RELIABILITY-BASED LOAD MANAGEMENT OF THE RED DEER RIVER BRIDGE

A Thesis Submitted to the College of Graduate Studies and Research in Partial Fulfilment of the Requirements for the Degree of

Master of Science

in the

Department of Civil and Geological Engineering
University of Saskatchewan
Saskatoon

By

Kristopher P. Jackson

PERMISSION TO USE

In presenting this thesis in partial fulfilment of the requirements for a Postgraduate degree from the University of Saskatchewan, I agree that the Libraries of this University may make it freely available for inspection. I further agree that permission for copying of this thesis in any manner, in whole or in part, for scholarly purposes may be granted by the professor or professors who supervised my thesis work or, in their absence, by the Head of the Department of the Dean of the College in which my thesis work was done. It is understood that any copying or publication or use of this thesis or parts thereof for financial gain shall not be allowed without my written permission. It is also understood that due recognition shall be given to me and to the University of Saskatchewan in any scholarly use which may be made of any material in my thesis.

Requests for permission to copy of to make other use of material in this thesis in whole or in part should be addressed to:

Head of Department of Civil and Geological Engineering
University of Saskatchewan
Engineering Building
57 Campus Drive
Saskatoon, Saskatchewan, Canada, S7N 5A9

ACKNOWLEDGEMENTS

The author wishes to express his sincere thanks to the project supervisors Dr. B. Sparling, and Dr. G. Sparks for their valuable guidance and support throughout the study. The author is also thankful for the contributions of advisory committee members Dr. L. Wegner, and Dr. P. Christensen.

The author also thanks Mr. Dale Pavier, Mr. Dave Messner, and Mr. Brennan Pokoyoway for their assistance in instrumenting the bridge and helping with the data collection. Special thanks go to Mr. Mazin Alwash for freely giving his time and knowledge in the data collection and finite element modeling portions of the study.

Thanks for financial support are extended to Saskatchewan Highways and Transportation and ISIS Canada.

ABSTRACT

This thesis presents the results of an investigation into the evaluation of a selected test bridge using instrumentation to obtain site-specific factors contributing to the evaluation, with the ultimate objective of improving the estimate of the bridge's reliability in order to assess allowable loading more accurately. The experimental portion of the research program involved instrumenting the test bridge with strain gauges, and recording field measurements using two forms of loading. The analytical portion of the research program involved the analysis of the bridge in the as-designed state, based on the design drawings and specification, followed by a re-analysis of the bridge using the site-specific factors measured on-site. The bridge was evaluated using methods outlined in the Canadian Highway Bridge Design Code CAN/CSA-S6-00 (CSA 2000).

The test bridge is located near the community of Hudson Bay, Saskatchewan. The bridge is constructed of steel-reinforced concrete, and there are three, three-span arch-shaped girders. There are also external steel bars added after initial construction to increase the midspan bending moment resistance. In total, 45 strain gauges were placed on the middle spans of the three girders to record strain induced by two forms of loading: controlled loading, in which a truck of known weight and dimensions was driven over the bridge in a number of pre-determined configurations, and in-situ loading, in which normal truck traffic was used. The current allowable loading on the bridge is a gross vehicle weight of 62.5 t, although increasing the allowable loading to 110 t has been proposed, along with two strengthening alternatives to make this increased loading feasible.

To provide a base-line analysis for comparison purposes, the bridge was first evaluated based strictly on information taken from the design drawings and specifications. The evaluation was performed using the load and resistance

factor method, in which load and resistance factors were used to account for uncertainty, as well as by the mean load method, in which statistical properties of the variable's parameters included in the design were used to account for uncertainty. The result of the load and resistance factor method was a live load capacity factor, indicating the overall "rating" of the bridge. In addition to the live load capacity factor, the mean load method was also used to determine the reliability index. The results of the as-designed analysis showed that the mean load method gave more conservative estimates of the bridge capacity. Furthermore, it was determined that, based on these assessments, the bridge would not have sufficient capacity to carry the proposed 110 t truck loads.

The bridge was re-evaluated using site-specific factors with the mean load method. Using the measured strains, statistical parameters were determined for live load effects, distribution factors, dynamic load allowance, and resistance. Statistical parameters that could not be obtained readily through testing were obtained from the literature. The results indicated that code-predicted estimates of a number of factors were highly conservative. Flexural and shear load effects in the girders were found to be less than 15% of the theoretical predictions, as a result of apparent arching action in the girders, generating significant axial forces. For this arching action to occur, horizontal restraint was required at the supports, either through unanticipated restraint in the bearings, or tension tie action of the tensile girder reinforcement. Furthermore, the dynamic amplification was found to be less than 1.0. The resulting reliability indices indicated that the bridge would be safe under the proposed increased allowable loading (110 t).

Finite element models were used to confirm the dynamic amplification observations and examine the effects of different degrees of bearing restraint. The model showed results similar to those measured for dynamic amplification. It was found that if the bearings were to become completely fixed against horizontal translation, the bridge would become overloaded as a result of

increased shear effects, demonstrating the need for proper bearing maintenance.

An analysis of relative costs was completed to determine the most cost-effective solution for hauling logs. Assumptions were made regarding truck and maintenance and operating costs. The results indicated that the most economic solution was to use the method outlined in the research to increase the allowable loading on the bridge to 110 t, over the strengthening alternatives and simply leaving the bridge in the current state.

TABLE OF CONTENTS

LIST OF TABLES

LIST OF FIGURES

CHAPTER 1 INTRODUCTION

1.1 PROBLEM DEFINITION

Bridges on highway networks constitute a vital part of the surface transportation network, so that the national economic status is directly related to the transportation network. Millions of dollars of products are transported to market in Canada each day, mainly by truck transportation. Despite their obvious importance, in many circumstances bridges are the limiting factor on a haul route; they do not have sufficient capacity to carry the increasingly heavy loads demanded to sustain today's economy. However, load-carrying capacities are generally determined based on conservative design and evaluation standards; therefore, the capacity of a bridge may be much higher than initially thought. Increased certainty regarding actual load-carrying capacity may allow truck loads to be increased, resulting in higher payloads at significantly lower hauling costs.

The only way to determine the actual load-carrying capacity of a bridge is through the use of field testing data incorporated into reliability-based assessment methods. Measurements taken at a bridge site can indicate actual material properties, geometry, and bridge behaviour that otherwise must be assumed from codes and bridge plans, thereby reducing the inherent uncertainty. Recent technological advancements have made field testing relatively quick, simple, and economical. Significant work has been done on

using site-specific factors determined in field testing to improve the load rating of bridges. Often, reliability-based methods are used to indicate a suitable load rating for a bridge. Reliability-based methods have become the preferred choice in evaluating bridges using field measurements, because they easily incorporate the uncertainty in field measurements, providing a probability of failure rather than a deterministic load rating.

This study focuses on the Red Deer River Bridge, located near Hudson Bay, Saskatchewan. The bridge has been the focus of much attention because it lies on a heavy haul route used by the logging industry; as such, there are continual demands from industry to allow increasingly heavy loads to cross the bridge. However, evaluations based on the Canadian Highway Bridge Design Code CAN/CSA-S6-00 (CSA 2000), a reliability-based code, indicate that the bridge has insufficient load-carrying capacity to comply with the latest loading demands. As a result, the reliability estimate for the bridge must be increased to meet a minimum acceptable level before the allowable loading may be increased. Two strengthening alternatives have been proposed, which would allow the bridge meet minimum reliability requirements for the proposed loading increase. However, the strengthening options are costly, and will require partial bridge closure for installation. At the time when this study was initiated, the bridge owner, Saskatchewan Highways and Transportation, was considering other alternatives for increasing the allowable loading while maintaining a minimum acceptable level of reliability. A re-evaluation of the in-situ bridge reliability was one of the available options.

1.2 OBJECTIVES

The primary objective of this research was to apply a methodology for assessing a safe level of allowable loading on a bridge using information from on-site instrumentation in a reliability-based evaluation. Sub-objectives were as follows:

1. To study the differences in bridge ratings using two different CAN/CSA-S6-00 methods (CSA 2000), based on information available from the evaluation of the bridge plans and specifications;
2. To determine the effects on reliability of using site-specific statistical properties of the required parameters in place of those prescribed by CAN/CSA-S6-00 (CSA 2000);
3. To use the site-specific measurements to develop a better understanding of the structural behaviour of the bridge; and
4. To determine the economic feasibility of using structural monitoring and site-specific measurements, along with reliability-based methods, as a means to manage loading on a bridge.

1.3 SCOPE

This research involves the static analysis of the Red Deer River Bridge using methods outlined in the CHBDC (CSA 2000). Potentially critical locations at midspans and support regions were considered, along with additional locations where instrumentation was installed. Based on previous evaluations of the bridge by others (EarthTech 2002), the bridge girders were assumed to be the critical structural elements. A dynamic study of the bridge was not completed as part of the evaluation; dynamic load effects were considered only in terms of equivalent static loads. In the economic feasibility study, on-site monitoring was compared with the proposed strengthening alternatives, as well as an option assuming that the bridge is left as is, with no monitoring, while maintaining the current allowable loading.

1.4 METHODOLOGY

The Red Deer River Bridge was first evaluated based on CAN/CSA-S6-00 (CSA 2000) methods, considering both the current and proposed allowable

loading. The first stage of the research will be referred to as the "as-designed" analysis. In the so-called as-designed analysis, the bridge was evaluated based only on information derived from the bridge plans and specifications, using the two different reliability-based evaluation methods specified in CAN/CSA-S6-00 (CSA 2000). The first type of evaluation applied was the load and resistance factor method, while the second method was the mean load method. The as-designed analysis served two purposes: to demonstrate the differences in the results of the two methods in terms of a live load capacity factor, and to provide a base-line reliability index for comparison with the "in-situ" analysis, as discussed below.

The second stage of the research will be referred to as the "in-situ" analysis. In the so-called in-situ analysis, the bridge was re-evaluated using several site-specific factors determined from field measurements. In addition to using simple non-destructive evaluations to determine concrete strength, instrumentation was permanently fixed to the girders to measure strains induced by log truck loading. From the field data, site-specific statistical parameters relating to load effects (bending moment and shear), distribution factors (lateral load sharing between girders), dynamic load allowance (increase in load effects due to dynamic effects), and resistance (bending moment and shear) were determined. The mean load method was then used in the in-situ analysis to determine a representative reliability index.

The results of the as-designed analysis and the in-situ analysis were compared, with explanations proposed for any differences that were determined. Finite element models of the bridge were used to assist in generating possible explanations for observed behaviour; in particular, the numerical analyses were used to confirm the observed effects of dynamic loading.

An analysis of relative costs was implemented to determine the economic feasibility of using the research methodology to obtain information about in-situ bridge behaviour. The analysis of relative costs was based on a number of best-estimate cost assumptions. The costs of the proposed research methodology were compared with the costs of strengthening the girders, as well as with the costs of leaving the bridge as is.

1.5 THESIS ORGANIZATION

This thesis contains six chapters and five appendices. The remaining five chapters are organized as described below; appendices will be referred to as needed within the chapters.

The second chapter supplies background information that is relevant to the study. A review of the literature pertaining to the research program is presented. First, literature related to reliability-based methods of managing loading on bridges are reviewed, followed by summaries of published research pertinent to this study.

The third chapter provides a detailed description of the test bridge, as well as a description of the experimental program. In addition to the description of the bridge layout and bridge materials, the general bridge location and usage are discussed. Details of the instrumentation, test loading, and procedures are provided.

The fourth chapter contains the analysis methods used in the research. Both methods used in the as-designed analysis, the load and resistance factor method and the mean load method, are described in detail. The in-situ analysis methods include details of methods used in analysing the collected data.

The fifth chapter presents the results of both the as-designed analysis and the in-situ analysis. The results are compared and discussed, and potential issues and problem areas are examined. A finite element model of the bridge is presented, and the model results are discussed. An analysis of relative costs and expected costs of alternative strategies for load management are also included.

The sixth and final chapter summarizes the methods and results of the research program, and provides conclusions and recommendations for further research in the field of the study.

CHAPTER 2 LITERATURE REVIEW

2.1 INTRODUCTION

This chapter presents background material pertinent to the research program. Relevant published literature dealing with load management of bridges, improving bridge reliability, and bridge testing is reviewed.

2.2 LITERATURE REVIEW

2.2.1 The Need for Load Management

Although the use of bridge management systems is becoming more widespread, not all jurisdictions have adopted some form of rational management strategy for making decisions pertaining to bridge loading, maintenance and repair, and rehabilitation (MR&R). A key component in bridge management is managing loading on a bridge. When loading and load effects are better understood, more responsible decisions regarding MR&R can be made. Inadequate knowledge regarding a bridge's true strength and response to loading may lead to poor decision-making, often resulting in substantial costs associated with unnecessary MR&R activity and loading restrictions.

Several studies (Dunker and Rabbat 1995, Estes and Frangopol 2001 (a), Estes and Frangopol 2001 (b), Estes and Frangopol 2003, Stewart 2001,

Stewart and Rosowsky 1998, Nowak and Tharmabala 1989), have provided statistics regarding the state of the national bridge inventory in the United States, with recent papers estimating that 40-45% of that nation's bridges are structurally insufficient in some way. The cost of alleviating this problem is estimated to be as much as US$90 billion, in addition to the US$140 billion already spent each year in the United States to maintain over 600,000 bridges. Although similar statistics are unavailable for Canada, it is reasonable to assume the situation is similar. It is thought by some, though, that a large part of this problem is simply one of perceptions; many of the bridges in question may already have sufficient capacity, but MR&R is being performed unnecessarily because the load-carrying capacity is not adequately understood. Any savings which could be realized by optimizing the allocation of MR&R resources in a more rational manner would be highly beneficial to society as a whole.

In addition to unnecessary MR&R being performed at substantial costs, economic efficiency is also impaired by forcing the trucking industry to restrict haul weights. Ghosn (2000) stated that "there is a general feeling among transportation interests that excessive regulations and weight restrictions imposed on the trucking industry are hampering efforts to strengthen the nation's economy and plans to make it more efficient in a competitive world market." Furthermore, when bridges are posted with haul weight restrictions or closed entirely, there is the added inconvenience of detours and waiting, resulting in high user costs (Chajes et al. 1997). The effects of overly conservative predictions of the load carrying capacities of bridges are therefore far-reaching. Improved load management can assist in reducing potentially large costs imposed by uninformed decisions.

2.2.2 Reliability Theory

Reliability-based methods are becoming the most commonly used method of evaluation for managing bridge loading. In general, reliability-based methods use the probabilities of failure as a performance, or safety measure. The typical unit by which bridge safety is measured is the reliability index, as it provides a convenient measure of likely life cycle performance (Nowak 1989, Akgul and Frangopol 2003). The reliability index is inversely related to the probability of failure; as the probability of failure is reduced, the reliability index is increased.

The probability of failure of a structural system is related not only to expected load effect and resistance values, but also to the uncertainty which is present in estimating these values. For this purpose, it is generally assumed that load effects and resistance can both be summarized by normal probabilistic distributions, which can be fully characterized by a mean value and standard deviation. In that case, the reliability index can be determined from the following relationship (Nowak and Collins 2000):

$$\beta = \frac{\mu_R - \mu_Q}{\sqrt{\sigma_R^2 - \sigma_Q^2}} \qquad [2.1]$$

where μ_R and μ_Q are the expected mean values of the corresponding resistance and load effect, respectively, while σ_R and σ_Q are the associated standard deviations for those values.

To prevent failure, the resistance of a structural element must be larger than the load effects it experiences. However, even when the mean values of load effects and resistance are substantially separated, there remains some possibility of failure due to the chance that load effects are much higher than anticipated and/or the resistance is much lower. This can be represented

graphically, as shown in Fig. 2.1 (Nowak and Collins 2000). The region where the tails of the load effect curve and the resistance curve cross defines the likelihood of possible structural failure. A more direct indicator of the probability of failures can be obtained from the probability distribution representing the difference between resistance and load effect, where the region to the left of the origin represent the probability of failure, as shown in Fig. 2.1. The spread of the normal distributions in Fig. 2.1 is dependent upon the standard deviations of the load effects and resistance, which can generally be stated as a measure of uncertainty in the predictions of these parameters. As a result, there are two methods of reducing the probability of failure, and thereby increasing the reliability index: increasing the mean of resistance and/or decreasing the mean of load effects, and decreasing the uncertainty in the predictions of load effects and/or resistance. For an appropriate reliability index to be selected, all sources of uncertainty must be considered.

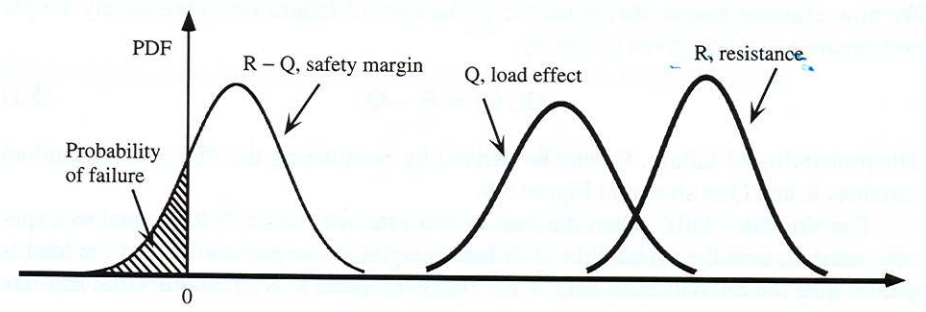

Figure 2.1. Loading and resistance normal distributions (taken from Nowak and Collins 2000).

2.2.3 Consequences of Target Reliability Selection

As stated previously, the outcome of most reliability-based analyses is a reliability index. Stewart and Val (1999) identified four main uses of bridge reliabilities:

- To compare a computed value with a target reliability;

- To estimate the cost effectiveness of various decisions affecting the reliability;
- To prioritize bridge MR&R in a bridge inventory; and
- To identify the likely mode of failure.

Comparing the estimated bridge reliability index with a target reliability index provides the basis for a reliability-based evaluation. A bridge can be considered safe when the computed reliability index is higher than the minimum allowable, or target reliability index. Stewart (2001) stated that comparing bridge reliabilities at any time with a target reliability can be extremely difficult. Although bridge reliability may be relatively easily determined, selection of an appropriate target reliability must be done by a calibration process, generally based on the reliabilities associated with a large number (minimum of 50, preferably several hundred) of new or well-performing bridges. It is for this reason that the target reliability may vary from country to country, or even between jurisdictions. It is also due to the fact that the perception of acceptable risk can vary between people and organizations; some are simply willing to accept more risk than others.

Possible outcomes of a bridge failure can include injuries and fatalities, financial loss, and environmental damage (Ryall 2001), leading to much more stringent bridge requirements (Das 1998). The level of aversion to these risks varies in different jurisdictions. Therefore, selection of a target reliability index essentially becomes an economical problem (Nowak 1997), in that selection of a low target reliability index can result in frequent failures, in which failure may be defined as the inability of the bridge to properly carry traffic, which can be very costly. However, selection of a high target reliability index may result in high initial and MR&R costs. In Canada, the minimum allowable reliability index is specified in the Canadian Highway Bridge Design Code CAN/CSA-S6-00 (CSA 2000), and it is a function of element behaviour, system behaviour, and inspection level. Generally, target reliability indices are around 3.0, although

several studies show very different values (Estes and Frangopol 1999, Frangopol et al. 2001).

Another issue with target reliabilities is that they generally tend to consider behaviour of a single structural component (Stewart et al. 2001). It has been argued that system reliability should be considered, as element reliability is not representative of the entire structural system, and system reliability can fall very low even if element reliabilities are acceptable (Estes and Frangopol 1999, Nowak and Collins 2000). However, in a study by Cheung and Li (2002), only girder reliability was considered, based on the argument that if a single girder failed the bridge could be considered to have failed.

2.2.4 Uncertainties in Bridge Evaluation

In a general sense, uncertainty in bridge evaluation is present in both loading and resistance, as presented in Figure 2.1. Statistical distributions are used to represent the uncertainty, considering each variable to be random. There are a number of different methods commonly employed to include uncertainty within a reliability analysis; in addition, the number of variables considered to be random, as opposed to deterministic, varies. This section discusses the different areas of uncertainty, and how they are included in reliability analyses.

In a low level reliability- based method, which Akgul and Frangopol (2003, 2004) refer to as a level 1 method, the reliability-basis is introduced in partial safety factors. Generally, modern design codes and standards utilize level 1 reliability-based methods, using load and resistance factors applied to deterministic nominal values. For example, the CAN/CSA-S6-00 (CSA 2000) load and resistance factor evaluation is a level 1 method, for which the partial factors have been developed based on statistical distributions measured at several bridge sites (CSA 2000). The calibration of level 1 methods has been

discussed by a number of authors (Nowak and Lind, 1979, Agarwal and Cheung 1987, Nowak 1994, Nowak and Grouni 1994, Nowak 1994, Nowak 1988, Nowak 1995, Nowak 1993).

The CAN/CSA-S6-00 (CSA 2000) mean load method is a level 2 reliability-based method (Akgul and Frangopol 2003, Akgul and Frangopol 2004). In a level 2 method, uncertainties in dimensions, resistances, and loads are considered as random variables, represented by a mean and standard deviation. Typically only the most significant variables are considered to be random, and simplified limit state design equations are used to calculate the reliability indices. In the mean load method, dead load effects, live load effects, resistance, and the dynamic load allowance, as well as the live load and dead load analysis methods, are treated as random variables.

Uncertainty in load effects, especially live load effects, can be substantial. Loads acting on bridges are relatively well defined, although the load effects induced by these loads are not. The manner in which load is distributed within a bridge dictates the magnitude of specific load effects. In the CAN/CSA-S6-00 (CSA 2000) mean load method, load distribution is more generally referred to as the load analysis method. Load distribution is uncertain because it is dependent on several factors that are difficult to accurately predict in a bridge evaluation (Nowak et al. 1999), such as the type and location of loading, as well as the configuration of the structure itself. Kim and Nowak (1997) stated that load effects depend on vehicle type, transverse position on the bridge, speed, and weight. Furthermore, load effects depend upon structural conditions, such as lateral load sharing mechanisms (diaphragms) and support conditions, which are also difficult to accurately include in an analysis. The uncertainty associated with dead load effects is less than that associated with live load effects. A study by Au et al. (2005) assumed that the dead load distribution (dead load analysis methods) was essentially deterministic.

Dynamic load amplification presents the greatest uncertainty in the mean load method (CSA 2000). Although the actual dynamic load effects in several studies used in the calibration of the code (CSA 2000) were found to be significantly less than the nominal values assumed for code analyses, the observed variation was substantial, a finding attributed to the fact that dynamic load allowance is highly site-specific and dependent on several factors. Although CAN/CSA-S6-00 (CSA 2000) defines dynamic load allowance as a function of "discrete and random irregularity of the riding surface, bridge static and vibratory deflections, and the dynamic effects of interaction between a moving vehicle and the bridge," other authors have stated that are several more contributing factors. Nassif and Nowak (1995(a)) stated that the dynamic load is "time variant, random in nature and depends on vehicle type, vehicle weight, axle configuration, bridge span length, road roughness and transverse position of truck on the bridge." As reported by Paultre and Proulx (1995), Humar and Kashif (1993) found on the basis of several studies that the dynamic amplification depended on the ratio of the first flexural frequency of the bridge to the vehicle's vibration frequency, the ratio of vehicle weight to total structure weight, and the vehicle speed.

Finally, there is overall uncertainty in both flexural and shear resistance. Uncertainty in resistance is largely due to differences in materials (strength, modulus of elasticity, cracking strength, chemical composition), fabrication (geometry and dimensions), and analysis (lateral distribution, idealized stress and strain distributions) from those initially assumed (Nowak and Szerszen 1998). There are often discrepancies between the calculated and actual flexural resistances, due to actual stiffnesses that are higher than predicted. Bakht and Jaeger (1990) found that increased stiffness could often be attributed to concrete with a higher modulus of elasticity than anticipated, interaction of the girders with secondary components such as barrier walls, and a higher degree than expected of composite action between deck and girders.

In a level 3 reliability-based method, simulation and numerical methods are used to evaluate reliability; traffic simulation models and deterioration models are also included (Akgul and Frangopol 2003, Akgul and Frangopol 2004). The list of random variables that may be included is extensive. Stewart (2001) described the different areas of uncertainty that may be included in a level 3 method:

- Model errors;
- Variability in material properties;
- Variability in workmanship and the environment;
- Spatial variations in material and other properties;
- Measurement and calibration errors;
- Variability in loading; and
- Assessment and deterioration processes.

A study by Estes and Frangopol (1999) detailed an extensive list of random variables considered in the reliability analysis of a steel-reinforced concrete bridge, in which 24 random variables were considered. Uncertainty in material properties was assumed to be present in:

- The yield strength of steel and compressive strength of concrete;
- The modulus of elasticity of the steel; and
- The weights of asphalt, steel, and concrete.

Uncertainty in workmanship was categorized in terms of:

- The cross-sectional area of the reinforcing steel within the concrete;
- The effective depth of the reinforcing steel; and
- The area of steel shear reinforcement along with the stirrup spacing.

Finally, a number of uncertainties related to loading were identified, including:

- Truck weights; and
- Amplification of loading caused by dynamic effects.

Deterioration models are often included in level 3 reliability-based methods, since the uncertainty in bridge evaluation can be compounded even further as a bridge ages. Val et al. (1998) described the most common contributor to deterioration of bridges as being related to the reinforcing steel. Corrosion of the steel is caused by chemical processes occurring within the concrete, including chloride contamination, alkali-silica reactions, sulphate attack, and carbonation. This break-down of the steel leads to reduced capacity of structural members as the cross-sectional area of steel is reduced, and the concrete spalls off in response to corrosion-induced pressure. Val et al. (1998) also stated that other factors such as fatigue and overloading can also significantly contribute to deterioration, making it even more difficult to predict bridge capacity with certainty.

Uncertainty can be significantly reduced through the use of field testing. Site-specific parameters may be determined to replace generic values prescribed by codes. Modelling uncertainty can be minimized by incorporating observed behavioural characteristics, such as load sharing and dynamic response, rather than assumed values. In addition, deterioration models are not required because existing properties and geometry can be obtained.

2.2.5 Reducing Uncertainty Through On-Site Testing

Several methods of reducing uncertainty have been proposed and discussed in the literature. Uncertainty in material properties and geometry can be reduced by performing non-destructive and partially-destructive evaluations. Stewart (2001) described how material properties can be better understood through the use of core testing, rebound hammer tests, and ultrasonic pulse velocity testing. Reinforcing steel dimensions can be determined by use of an electromagnetic covermeters. Furthermore, internal deterioration can be analysed by means of impact-echo techniques, half-cell potential tests, or resistivity measurements. Although the results of non-destructive evaluations

can often be subjective, time consuming, and difficult to interpret (Martin et al. 1998), most studies agree that different forms of site-specific data are beneficial.

Non- and partially- destructive evaluations are useful in determining material and geometric properties; however, full scale bridge testing is also required to obtain estimates of actual bridge behaviour. Bakht and Jaeger (1990) discuss the often surprising results obtained from bridge testing, stating that "bridge behaviour may be so deceptive that it can be understood only through a field test." Full scale bridge testing is typically used to determine live load effects, distribution factors, dynamic load effects, and bearing restraint. In the past, full scale bridge testing has not often been practical, due to the associated high costs and complexity levels; today, on the other hand, it has become relatively inexpensive (Moses et al. 1994, Schulz et al. 1995). In most cases, the findings of full scale bridge testing have been beneficial, indicating lower response levels than anticipated. Nowak and Zhou (1990) often found that bridge testing indicated that there were considerable differences between the predicted bridge capacity and the capacity determined by on-site evaluation. Based on several field tests in Ontario, Bakht and Jaeger (1990) stated that "large differences between the calculated and actual load-carrying capacities of bridges have been encountered in so many instances that they are no longer included in the surprises of bridge testing…fortunately, in most cases, the errors in the mathematical modeling of the structure are on the safe side." However, it should be noted that regardless of the amount of data collected, a significant amount of engineering judgement is required in interpreting results (Schulz et al. 1995).

Finally, uncertainty in loading can be reduced by placing stricter controls on truck traffic. Asantey and Bartlett (2005) discussed the benefits with regard to reliability of using stringent loading control methods. The use of weigh scales near bridges would reduce occurrence of overweight trucks, or at least provide

knowledge of the actual truck weights. Better enforcement of weight limit laws would discourage the practice of hauling overweight loads, as strong financial consequences would be placed on truck drivers and owners (Peterson 2001). Furthermore, the benefits of on-board scales installed in trucks ensure legal payloads, except in the case of deliberate non-compliance, and are especially beneficial in the logging industry (Talbot 1999).

2.2.6 Related Studies

2.2.6.1 Improving Bridge Rating and Reliability

Several studies have been completed which were similar to the work undertaken in this research. Generally, the study objectives were aimed at increasing the bridge reliability or bridge rating by determining site-specific factors through field measurements. In all the reported studies, information was obtained through the use of strain gauges installed on the bridge girders, usually on the top and bottom flanges. Two forms of loading were often utilized: controlled loading, and normal truck traffic. Controlled loading usually involved using test trucks of known weights and dimensions, driving over the test bridges at a number of predetermined speeds and configurations. The test trucks were run across the bridge at low speeds to produce pseudo-static loading, in which the trucks are moving, although so slowly that the response is essentially static, as well as at typical travel speeds. In several cases, controlled loading was used to "calibrate" the strain measurements to truck weights and load effects. Such a method was often referred to as a weight-in-motion (WIM) system (Nowak et al. 2000, Ghosn et al. 1986, Nassif and Nowak 1995 (a), Laman and Nowak 1995, Nowak and Nassif 1992, Kim et al. 1995, Kim et al 1999), while Chajes et al. (2000) refer to the method as a stress-in-motion system. In all these studies, the bridge was essentially used as a scale. In contrast, tests involving normal truck traffic measured the load effects caused by trucks travelling in an unregulated fashion in the flow of traffic.

Chajes et al. (2000) summarized the advantages and disadvantages of using controlled and normal truck loading. Controlled loading has the advantage of a known vehicle weight, and therefore accurate quantification of response, while the disadvantages include the requirement of bridge closure for testing and the fact that the observed response represents a snapshot in time only. On the other hand, normal truck traffic has the advantage of representing real traffic conditions, as well as allowing the bridge to remain open; however, the truck weights in this case are unknown, and the limited random data does not allow certain parameters to be evaluated. Kim and Nowak (1997) identified several advantages of using normal truck traffic, including:

- No disturbance of normal traffic;
- The use of a variety of truck types;
- A diversity of lateral positions of the trucks;
- A variety of speeds;
- Cost effectiveness (no bridge closure and traffic control is required);
- Ease of testing; and
- Strain data that is representative of the actual loading conditions.

It has been recommended that a combination of controlled loading and normal traffic should be used in bridge testing (Paultre et al. 1995).

As mentioned previously, one aspect of bridge behaviour that can be studied using on-site testing is the dynamic response. In general, there were two methods typically used for determining the dynamic load allowance. Both methods used the following equation to obtain the dynamic load allowance (Nassif and Nowak 1995 (a), Nassif and Nowak 1995 (b)):

$$I = \frac{D_{dyn}}{D_{stat}} \qquad [2.2]$$

where D_{dyn} is the dynamic component of the response at any point (the total response less the static response), and D_{stat} is the corresponding response to

static loads. Generally, the response considered was measured strain. One reported method of determining the dynamic load allowance was to obtain D_{stat} from pseudo-static truck passes, and D_{dyn} from dynamic passes using a comparable truck. Another method of determining the dynamic load allowance was to use the "raw" strain measurements from uncontrolled truck loading tests as the dynamic response, filtering out the low frequency pseudo-static response from the strain time-histories to obtain the static response, D_{stat}. The dynamic component of the response, D_{dyn}, is taken as oscillation height above the static response.

Distribution factors were typically determined in a similar manner in all the reported studies. The distribution factor at a girder was taken as ratio of the response at that girder to the sum of the responses in all girders (Kim and Nowak 1997):

$$GDF_i = \frac{M_i}{\sum_{j=1}^{k} M_j} = \frac{ES_i\varepsilon_i}{\sum_{j=1}^{k} ES_j\varepsilon_j} = \frac{\frac{S_i}{S_l}\varepsilon_i}{\sum_{j=1}^{k}\frac{S_j}{S_l}\varepsilon_j} = \frac{\varepsilon_i w_i}{\sum_{j=1}^{k}\varepsilon_j w_j} \qquad [2.3]$$

where M_i is the bending moment in the *i*th girder of girders 1 to *k*, E is the modulus of elasticity of the girder material, S_i is the section modulus of the *i*th girder, ε_i is the strain in the *i*th girder, S_l is the typical interior girder section modulus, and w_i is the ratio of the section modulus of the *i*th girder to the section modulus of a typical interior girder. Usually, strain measurements were used to determine the distribution factors. When a single test truck was used, linear superposition was assumed so that multiple lane loading could be approximated as the sum of multiple single lane loadings.

Au et al. (2005) carried out a study very similar to that undertaken in this research program, in which a simply supported steel box-girder bridge in Ontario was instrumented in order to obtain site-specific statistical parameters

of some of the variables used in the mean load method in CAN/CSA-S6-00 (CSA 2000). In the study, the bridge was evaluated using the load and resistance factor method, the mean load method, and then re-evaluated using the mean load method with site specific data.

Strain gauges were installed on the girder webs and on the bottom flanges. The maximum and minimum strains were recorded to obtain the maximum response under load. A single test truck was used to calibrate strain response to load effect, and the dynamic load allowance was determined using pseudo-static and dynamic truck passes. The only load effects considered in the study were bending moments, which were determined from the strains calibrated to known truck weights, and therefore were not determined by bending moment analysis methods. Site-specific statistical parameters were used in the mean load method (CSA 2000) to determine live load capacity factors. No site-specific information was determined regarding dead load effects.

The study found that the load and resistance factor method and the mean load method using code recommended parameters (CSA 2000) gave comparable live load capacity factors. The live load capacity factor of the bridge was increased by 4% when the mean load method was used, as compared to that predicted by the load and resistance factor method. When the mean load method was used to re-evaluate the bridge using site-specific information from field measurements, the live load capacity factor was increased 57% from the initial mean load method evaluation. Resulting reliability indices were not discussed. The study concluded that using site-specific statistical parameters in the mean load method resulted in improved live load capacity factors, leading to economic benefits which outweighed the cost of data collection and analysis.

A study by Cheung and Li (2002) described a reliability-based evaluation of a slab-on-girder bridge using reliability theory, rather than the CAN/CSA-S6-00 (CSA 2000) methods of analysis. The study was theoretical, and statistical parameters characterizing several variables used in analysing loading and resistance were assumed based on the results from previous studies. The focus of the study was the behaviour of the bridge girders, as girder failure would result in bridge closure.

Girder sections were evaluated using the assumed statistical parameters from the literature and conventional bending moment analysis techniques. The location of the neutral axis was adjusted until the net axial forces based on the assumed strain distributions were zero, at which point the bending moment was determined. The study concluded that reliability assessment should be performed on all bridge designs and evaluations, as idealized code requirements cannot take into account the influence of different factors on particular bridges. The authors stated that bridges considered safe in a load and resistance factor evaluation often have unsatisfactory reliability indices. This fact was demonstrated by an example slab-on-girder bridge. Furthermore, the authors showed that a simple change, such as the addition of sidewalks on the example bridge, reduced the probability of failure by 83%, while no change was registered when the load and resistance factor method was used.

Chajes et al. (2000) developed a methodology for improving the accuracy of bridge capacity evaluation using field measurements, determined from load testing and in-service monitoring. A slab-on-steel girder bridge in Delaware provided the basis of the study. The bridge was instrumented with 32 strain gauges, most of which were concentrated in midspan locations. Two forms of testing were utilized in the study: diagnostic load testing, in which controlled loading was used, and in-service monitoring, in which normal truck traffic was used and monitored over a ten week period.

In the study, measured strains and basic principles of structural behaviour were used to determine live load distribution, support restraint, flexural resistance, and effects of impact (dynamic load allowance). As only one test truck was used in the controlled loading tests, the distribution factors determined from Equation 2.3 for loading on single lanes were superimposed for multiple lane loading. Overall load effects along the lengths of the girders were used as an indication of the degree of fixidity in the supports. Bending moments were determined using the neutral axis location interpolated on the basis of the measured top and bottom flange strains, assuming that plane sections remained plane. The site-specific factors were used according to the rating factor method specified by AASHTO (1994 (b)). The bridge rating was increased due to a 15% improvement in distribution factors, a general improvement in dynamic load allowance (ranging from 0.0 to 0.26, as opposed to the AASHTO value of 0.27), and generally low stresses. The methodology outlined in the study allowed the bridge owner in the area, Delaware Department of Transportation, to remove load restrictions on some bridges, and to permit access of super-loaded trucks. Furthermore, plans for bridge replacements were postponed.

Nowak et al. (2000) carried out a study investigating the control of live loading on bridges. The objective of the study was to monitor and control various live loading parameters. The study considered a number of slab-on-steel girder bridges in the Detroit area. Portable strain gauges were installed on the bottom flanges only of the girders at several locations, and data was recorded for 2-3 weeks at each bridge. The measured strains were calibrated using test trucks to generate statistical distributions of gross vehicle weight. Considering the gross vehicle weights, bending moments and shear forces were determined analytically.

The distribution factors were determined from the static strain data. Multiple trucks were driven across the bridge to obtain distribution factors for multiple lane loading, rather than using the previously discussed superposition

technique. Truck passes were run pseudo-statically, and at two travel speeds to determine the dynamic load allowance. The study found that distribution factors were lower than those given by AASHTO (1998), ranging from 15% to 75% of the code-predicted values for two-lane loading, indicating that there was more load sharing than predicted. Furthermore, distribution factors determined using two test trucks were comparable to those determined using linear superposition. It was also found that the dynamic load allowance was lower than the code-specified value, and that it decreased with increasing static load effect. For two trucks side by side, the dynamic load allowance was determined to be less than half of the code specified value.

A study by Ghosn et al. (1986) used field measurements from strain gauges on five steel girder bridges in Ohio to obtain statistical parameters for several variables which were incorporated into a reliability analysis. The strains measured at the bridges in the study were calibrated using a single test truck. After the test truck calibration, 600 truck loading events in normal traffic were considered during four hours of continuous data acquisition. Distribution factors were determined for multiple lane loading by the method of superposition, as occurrences of two side by side trucks on the bridges were very rare. Dynamic load allowances were estimated from the response strain record using a filtering technique. Measured stresses were used to determined live load effect statistical parameters. The study concluded that the load effects were significantly smaller than the predicted values, a result attributed to composite action, as well as effective section modulus increases due to sidewalks, barriers, and the asphalt surface. The measured maximum stresses were 28% of the stresses calculated assuming no composite action, and 44% of those assuming composite action. Furthermore, the code-predicted values of distribution factors and dynamic load allowances were found to be highly conservative; the measured dynamic load allowance of 0.1 was significantly less than the AASHTO-prescribed value of 0.28, while the maximum measured distribution factor was 75% of the code-prescribed value (AASHTO 1983). The

use of site-specific data resulted in improved bridge ratings; on average, ratings were improved 30% from AASHTO values (AASHTO 1983). Although the study noted the occurrence of several over-loaded trucks, bridge safety was not impaired.

Nowak and Tharmabala (1989) performed a study on a steel truss bridge, with the objective of combining structural reliability analysis with bridge test results to improve reliability. The bridge was instrumented with strain gauges to obtain measurements of axial strain. Two test trucks were used to carry out controlled loading. Axial stresses in the members were determined from the strains, indicating load distributions in the various truss members. Furthermore, the dynamic load allowance was determined using pseudo-static and dynamic truck passes. Reliability indices were determined using reliability theory for each truss member, and the lowest reliability index was taken as the bridge reliability. The general findings of the study were that the reliability indices computed from field measurements were 30% to 55% higher than those based on conventional analysis methods prior to the bridge testing, primarily as a result of measured axial forces which were lower than those calculated.

Chajes et al. (1997) completed a study on a slab-on-steel girder bridge in Delaware. The objective of the study was to improve estimates of the allowable load rating of the bridge by determining the degree of support restraint, composite section properties (neutral axis location and moment of inertia), and distribution factors. The bridge was instrumented with strain gauges on the top and bottom flanges of the girders. The top flanges of the girders were concrete-encased; therefore, longer strain gauge lengths were used to avoid measurements of localized stresses in cracked concrete. Loading was applied in a pseudo-static manner only, with a single test truck of known weight driven across the bridge at 8 kph. Readings were taken at a sampling frequency of 32 Hz.

Using the measured top and bottom flange strains, and assuming plane strain conditions, the neutral axis was located, allowing a better estimate of the effective moment of inertia of the section. The degree of support restraint was determined considering the measured longitudinal strain distribution, combined with finite element model results. The predicted longitudinal strain distributions were determined from the finite element model for two cases: the supports at both ends of the spans being rigidly fixed, and pinned. Comparing the results of the measured and predicted strain distributions gave an indication the actual fixity of the girders.

Test results indicated that there was a high degree of composite action, an increase in the moment of inertia over predicted values, some degree of end fixity (estimated to be 20% fixity), resulting in an increase in stiffness over calculated levels. In addition, the code-predicted distribution factors were found to be conservative by a margin of 28% (AASHTO 1989). The final result of load rating suggested that the bridge likely did not need to be posted for low loading, as the load-carrying capacity was determined to be substantially higher than was previously indicated. Although the study determined that there was little axial force in the girders, it was noted that unanticipated end restraint could lead to significant axial loads. In cases where axial forces are large, the authors indicated that girder curvatures could be used to determine some of the needed parameters.

A study similar to that of Chajes et al. (1997) was completed by Reid et al. (1996), using a slab-on-steel girder bridge in Delaware. The objective of the study was to improve the estimate of the load rating of the test bridge by measuring the same site-specific parameters as those considered in the study by Chajes et al. (1997). Furthermore, the dynamic load allowance for the bridge was determined. A total of 32 strain gauges were placed on the girders, with an emphasis placed on the midspan regions of the girders. The bridge was loaded using a single test truck, moving pseudo-statically and dynamically.

The results of the study indicated that some composite action was occurring, and that there was a small degree of support restraint (5%). The distribution factors and dynamic load allowance were found to be "very similar" to those predicted by the AASHTO formula (AASHTO 1989). The bridge rating was increased due to the improvements in measured factors, and the results were extrapolated to permit higher loading.

A study by Barnes et al. (2003) focused on obtaining site-specific estimates for distribution factors, dynamic load allowance, and stresses in a high-performance prestressed concrete bridge. Strain gauges were mounted on the reinforcing bars in the top and bottom flanges prior the casting of the concrete. Loading was applied using a single test truck, as well as with two trucks travelling side by side, both pseudo-statically and dynamically. Distribution factors were determined combining the single test truck passes and using superposition, and from the two test trucks without superposition. Stresses at the bottoms of the girders were considered, as the authors stated that they tend to control the design for live load. The dynamic load allowance was determined from the pseudo-static and dynamic truck passes. It was found that the theoretical calculations, based on AASHTO methods (AASHTO 1996), overestimated all of the factors determined from the field measurements. The code-computed bottom flange stresses were 85% larger than the measured values, the measured distribution factors ranged from 12% to 47% less than the computed values, and the average measured dynamic load allowance of 0.12 was 36% of the AASHTO value of 0.33.

2.2.6.2 Improving Specific Factors

A number of studies have focused on the use of bridge testing as a means of determining different factors, without the specific consideration of estimating bridge reliability. A study by Kim and Nowak (1997) focused on

determining distribution factors and dynamic load allowances for two steel I-girder bridges in Michigan. Strains measured from the lower flanges at midspans were used for evaluation. A total of 130 trucks travelling in normal traffic were used to load the bridges. The dynamic load allowance was determined by separating the static and dynamic response components by signal filtering. The distribution factors were determined using the filtered static strains with Equation 2.3, applying the principle of superposition to account for two lane loading. It was found that the distribution factors and the dynamic load allowances were consistently lower than those determined by AASHTO methods (AASHTO 1992, AASHTO 1994 (b)), and that the discrepancy relative to AASHTO values in the results was similar for the two bridges. The code values of distribution factors were 16% to 28% higher than the measured values, while the measured dynamic load allowances were less than two-thirds of the code-prescribed values. It was also determined that the measured dynamic load allowances decreased as the static strain level increased.

Three studies which focused on determining only distribution factors are summarized below.

Fu et al. (1996) attempted to determine the distribution factors for four steel I-girder bridges in Maryland, using strain measurements taken at the bottom flanges of the girders. Two test trucks were used, travelling at typical bridge speeds. Since it was suggested that static strains alone should be used in determining distribution factors, the dynamic component of the measured strains was filtered out. Rather than using Equation 2.3, the authors developed a root-mean-square method for calculating distribution factors. It was found that the distribution factors were independent of the magnitude and configuration of the truck load, although the transverse position on the bridge did affect results. The measured distribution factors were consistently lower than those predicted by AASHTO code methods (AASHTO 1994 (b)).

Huang et al. (2004) also measured site-specific distribution factors. A highly skewed slab-on-steel girder bridge was equipped with 40 strain gauges on the top and bottom flanges of the girders. Thirteen pseudo-static truck passes were made using two test trucks, travelling solo and side-by-side. Bending moments were determined using the computed locations of the neutral axes based on measured strain distributions. The distribution factors were determined using Equation 2.3 applied to bending moments. It was found that the girders nearest to the load carried most of the load, and that the distribution factors remained less than or comparable to the theoretical values. It was also determined that while distribution factors were over-predicted using AASHTO methods (AASHTO 1994 (b)) in the positive bending moment regions, they were "accurate, but not conservative" in the negative bending moment regions.

Nowak et al. (1999) completed a study in which distribution factors were determined for five slab-on-steel girder bridges in Michigan, using strain gauges installed on the bottom flanges at midspans. The study obtained distribution factors for test trucks travelling pseudo-statically and at regular highway speeds. A single test truck was used, and the superposition principle was applied to determine the distribution factors for multiple lane loading. The measured distribution factors were determined to be well below the AASHTO-specified values for both truck speeds (AASHTO 1996, AASHTO 1998, AASHTO 1994 (a)).

Several other studies focused only on determining the site-specific dynamic load allowance through the use of field measurements. Two similar studies by Nassif and Nowak (1995 (a), 1995 (b)) determined the dynamic load allowances by girder of four slab-on steel girder bridges in Michigan. The strain gauges installed on the bottom flanges near midspan were calibrated using a test truck, although normal truck traffic was used to determine the dynamic load allowances. The strain time-histories were run through a fast fourier transform, which indicated the static component of the response. It was determined that

the average dynamic load allowances were in the range of those predicted by the AASHTO method (AASHTO 1992). It was also found that the dynamic load allowance decreased with increasing static response, and that the dynamic component of the response was practically independent of the static component. The measured dynamic load allowance decreased with an increase in speed, which is contradictory to what is specified in CAN/CSA-S6-00 (CSA 2000). Furthermore, the measured dynamic load allowance was larger in the exterior girders, although this was attributed to the fact that the static response was much lower in those girders.

Chan and O'Connor (1990) carried out a study to determine the effects of dynamic load on a slab-on-steel girder bridge located in Australia, fitted with strain gauges on the webs of the girders. A test truck was used to calibrate measured strains to bending moments in the section. A linear relationship was developed, such that bending moments from normal truck traffic were predicted from the measured strains. The weights of the trucks in the normal flow of traffic were known from a nearby weigh scale. The dynamic load allowance was determined by filtering the dynamic component of bending moment from the overall bending moment. A high dynamic load allowance relative to theoretical values was determined for the bridge for some combinations of GVW and span length (MTC 1983). It was also found that dynamic load allowance decreased with increasing truck weight.

Paultre et al. (1995) completed a study outlining dynamic testing procedures for bridges. Three bridges of different construction located in Quebec were equipped with various forms of instrumentation, although strain gauges were used in the determination of the dynamic load allowances. Dynamic load allowances were determined by the two methods discussed in Section 2.2.6.1: through filtering, and from pseudo-static and dynamic truck passes. In controlled testing, two test trucks were driven over the bridges in a number of different configurations, including one following another. A dynamic

load allowance was determined for all load configurations on each bridge. Finite element models, calibrated based on natural frequencies and mode shapes, were created for each of the bridges tested, and used for the purposes of comparison. It was determined that the measured dynamic load allowances were generally quite large, compared to those generally specified by codes, although no comparisons to codes were drawn, as the article discussed different testing procedures. The dynamic load allowances resulting from the different controlled loading configurations varied considerably, and no trend in the results was noted.

An extensive study was undertaken by Billing (1984) in which 27 bridges of various configurations in Ontario were dynamically tested using strain gauges to record responses. Controlled loading was performed using two test trucks in various configurations, including one following another, at speeds of 16 kph and 48 kph. Normal truck traffic was also used as a form of loading. The dynamic load allowances were determined by filtering the static response from the strain time-histories. Only strains from the largest positive regions of the girders were considered in the study. It was determined that the dynamic load allowances were generally lower than expected from the Ontario Highway Bridge Design Code (MTC 1979), although some were found to be very high, with significant variability in the measurements. It was also determined that the dynamic amplifications were approximately equal in the positive and negative bending moment regions of continuous girders. The results showed that the dynamic load allowances were typically reduced for higher loading, and increased for the cases where two test vehicles were following one another. Due to the extensive results, the reader is referred to the article for numerical findings.

2.2.6.3 Trends and Gaps in the Literature

The reported studies previously discussed had goals of either increasing reliability estimates using site-specific field measurements, or measuring

specific parameters contributing to bridge evaluations. Generally, the studies showed similar trends in both the methodologies and the results. Similar testing procedures were used throughout the reported literature, which can be summarized as follows:

- The use of strain gauges, generally fixed to the bottom flanges of the girders, and an automated data acquisition system;
- The use of controlled loading, often using only a single truck and linear superposition to determine multiple lane loading effects; and
- The use of normal truck traffic to measure "real" results.

Furthermore, similar analytical methods and techniques were applied through the reported studies. There is a wide base of literature covering the determination of dynamic load allowance and distribution factors, generally using the methods discussed previously in this section. In studies aiming to increase the load rating of a bridge, load effects were typically measured in terms of stresses and bending moments. There was a general trend, however, not to determine these effects by conventional methods, but by the "calibration" of the measurements to known vehicle weights. The results of the reported studies were typically beneficial, with lower dynamic load allowances, distribution factors, and load effects than those determined theoretically, or specified in codes, resulting in improved bridge load ratings.

Despite the vast amount of literature that exists pertaining to this study, there were still gaps in the previous research. A key issue that has had little exposure is the use of field measurements in the Canadian-based code, CAN/CSA-S6-00 (CSA 2000). Although the study by Au et al. (2005) most closely resembles the work carried out in this research program, in that it measured site specific parameters for use in CAN/CSA-S6-00 (CSA 2000), there were some clear differences that can also be noted in many of the other reported studies. The first clear difference is that only one of the studies discussed above quantified a bridge rating in terms of a reliability index (Ghosn

1986); rather, bridge rating values were used, which do not describe the risk associated with the passage of a particular type of truck. Secondly, the Au et al. (2005) study, along with most of the other reported studies, determined bending moments from a "calibration" to known truck weights, rather than determined them from conventional methods. The studies by Cheung and Li (2002), Chajes et al. (1997, 2000), and Reid et al. (1996), were the exceptions. None of the reported studies determined shear forces induced in the girders by vehicle loading. Finally, there appears to be little in the published literature pertaining to test bridge girders that were constructed of reinforced concrete; rather, steel girders with concrete deck slabs were typically chosen.

CHAPTER 3 EXPERIMENTAL PROGRAM

3.1 INTRODUCTION

Details of the bridge and bridge site considered in the research program are presented in this chapter, as well as a description of the instrumentation and testing procedures included in the experimental portion of the program. Included with the bridge and bridge site details are the traffic conditions at the site and the material properties and dimensions of the bridge girders. The experimental portion of the research program was carried out to obtain site-specific data to generate a better estimate of the in-situ live load capacity factor and reliability index, relative to those obtained from the as-designed analysis, using values specified on the design drawings and in CAN/CSA-S6-00 (CSA 2000).

3.2 BRIDGE DESCRIPTION

3.2.1 Bridge Location and Use

The Red Deer River Bridge provides a crossing over the Red Deer River on Provincial Highway #9, approximately one kilometre south of the town of Hudson Bay, located in north-eastern Saskatchewan. The highway and bridge carry two lanes of traffic, travelling in opposite directions. A Saskatchewan Highways and Transportation weigh scale located north of the bridge is used to

record the gross vehicle weight and axle weights of trucks travelling along the route, providing a means for controlling loading on the bridge. The speed limit over the Red Deer River Bridge is 100 km/hr.

Weyerhaeuser Canada operates a timber mill south of the town, near the bridge, which manufactures oriented strand board. Therefore, large quantities of logs are hauled across the bridge for processing in the mill. Due to the large quantities hauled by Weyerhaeuser, the company holds a bulk haul permit, allowing them to carry loads higher than those typically allowed on such a corridor. Weyerhaeuser is part of the Heavy Haul Agreement with Saskatchewan Highways and Transportation (Sparks 2005), which regulates the bulk haul permit system, provided that 50% of the profits earned on the additional loading are shared with Saskatchewan Highways and Transportation.

3.2.2 Bridge Description

The Red Deer River Bridge, shown in Fig. 3.1, was constructed in 1956, using conventional steel reinforced concrete. The end spans are 30.92 m in length, while the middle span is 38.66 m in length. The deck is supported by three varying-height, continuous girders. The girders and deck were constructed integrally; therefore, the girders were considered to act as T-beams in strength evaluations, incorporating an "effective" portion of the deck, as outlined in the CHBDC (CSA 2000). The bridge is symmetrical about a longitudinal center-line, and is also symmetrical about the lateral line through the mid-span of the bridge. The bridge was not designed to be skewed in any direction; it is approximately level along the entire length, and is roughly perpendicular to the embankments on both sides of the river. Connecting the three girders are a number of concrete diaphragms. The diaphragms are located at the piers and abutments, as well as at the halfway and quarter points of the girder lengths. The diaphragms increase overall superstructure stiffness and assist in distributing live load laterally between the girders.

Figure 3.1. The Red Deer River Bridge.

A typical girder cross-section is shown in Fig. 3.2. There is both tensile and compressive principal steel reinforcement to resist flexural action, and stirrups are provided to resist shear forces. The girders were strengthened in 1988 using external steel bars, which were attached with bolted brackets to the bottom faces of the girders in the positive bending moment regions of all three spans. A photograph of the external steel bars with brackets and end bolts is shown in Fig. 3.3. The external bars were each pre-tensioned to a force of 25 kN, essentially to keep slack out of the bars, and ensure that they were fully effective in contributing to the resistance of the composite section. The external bars are conventional No. 30 steel reinforcing bars. Fig. 3.4, shows the bridge girders in elevation view, displaying the general dimensions, and location of the external steel bars (DHT 1956).

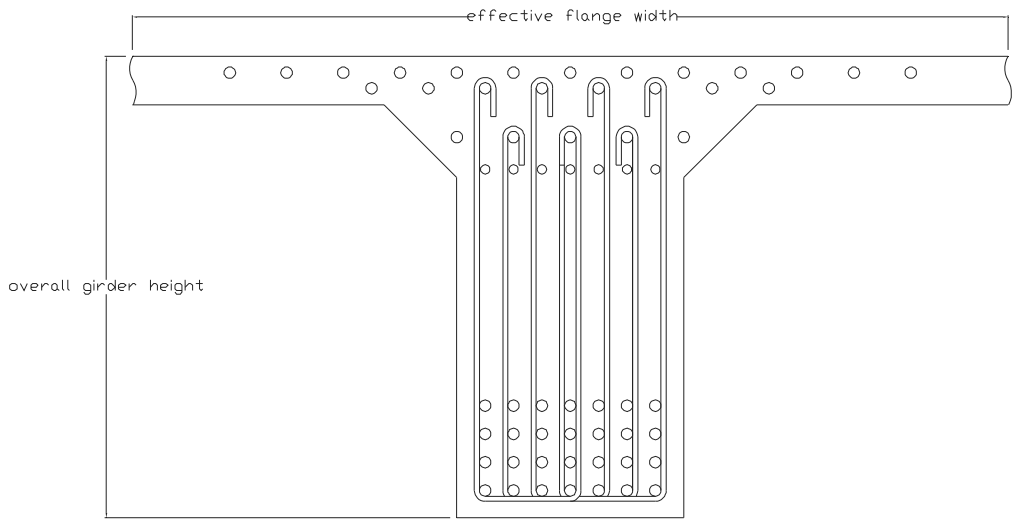

Figure 3.2. Typical cross-section of a bridge girder.

Figure 3.3. Ends of external steel reinforcing bars.

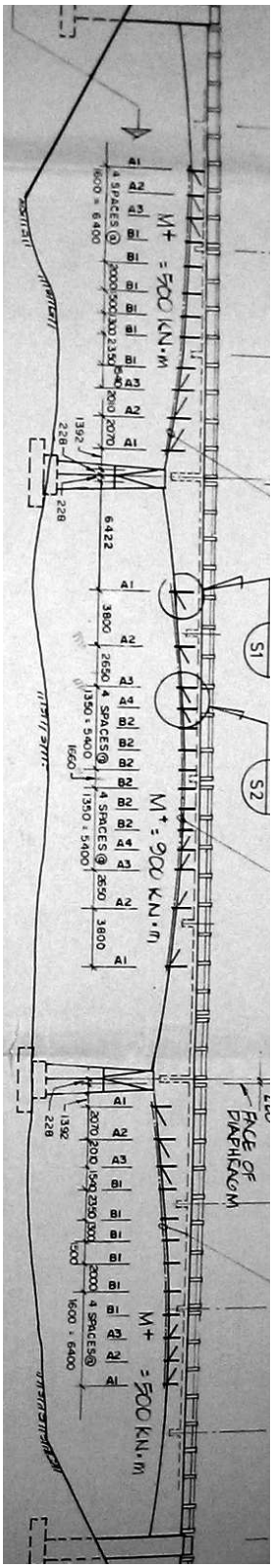

Figure 3.4. Elevation of Red Deer River Bridge (Reid Crowther and Partners Ltd. 1989).

As illustrated in Fig. 3.4, the girder depth varies non-linearly along the length of the girders. Only selected critical locations, along with those at which instrumentation was installed, were considered for analysis. The critical locations considered were at the piers, where girder depth, negative bending moments, and shear are the greatest, and at the midspans of each span, where the depth of the girders is lowest, and the positive bending is greatest. Five instrumented locations on the middle span of each girder were also analysed.

The cross-sectional details at the selected locations are summarized in Appendix A. A typical girder cross-section with dimensions is shown in Fig. A.1. Dimensions shown as numerical values on Fig. A.1 remain constant for all cross-sections, while those shown as variables change with location; values for these variable dimensions can be found in Table A.1 for the selected girder locations.

Further possible strengthening of the Red Deer River Bridge girders to accommodate possible increases in loading requested by the logging industry had been proposed at the time of writing. Two different strengthening alternatives were initially proposed (Earth Tech 2002): steel plates attached to the bottom faces of the girders in the positive bending moment regions, or fibre-reinforced polymer (FRP) sheets applied to the same areas. According to the design report (Earth Tech 2002), the strengthened bridge girders would enable the allowable loading on the bridge to be increased from 62.5 t to 110 t for permit holders. In the summer of 2006, SHT opted to strengthen the girders with the steel-plate option.

3.2.3 Bridge Materials

Estimates of material properties required for girder evaluation were obtained from various sources. When possible, information from design

documents was used; however, in other cases, the necessary values were inferred from published literature or CAN/CSA-S6-00 (CSA 2000).

As the yield strength of the internal steel reinforcing bars was not specified in the original design (DHT 1956), an assumed yield strength of 275 MPa was adopted in accordance with the guidelines provided in CAN/CSA-S6-00 (CSA 2000) for bridges constructed between 1956 and 1978. The yield strength assumption is also consistent with the allowable stress values used in the report for the proposed girder strengthening (Earth Tech 2002). The external steel reinforcing bars added in 1988 were specified in the design drawings (Reid Crowther and Partners Ltd. 1989) as being Grade 60, which have a nominal yield strength of 60 ksi, or 414 MPa.

Both the internal and external steel bars were assumed to have a modulus of elasticity of 200000 MPa. Hooke's Law relates stress and modulus of elasticity to strain:

$$\sigma = E\varepsilon \leq \sigma_y \qquad [3.1]$$

where σ is stress, E is modulus of elasticity, and ε is strain. Considering Hooke's Law, the yield strain of the internal steel reinforcing bars was taken as 0.00138, and the yield strain of the external steel reinforcing bars was taken as 0.00207. In-situ estimates of actual steel properties are discussed in Section 4.2.5.1.

The ultimate compressive strength of the concrete was specified on the design drawings as 3000 psi, or 20.7 MPa (DHT 1956). As specified in CAN/CSA-S6-00 (CSA 2000), an empirical formula to be used for estimating the corresponding concrete modulus of elasticity as follows:

$$E_c = \left(3300\sqrt{f_c'} + 6900\right)\left(\frac{\gamma_c}{2300}\right)^{\frac{3}{2}} \qquad [3.2]$$

where f'_c is the ultimate compressive strength of the concrete in MPa, and γ_c is the concrete density in kg/m^3, generally assumed to be 2350 kg/m^3. Using Eq. 3.2, the modulus of elasticity of the concrete was determined to be 22630 MPa based on the specified concrete strength. In-situ estimates for the actual concrete strength are discussed in Section 3.3.3.

3.3 DATA COLLECTION

3.3.1 Instrumentation and Data Acquisition

The main portion of the experimental program in the study comprised the monitoring of load effects on the Red Deer River Bridge for use in determining the in-situ response characteristics. The purpose of the on-site data collection program was to obtain better estimates of different variables relating to the structural reliability of the bridge.

The primary source of data from the bridge monitoring came from strain gauges installed on the bridge girders. The strain gauges were installed on the center spans of all three girders, as shown in Fig. 3.6, in August 2004. In total, 45 strain gauges were used, with fifteen strain gauges placed on each girder, arranged in five vertical lines, each of which contained three gauges. The strain gauges were installed at the same locations along the lengths of each of the three girders. Vertical lines of three strain gauges were used to provide a reliable indication of the strain distribution over the girder, which, in turn, also allowed girder curvatures to be estimated. The vertical arrangement of gauges is shown in Fig. 3.5.

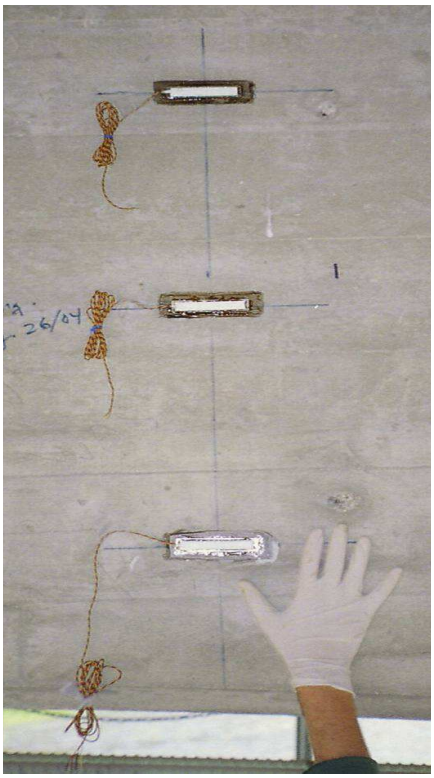

Figure 3.5. Typical strain gauges arranged in a vertical line on the girder webs.

The locations of the vertical lines of strain gauges were chosen to represent different conditions along the lengths of the girders. The locations of the strain gauges with respect to the north abutment and the bottom face of the girder section are shown in Table 3.1. Fig. 3.6 shows the strain gauge arrangement graphically in profile and plan views. The strain gauges were placed on the inside faces of girders to prevent exposure to the elements, as well as to reduce the potential for vandalism, as can be seen in Figure 3.6. The five vertical lines of three strain gauges were distributed along the middle spans of each girder, arranged in a symmetric manner about the central diaphragm; the middle vertical line of strain gauges, though, was shifted 1.43 m south of the diaphragm.

For convenience, the vertical lines of gauges were numbered using a two number designation. The first number in the designation referred to the girder

number. The girders were numbered one through three, where girder one was on the east side of the bridge, girder two was in the center, and girder three was the west-most girder. The second number in the designation referred to the vertical line of gauges. The vertical lines of gauges along each girder were then numbered consecutively from one through five, in the north to south direction.

Ideally, the group of three strain gauges would have been uniformly distributed over the full height of the girder in order to maximize the precision of the strain distribution estimates. However, due to physical limitations during installation, only certain portions of the girders could be safely accessed, restricting possible vertical locations of the gauges at some girder sections. In some cases, all three gauges were below the neutral axis, and significant extrapolation was necessary to define the strain distribution over the entire girder height.

Table 3.1. Strain gauge locations.

		Distance from bottom face of girder (mm)		
Strain gauges	**Distance from north pier (m)**	**Lower strain gauge**	**Middle strain gauge**	**Upper strain gauge**
north end	2.73	292	737	1181
north second	11.89	127	483	838
middle	20.76	102	381	660
south second	26.79	127	483	838
south end	35.95	292	737	1181

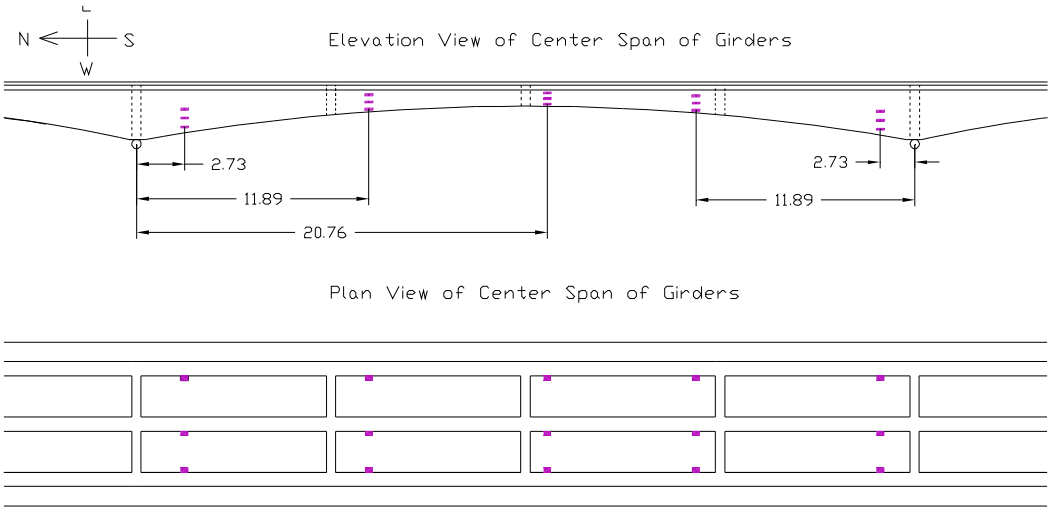

Figure 3.6. Strain gauge locations on the center span of the girders.

Prior to strain gauge installation, the concrete surface was prepared by removing dust and dirt with a wire brush, and was lightly sanded. The strain gauges were applied to the bridge girders using a quick-drying epoxy provided with the strain gauges, which fully covered the lead wires as well as the gauges, to protect against exposure to the elements. The lead wires from the strain gauges were soldered to shielded wires which were run to the north abutment. The wires at the north abutment were coiled into locked electrical boxes to protect them from exposure and vandalism. The arrangement allows a user to collect data conveniently by facilitating a connection to the data acquisition system and a notebook computer, since the wires plug directly into the data acquisition system. The strain gauges and wiring were installed by a crew of four persons over a period of three eight-hour days in August 2004. A bridge inspection truck equipped with a boom was used to access the underside of the bridge, as shown in Fig. 3.7.

Figure 3.7. Bridge inspection truck used to install strain gauges.

The strain gauges selected for use in this study were model WFLM-60, waterproof gauges intended for use with concrete, manufactured by the Tokyo Sokki Kenkyujo Company, of Tokyo, Japan. Although the strain gauge was 60 mm long and 0.7 mm wide, the backing was 90 mm in length, and 18 mm in width. The long gauge length is particularly useful with concrete, since it effectively averages the strain over the gauge length, thereby attenuating the influence of highly localized strains at the location of a small crack in the concrete. The strain gauges were a 3-wire system, manufactured with the lead wires in place, featuring a resistance of 120 Ω. The strain gauge is shown in Fig. 3.8, with the actual strain gauge shown in black, and the backing shown in the lighter grey.

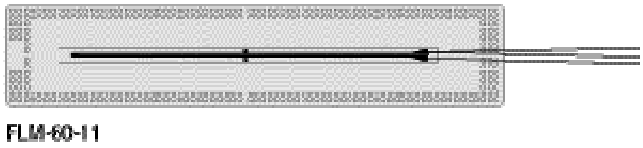

Figure 3.8. WFLM-60 Strain gauge used at Red Deer River Bridge (taken from Tokyo Sokki Kenkyujo Company 2006).

Strain gauge data was collected and stored electronically using the data acquisition system and notebook computer arrangement shown in Fig. 3.9. The data acquisition system consisted of a model SCXI-1001 chassis, containing twelve combination model SCXI-1121 isolation amplifiers and model SCXI-1321 connector modules, all manufactured by National Instruments, of Austin, Texas. As each combination module contained four channels, a total of 48 separate instruments could be read simultaneously. However, since additional instrumentation was also being monitored for other purposes, the strain gauges were divided into two arrangements which were monitored separately, denoted as east and west arrangements in Table 3.2. Relating the data from the two arrangements was achieved by using one reference set of strain gauges (2-2), which was included in both arrangements.

Figure 3.9. Data acquisition system and notebook computer.

Table 3.2: Arrangements of strain gauge groups for simultaneous monitoring.

Strain Gauge Locations		
Girder	West Arrangement	East Arrangement
1		1-1
		1-2
		1-3
		1-4
		1-5
2		2-1
	2-2	2-2
		2-3
	2-4	
	2-5	
3	3-1	
	3-2	
	3-3	
	3-4	
	3-5	

The acquisition of data was controlled using Labview 7 software (National Instruments Corporation 2003). Strain readings were obtained at a sampling rate of 3000 Hz, and stored electronically. A reduction in the influence of random measurement noise was achieved by subdividing data into packets of 100 consecutive readings, each of which were averaged, resulting in a condensed strain time-history with an effective sampling rate of 30 Hz that was used in subsequent evaluation. However, as the fundamental natural frequency of the Red Deer River Bridge was approximately 2.5 Hz, the effective sampling rate of 30 Hz still met the criteria proposed by Kim and Nowak (1997) that the sampling frequency should be 10 to 20 times the dominant frequency of the measured process.

3.3.2 Loading

3.3.2.1 Overview

Data collection was carried out at the Red Deer River Bridge over a two day period, on September 29 and 30, 2005. Two types of loading were carried out at the bridge: controlled loading and ambient loading.

3.3.2.2 Controlled Loading

Controlled loading involved the use of a truck of known weight and dimensions, travelling over the test bridge in predetermined configurations, at known speeds. The test truck used in controlled loading was a five-axle gravel truck provided by E.G. Services of Hudson Bay, Saskatchewan. A photo of the test truck is shown in Fig. 3.10. The truck was weighed at a nearby Saskatchewan Highways and Transportation scale to determine the gross weight (51660 kg) and the axle weights, described in Table 3.3. In this table, the axles distances are to the center of the axle group. The axle width was 2.6 m. This truck was used throughout the controlled loading tests, and was approximately representative of typical vehicle loading on the bridge.

Figure 3.10. Test truck for controlled loading.

Table 3.3. Test truck axle weights and dimensions.

Axle group	Number of axles	Weight (kg)	Distance from steer axle (m)	Inter-axle spacing (m)
Steer	1	4800	0	N/A
Drive	2	20490	6.23	1.64
Rear	2	26370	15.42	1.64

For the purposes of this study, the controlled loading was used to investigate the dynamic load allowance, which is discussed in Section 4.3.7. The dynamic load allowance can be determined using controlled loading by comparing the strains induced by static or pseudo-static loads to those induced by dynamic loads for the same loading configuration. In pseudo-static loading, the test truck was driven across the bridge at a crawl speed of between 5 and 10 kph, as controlled by an experienced truck driver. For the dynamic loading, the truck was driven across the bridge under typical operating speeds, which, in the case of the Red Deer River Bridge, was between 80 and 90 kph, based on the judgement of the truck driver. The test truck was alternately driven north and south across the bridge under pseudo-static loading or dynamic loading, using both the east and west lanes, to provide for all possible loading conditions. A summary of the controlled truck passes under static and dynamic loading is presented in Table 3.4.

Table 3.4. Controlled Loading Summary.

Direction of travel	Lane	Strain gauge arrangement	Number of pseudo-static passes	Number of dynamic passes
Southbound	West	West	4	2
		East	2	2
	East	West	1	2
		East	2	2
Northbound	West	West	2	2
		East	2	3
	East	West	3	2
		East	2	2

In CAN/CSA-S6-00 (CSA 2000), the governing load case on a two-lane bridge, regardless of designed direction of travel, is defined as two trucks travelling side by side in the same direction, a load condition that could occur in an over-taking situation. For the bridge in this study, there was difficulty in actually testing for such a scenario, primarily for safety reasons. Thus, only one test truck was used, and the load effects comparable to the design over-taking condition were approximated by superimposing the results from the test vehicle travelling in each of the two lanes separately, as discussed in Section 4.3.6.

3.3.2.3 Ambient Loading

The other form of loading considered in this study was ambient loading. For this purpose, ambient loading referred to load applied to the bridge by the regular flow of uncontrolled traffic. However, only loaded trucks were considered, as the load effects of personal vehicles such as cars, pick-up trucks, motorcycles, and unloaded trucks were found to be minimal when compared with those caused by loaded truck traffic. The speed of the trucks was dictated by existing traffic conditions and, although thought to be at typical highway speeds, were not measured. An attempt was made to make the data

collection process as inconspicuous as possible, so as not to disrupt the traffic flow or speed.

A typical log truck used in the Red Deer River Bridge area is shown in Fig. 3.11. The gross weights of the loaded log trucks in the ambient testing were obtained from a nearby scale operated by Weyerhaeuser Canada, used to weigh all log truck traffic on the corridor. Table B.1 in Appendix B lists the tare and gross weights of all the Weyerhaeuser-operated trucks. The mean gross weight of the log trucks was determined to be 64710 kg, with a standard deviation of 5490 kg. Since the legal weight limit for the permit-holding log trucks was 62500 kg, the trucks were therefore generally overloaded, although the limited size of the sample population may not have been representative of typical traffic. However, an article in *Timber Harvesting* (Peterson 2001) reported that a Wisconsin study found similar results, with 78 log trucks out of 86 surveyed being overloaded, a trend that is generally thought to be common in the logging industry. In addition to log trucks, other large trucks configured with five to nine axles were also observed. No weights were available for these non-logging vehicles.

Figure 3.11. Weyerhaeuser-operated log truck at the Red Deer River Bridge.

Data were recorded for trucks travelling both northbound and southbound across the bridge. Unlike the controlled loading tests, all trucks in the ambient tests travelled in the proper (right-hand) lane corresponding to their direction of travel. In total, 99 ambient loading events were monitored, although only 28 of these ultimately provided useful data. The remaining 71 loading events were recorded for vehicles which did not generate sufficiently large strains to enable meaningful analyses.

Data collection was performed intermittently, generally starting shortly before a truck entered onto the bridge, and stopping shortly after a truck had exited the bridge. In some cases, there were other vehicles on the bridge simultaneously with the truck of interest, although the other vehicles were in all cases personal vehicles which likely produced negligible load effects.

3.3.3 Non-Destructive Evaluations

3.3.3.1 Overview

Non-destructive evaluation was used at the Red Deer River Bridge to obtain better estimates of the ultimate compressive strength of the concrete. Rebound hammer tests were carried out at a number of locations on the bridge deck and bridge abutments.

3.3.3.2 Rebound Hammer

The rebound hammer used in these tests, shown in Fig. 3.12, was manufactured by Soiltest Engineering Test Equipment, based in Chicago, Illinois. Rebound hammer tests are dependent upon the angle of inclination of the rebound hammer; in this study, all rebound hammer tests were performed by holding the instrument vertically, as the bridge deck was being tested. A hammer number was recorded, which corresponded to an approximate ultimate

compressive strength of concrete. Rebound hammer testing was done at five locations on the bridge deck: the north-east corner, the north-west corner, the south-east corner, the southwest corner, and approximately at the middle of the deck.

Figure 3.12. Rebound hammer used in non-destructive evaluations.

A calibrated graph provided by the rebound hammer manufacturer related the measured hammer number to the ultimate compressive concrete strength. However, the rebound hammer was also calibrated at the University of Saskatchewan following testing at the bridge site, using concrete cylinders which were fabricated in the laboratory. The 21 concrete cylinders which were tested were 150 mm (six inches) in length, and 75 mm (three inches) in diameter. The concrete cylinders were randomly made using four different concrete mixes, the only difference between them being the water content. The concrete cylinders were made from a mix containing 32.5 kg of coarse aggregate, 22.0 kg of fine aggregate, 8.0 kg of type 30 cement (high-early strength), and various amounts of water, ranging from 2.5 L to 2.9 L. Furthermore, some of the cylinders contained 50 mL of an air-entraining admixture. The cylinders were moist cured for 14 days in a calcium-chloride bath.

Calibrating the rebound hammer number to the ultimate compressive strength was done following the testing procedure outlined in ASTM Standard C805-02 (Standard Test Method for Rebound Number of Hardened Concrete) (ASTM 2002). Each concrete cylinder was loaded to a uniaxial stress of approximately 7 MPa in a material testing machine located in the laboratory, as shown in Fig. 3.13. Under the applied stress of 7 MPa, rebound hammer tests were carried out on the sides of the concrete cylinders. Ten rebound hammer tests were completed on each concrete cylinder, with locations chosen around the entire circumference. The mean value of the readings was taken as the rebound hammer number for that cylinder. Upon obtaining the rebound hammer number, each cylinder was loaded to failure to determine the ultimate compressive strength. A calibration curve was created to determine ultimate compressive strengths to use in the in-situ analysis.

Figure 3.13. Loading concrete test cylinder to failure.

The results of the rebound hammer calibration can be found in Appendix C, while Fig. 5.20 in Chapter 5 displays the rebound hammer number vs. ultimate compressive strength of concrete graphically.

CHAPTER 4 ANALYTICAL PROCEDURES

4.1 INTRODUCTION

This chapter presents the analytical methods used in evaluating the Red Deer River Bridge in the as-designed state, as well in its assessed in-situ condition. The variables and assumptions used in the analyses are presented; in addition, the equations and methods used in evaluating load effects and resistance in both flexure and shear are outlined. Procedures used in the determination of reliability are also presented.

4.2 AS-DESIGNED ANALYSIS

4.2.1 Overview

To provide a basis of comparison for the "in-situ" analyses carried out in this study, the bridge in question was first evaluated using the conventional methods outlined in CAN/CSA-S6-00 (CSA 2000). This "as-designed" analysis was based on the assumption of flexural behaviour in the girders, information provided on the engineering drawings and specifications, and on the methods provided in CAN/CSA-S6-00 (CSA 2000). As such, it is representative of the approach which would be used by practicing bridge engineers in the evaluation of an existing bridge in the absence of more specific information. For the

purposes of this comparison, only ultimate limit state conditions were assessed; fatigue and serviceability limit states were not explicitly considered.

There are two alternatives for evaluating bridges presented in CAN/CSA-S6-00 (CSA 2000): the load and resistance factor method and the mean load method. In both cases, the nominal load effects and resistance must be determined. Therefore, methods for defining the nominal load effects and resistances are first presented in the subsequent sections, followed by a description of the code evaluation methods.

4.2.2 Loading

4.2.2.1 Live Load

Logging trucks represent the governing vehicular loads for the bridge in question. Under a heavy haul agreement with Saskatchewan Highways and Transportation (Sparks 2005), a selected forestry company is permitted to use trucks with gross vehicle weights (GVW) of 62 500 kg (62.5 t), exceeding normal highway load regulations. The typical configuration for a 6-axle logging truck with a 62.5 t GVW and an axle width of 2.6 m is shown in Fig. 4.1. As shown, the 6-axle truck consists of three axle groups. Experience from across Canada suggests that there is generally good compliance with similar heavy haul permit programs, with few reported instances of significant overloading (CSA 2000).

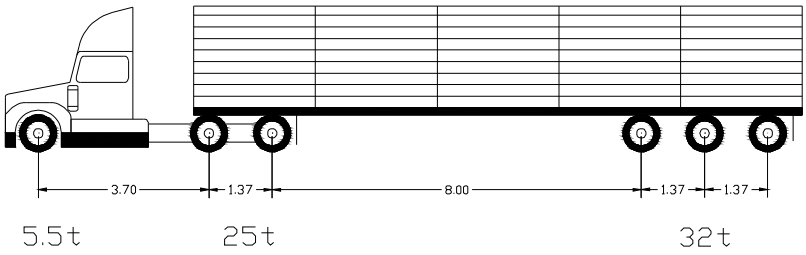

Figure 4.1. Schematic of a 6-axle 62.5 tonne logging truck.

To increase timber haul efficiency, a proposal has been made to increase the allowable GVW to 110 000 kg (110 t), the largest size truck currently used by the logging industry. As shown in Fig. 4.2, a possible configuration for this truck size is an 11-axle truck with four axle groups. The axle width remains 2.6 m.

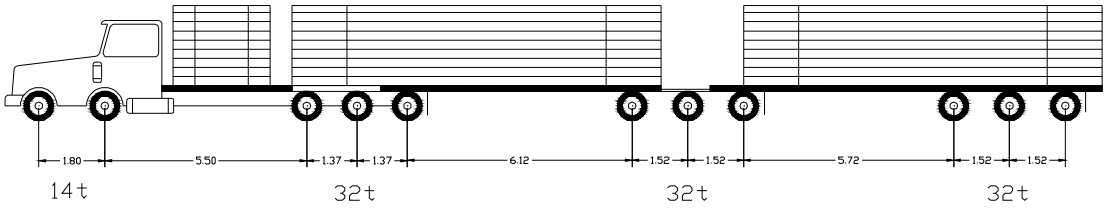

Figure 4.2. Schematic of an 11-axle 110 tonne log truck.

4.2.2.2 Dead Load

Dead load on the bridge is caused by the self-weight of the structure, which is primarily reinforced concrete and assumed to have a density of 2350 kg/m^3. Dead load was separated into three components, as specified in CAN/CSA-S6-00 (CSA 2000). The first type of dead load, D1, includes the weight of factory-produced components and cast-in-place components, excluding bridge decks; for the bridge in question, only the girders were included. The second form of dead loading, D2, includes the weight of cast-in-place decks. In this study, the integrally poured sidewalks and barriers were also included in this category. The third and final type of dead load, D3, is the weight of the asphalt wearing surface, which was assumed to be 90 mm thick for the evaluation.

Due to the varying girder depth, dead load was determined separately for ten sections of each span of the girders; therefore, each section length was 3.09 m in the end spans, and 3.87 m in the middle spans. The weight of the webs of the girders was the only portion of the dead load that varied from section to section. Dead load components D2 and D3 were constant over all

sections. For simplicity, the self weight of the diaphragms between girders were assumed to be spread uniformly over the length of the bridge.

4.2.2.3 Bridge Girder Model

Due to the complex geometry of the bridge girders in question, a two-dimensional finite element model was used to determine the load effects to be used in the as-designed analysis, as shown in Fig. 4.3. The model was created in the structural analysis software P-Frame^{TM} V6.21 (Softek 2006), and consisted of a three-span continuous beam, pin-connected (restraint in the horizontal and vertical directions, with no rotational restraint) at one end, with rollers (only vertical restraint) at the remaining supports. As such, the model allowed only bending moments and shear forces to develop; no axial force could be generated as horizontal reactions could not be sustained. The model was divided into segments of the same length as those used to generate the dead load estimates discussed in Section 4.2.2.2. Each girder segment was modelled using a beam-column element that had a constant cross-sectional area and, therefore, moment of inertia. The height of the girder in each section was taken as the average of the actual girder heights over the length of the section. Gross section properties were used, assuming concrete with a uniform modulus of elasticity of E=22,630 MPa.

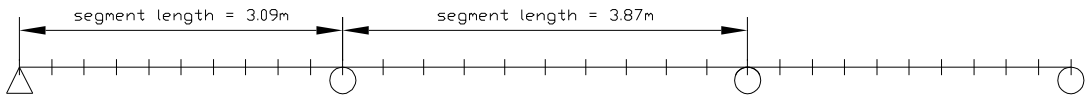

Figure 4.3. Bridge girder model used in the as-designed analyses.

4.2.2.4 Analysis of Load Effects Using the Girder Model

The bridge girder model was used to determine nominal bending moments and shear forces at the locations discussed in Section 3.3.1. For

each specified location, there were different truck locations which induced the governing load effect. Furthermore, the critical truck placement for one analysed location was typically different for the governing bending moment and governing shear. Influence lines were used to determine the truck locations which induced governing load effects, as summarized in Tables B2 and B3 in Appendix B.

Factored load effects were determined by applying the load factors discussed in Sections 4.2.4.1 through 4.2.4.4 to the nominal load effects obtained from the bridge girder model analysis. Factored dead load effects were determined using:

$$D_f = \alpha_i D_i \qquad [4.1]$$

where D_i is the *i*th nominal dead load effect and α_i is the *i*th dead load factor. Live load effects were determined in a similar manner; however, additional factors and allowances were also applied as follows to recognize various influences associated with the live load:

$$L_f = \alpha_L L(R_L)(1+I)(DF) \qquad [4.2]$$

where α_L is the live load factor, L is the nominal live load effect, R_L is the multiple lane loading factor (see Section 4.2.4.2), I is the dynamic load allowance (see Section 4.2.4.3), and DF is the distribution factor for the location under analysis (see Section 4.2.4.4).

4.2.3 Resistance

4.2.3.1 Effective Section Properties

Resistance to bending and shear was determined using methods specified in CAN/CSA-S6-00 (CSA 2000). The girders and deck of the bridge

were poured integrally and, thus, were assumed to behave as T-beams, including an effective top flange width from a portion of the bridge deck. The effective flange width was determined using the following formula:

$$\frac{B_e}{B} = 1 \qquad [4.3]$$

where B_e and B are the dimensions shown in Fig. 4.4 (taken from CSA 2000 Fig. 5.8.2.1), in which B_e is the effective flange width. As defined in CAN/CSA-S6-00 Eq. 4.3 is only valid for cases where:

$$\frac{L}{B} > 15 \qquad [4.4]$$

where L is the length of the positive or negative region of dead load moment for continuous spans. Here, the lengths of the various moment regions were determined from the dead load bending moment diagram generated from the bridge girder analysis model. For the internal girder, the total effective top flange width was taken to be 2.74 m, while for the external girders, it was taken to be 2.64 m.

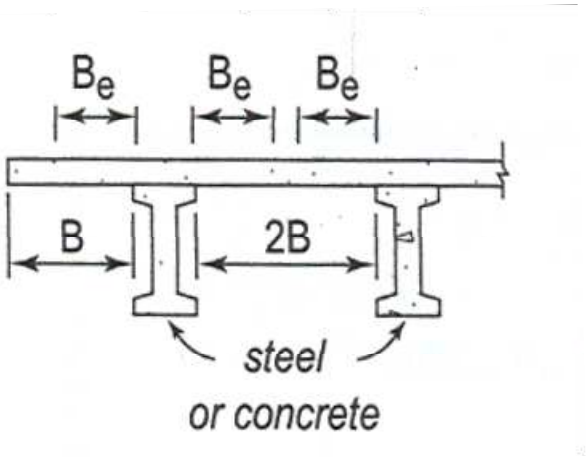

Figure 4.4. Effective flange width (taken from CSA 2000).

4.2.3.2 Bending Moment Resistance

Bending moment resistance was determined using the conventional methods in CAN/CSA-S6-00 (CSA 2000), although the bridge in question presented some unique challenges due to the external steel bar strengthening which was carried out in 1988. The external bars were installed after the bridge was initially constructed; therefore, initial strains already present in the girder as a result of self-weight were not experienced by the external bars. To compensate for this fact, the estimated strains in the external bars at ultimate conditions were reduced by the strain those bars would have undergone due to the bridge self weight. In the resistance calculations, a linear strain distribution, along with perfect strain compatibility, was assumed.

Strains due to self weight were estimated assuming linear behaviour, based on the transformed cross-section approach, which enables the application of linear flexural theory to composite sections by converting all materials present in the section to equivalent areas having a common modulus of elasticity. In this case, the modulus of elasticity of the reinforcing steel was transformed to that of the concrete by means of the modular ratio:

$$n = \frac{E_s}{E_c} \qquad [4.5]$$

(for which it was assumed that the steel modulus E_s=200,000MPa, and the concrete modulus E_c=22,630MPa). The following formula was used to determine the location of the neutral axis, assuming that the tensile region of the section was fully cracked and ineffective:

$$\bar{y}_t A_t = \sum_i y_i A_{ti} \qquad [4.6]$$

where $\bar{y}_t$ is the height to the centroid of the transformed section from some reference axis, A_t is the cross-sectional area of the transformed section, y_i is the height to the centroid of the *i*th component of the transformed section relative to the reference axis, and A_{ti} is the cross-sectional area of the *i*th component of the transformed section.

With the location of the neutral axis of the transformed cracked cross-section, the transformed cracked moment of inertia was determined using the parallel axis theorem:

$$I_t = \sum_{i_c} \left[I_{c_i} + A_{c_i} \left(y_{c_i} - \bar{y}_t \right)^2 \right] + \sum_{i_s} A_{ts_i} \left(y_{s_i} - \bar{y}_t \right)^2 \qquad [4.7]$$

where I_{ci} is the moment of inertia of the ith concrete section about its own centroidal axis, A_{ci} is the cross-sectional area of the ith concrete section, y_{ci} is the height to the centroid of ith concrete section, A_{tsi} is the transformed cross-sectional area of the ith layer of reinforcing steel, and y_{si} is the height to the ith layer of reinforcing steel. The moment of inertia of the steel about its own axis was neglected.

The normal stress profile due to self weight was determined using the flexure formula, given as:

$$\sigma = n\left(\frac{M_D y}{I_t} \right) \qquad [4.8]$$

where n is the modular ratio (which may be taken as 1.0 for concrete elements), σ is the stress at a distance "y" from the centroidal axis, M_D is the bending moment caused by the self weight. The required corresponding strains were then determined from Eq. 3.1.

At ultimate conditions, concrete compressive stresses are known to follow an approximately parabolic distribution over the compressive zone of a reinforced concrete flexural member. However, CAN/CSA-S6-00 permits concrete compressive stresses to be idealized by an equivalent uniform (Whitney) stress block, characterized by two parameters, α_1 and β_1, where:

$$\alpha_1 = 0.85 - 0.0015 f_c' \qquad [4.9]$$

$$\beta_1 = 0.97 - 0.0025 f_c' \qquad [4.10]$$

and f'_c is the ultimate compressive strength of the concrete. An ultimate concrete crushing strain of 0.0035 is also specified. The total height of the concrete stress block, a, is determined from the following relationship:

$$a = \beta_1 c \qquad [4.11]$$

where c is the depth to the neutral axis from the compressive face of the girder.

As the first step in the analysis of the flexural resistance, the neutral axis of the girder section at its ultimate limit state was located by balancing the net internal compressive and tensile forces in the section. There were two components of compressive forces which were considered in the girder sections: those in the concrete, and those in the compressive reinforcing steel. Similarly, tensile forces were provided by the tensile reinforcing steel and the external steel bars; concrete in the tensile zone was ignored. Since the girder sections for this bridge were composed of rectangular components, the compressive force in the concrete was determined using the following:

$$C_c = \phi_c \alpha_1 f_c' \sum_i b_i h_i \qquad [4.12]$$

where ϕ_c is the material resistance factor for concrete, discussed in Section 4.2.4.1, b_i is the width of the *i*th component of the concrete stress region, and h_i

is the height of the *i*th component of the concrete within the compressive stress block region. The force in the compression reinforcing steel, allowing for the concrete displaced by the bars, was determined by:

$$C_s = A_s'\left(\phi_s f'_s - \phi_c \alpha_1 f_c'\right) \qquad [4.13]$$

where A'_s is the total cross-sectional area of the compressive reinforcing steel, which varies among the different sections of the girders, and f_s is the stress in the compressive reinforcing steel. The material resistance factor for steel, ϕ_s, is discussed in Section 4.2.4.1.

The force in the tensile reinforcing steel is given by:

$$T_s = A_s \phi_s f_s \qquad [4.14]$$

while the force in the external steel bars is given by:

$$T_{se} = \phi_s \left(A_{se} f_{se} + n_e F_{ps}\right) \qquad [4.15]$$

where A_s is the total cross-sectional area of the internal tensile reinforcing steel, A_{se} is the total cross-sectional area of the external steel bars, n_e is the number of external steel bars, and F_{ps} is the initial (nominal) prestressing force in each external bar. However, as was discussed previously in this section, the strains, and therefore stresses, in the external steel had to be adjusted to account for initial self weight strains. Eq. 4.15 then becomes:

$$T_s = \phi_s \left[A_{se} E_{se} \left(\frac{f_{se}}{E_{se}} - \varepsilon_{sei} \right) + n_e F_{ps} \right] \qquad [4.16]$$

where ε_{sei} is the required adjustment for self weight effects. It should be noted that Eq. 4.16 is only valid if the stresses in the external bars remain in the elastic range, which was found to be true in this study.

For cases where the steel did not yield, the stress in the steel was determined from geometry, considering the linear strain distribution through the girders. For example, if the *i*th layer of the compressive steel reinforcement did not yield, the stress was determined by:

$$f_{si} = \varepsilon_{cu}\left(\frac{c - d'_{si}}{c}\right)E_s \qquad [4.17]$$

where ε_{cu} is the assumed crushing strain in the concrete (0.0035), and d_{si}' is the depth from the top face of the girder to the *i*th layer of compressive steel. Similarly, if the ith layer of the tensile steel reinforcement did not yield, the stress was determined by:

$$f_{si} = \varepsilon_{cu}\left(\frac{d_{si} - c}{c}\right)E_s \qquad [4.18]$$

where d_{si} is the depth from the top face of the girder to the *i*th layer of tensile steel.

The bending moment resistance of a section was determined by considering the internal moment within the section, formed by couples of the tensile and compressive force components. Considering bending moments taken about the neutral axis of the section, the bending moment resistance can be expressed as:

$$M_r = \sum_i C_{si} y'_{si} + \sum_i C_{ci} y_{ci} + \sum_i T_{si} y_{si} + T_{se} y_{ext} \qquad [4.19]$$

where C_{si} is the force in the ith layer of compressive steel reinforcing bars (given by Eq. 4.13), y'_{si} is the distance from the centroid of the ith layer of the compressive bar group to the neutral axis, C_{ci} is the compressive force in the ith component of the concrete (given by Eq. 4.12), y_{ci} is the distance from the centroid of the ith concrete component to the neutral axis, T_{si} is the force in the ith layer of tensile steel reinforcing bars (given by Eq. 4.14), y_{si} is the distance from the centroid of the ith layer of the tensile bar group to the neutral axis, T_{se} is the force in the external steel bars (given by Eq. 4.16), and y_{ext} is the distance from the centroid of the external steel bars to the neutral axis.

4.2.3.3 Shear Resistance

The shear resistance of a girder section was determined based on the methods outlined in CAN/CSA-S6-00 (CSA 2000), which are based on the compression field theory of shear analysis (Collins and Mitchell 1990, Vecchio and Collins 1986). In this approach, the total shear resistance of a steel reinforced concrete girder is taken to be the sum of the shear resistance of the concrete, V_c, and the shear resistance of the steel stirrups, V_s:

$$V_r = V_c + V_s \qquad [4.20]$$

where V_c is the given by the expression:

$$V_c = 2.5\beta\phi_c f_{cr} b_v d_v \qquad [4.21]$$

Here, f_{cr} is the cracking strength of the concrete, given by the following expression for normal-density concrete:

$$f_{cr} = 0.4\sqrt{f'_c} \qquad [4.22]$$

The variable b_v is the effective girder width within the effective shear depth, d_v, which was defined as the width of the web for the T-girder section in question. The effective shear depth was taken as the distance, measured perpendicular to the neutral axis, between the resultants of the tensile and compressive forces generated due to flexure. However, the effective shear depth must not be less than 90% of d, the effective depth from the extreme compression fibre in the concrete to the centroid of the tensile force. The factor β was taken from Table 4.1 (reproduced from CAN/CSA-S6-00 (CSA 2000)), and accounts for the shear resistance of cracked concrete. The variable β was determined on a trial and error basis, and is dependent upon other variables, as discussed in the following paragraphs.

The nominal shear stress, v, must be determined in order to use Table 4.1 to determine the value of β. The nominal shear stress is calculated by:

$$v = \frac{V_f - \phi_p V_p}{b_v d_v} \qquad [4.23]$$

where V_f is the factored shear force in the girder section, and ϕ_p and V_p are the prestress resistance factor and component of the effective prestressing forces acting to resist the applied shear, respectively. Conservatively, V_p was taken as zero for all sections analysed in the Red Deer River Bridge, even though some of the external prestressing bars were inclined and thus may have contributed to the shear resistance.

Table 4.1. Values for β and θ for sections with at least minimum transverse reinforcement (taken from CSA (2000)).

$\frac{v}{\phi_c f_c'}$		Longitudinal Strain, ε_x						
		≤ 0.0000	≤ 0.00025	≤ 0.0005	≤ 0.00075	≤ 0.0010	≤0.0015	≤ 0.0020
≤ 0.050	β	0.405	0.290	0.208	0.197	0.185	0.162	0.143
	θ	27.0°	28.5°	29.0°	33.0°	36.0°	41.0°	43.0°
≤ 0.075	β	0.405	0.250	0.205	0.194	0.179	0.158	0.137
	θ	27.0°	27.5°	30.0°	33.5°	36.0°	40.0°	42.0°
≤ 0.100	β	0.271	0.211	0.200	0.189	0.174	0.143	0.120
	θ	23.5°	26.5°	30.5°	34.0°	36.0°	38.0°	39.0°
≤ 0.125	β	0.216	0.208	0.197	0.181	0.167	0.133	0.112
	θ	23.5°	28.0°	31.5°	34.0°	36.0°	37.0°	38.0°
≤ 0.150	β	0.212	0.203	0.189	0.171	0.160	0.125	0.103
	θ	25.0°	29.0°	32.0°	34.0°	36.0°	36.5°	37.0°
≤ 0.200	β	0.203	0.194	0.174	0.151	0.131	0.100	0.083
	θ	27.5°	31.0°	33.0°	34.0°	34.5°	35.0°	36.0°
≤ 0.250	β	0.191	0.167	0.136	0.126	0.116	0.108	0.104
	θ	30.0°	32.0°	33.0°	34.0°	35.5°	38.5°	41.5°

The effective longitudinal strain in the section, ε_x, is computed from the following formula:

$$\varepsilon_x = \frac{0.5N_f + 0.5\left(V_f - \phi_p V_p\right)\cot\theta + \frac{M_f}{d_v} - A_{ps} f_{po}}{E_s A_s + E_p A_{ps}} \leq 0.002 \qquad [4.24]$$

where N_f is the factored axial load acting normal to the cross-section and occurring simultaneously with V_f; in the as-designed analysis N_f was taken as zero, in accordance with the assumption of pure flexural behaviour in the girders. The variable M_f is the factored bending moment in the section occurring simultaneously with V_f. The angle of inclination of the principal diagonal compressive stresses to the longitudinal axis of the member, θ, is determined iteratively from Table 4.1, along with β.

The shear resistance of the steel stirrups, V_s, is determined from Eq. 4.28:

$$V_s = \frac{\phi_s f_y A_v d_v \cot\theta}{s} \qquad [4.25]$$

where s is the spacing of the steel stirrups parallel to the longitudinal axis of the girder, and A_v is the cross-sectional area of shear reinforcement perpendicular to the axis of the girder, within the spacing distance, s.

4.2.4 Load and Resistance Factor Evaluation

A commonly used method of designing and evaluating bridges is the load and resistance factor method, in which partial safety factors are applied to loading and resistance to account for the uncertainty present in both. Factors applied to loading typically increase the loading effect from its nominal value, and as such, are greater than 1.0. However, other factors may reduce the conservatism of the method by featuring load factors which are less than 1.0; for example, certain circumstances have a low probability of occurrence. Factors applied to resistance are less 1.0, making estimates of resistance more conservative. The benefits of the load and resistance factor method are that it is quick, efficient, safe, and economical (Akgul and Frangopol 2003).

4.2.4.1 Load and Resistance Factors

Partial safety factors assigned to resistance take the form of material resistance factors, accounting for variability in material properties and workmanship. Material resistance factors were applied to the two materials present in the bridge girders: concrete and steel. CAN/CSA-S6-00 (CSA 2000) specifies that the concrete resistance factor, ϕ_c be taken as 0.75, while the reinforcing steel resistance factor, ϕ_s be taken as 0.9. The larger factor applied

to steel reflects the fact that there is typically better quality control in steel production.

The selection of load factors is dependent upon the target reliability index of the structural element, which represents the minimum acceptable level of safety. A detailed discussion of the reliability index can be found in Section 4.2.5.3. The target reliability index itself is a function of three factors specified in the CAN/CSA-S6-00 (CSA 2000): system behaviour, element behaviour, and inspection level, each of which contains three levels. Table 4.2 (reproduced from CAN/CSA-S6-00 (CSA 2000)) summarizes the selection procedure for the appropriate target reliability index.

System behaviour considers the effects of element failure on failure of the overall structural system; levels S1 through S3 may be applied as follows:

- S1 is applied to systems where element failure leads to total collapse;
- S2 is applied to systems where element failure probably will not lead to total collapse; and
- S3 is applied to systems where element failure leads to local failure only.

For the bridge in question, level S2 was selected, as a single girder failure typically does not lead to complete structural failure in multigirder continuous systems. Element behaviour considers the manner in which individual elements fail; similar to system behaviour, levels E1 through E3 may be applied, as follows:

- E1 is applied to elements where sudden loss of capacity can occur with little or no warning;
- E2 is applied to elements where sudden failure can occur, but post-failure capacity will be retained; and
- E3 is applied to elements where failure will occur gradually, with warning of the probable failure.

Level E2 was used in considering shear, where girder failure can occur suddenly, while level E3 was used in considering bending, where it was assumed that girder failure will occur gradually, as the steel should yield prior to crushing of the concrete.

Selection of the inspection level was based on the results of a bridge inspection, which must be carried out prior to the evaluation; levels INSP 1 through INSP 3 may be applied, as follows:

- INSP 1 is applied to components which are not inspectable;
- INSP 2 is applied to components where the inspection was carried out to the satisfaction of the evaluator and the results are recorded and readily available; and
- INSP 3 is applied where inspection of critical components has been carried out by the evaluator and the final evaluation calculations account for all information obtained during this inspection.

The Red Deer River Bridge was inspected by a private consultant prior to the proposed strengthening, and was assigned level INSP2 (EarthTech 2002), indicating a satisfactory inspection. Based on Table 4.2 the resulting target reliability indices for the bridge in question were 3.0 for bending moment and 3.25 for shear.

Table 4.2. Target reliability index for PB (Bulk Permit) traffic (reproduced from CAN/CSA-S6-00 (CSA 2000)).

		Inspection Level		
System Behaviour	**Element Behaviour**	**INSP1**	**INSP2**	**INSP3**
S1	E1	4.00	3.75	3.75
	E2	3.75	3.50	3.25
	E3	3.50	3.25	3.00
S2	E1	3.75	3.50	3.50
	E2	3.50	**3.25**	3.00
	E3	3.25	**3.00**	2.75
S3	E1	3.50	3.25	3.25
	E2	3.25	3.00	2.75
	E3	3.00	2.75	2.50

The dead load factors based on the target reliability indices are summarized in Table 4.3. The magnitudes of factors used in load and resistance factor evaluations reflect the degree of uncertainty present in the corresponding variable. For example, the factors for dead load D3 were the largest, indicating considerable uncertainty in loading caused by the wearing surface. Dead load categories (D1, D2 and D3) are described in Section 4.2.2.2.

Table 4.3. Dead load factors.

Element	**Factor**	**Flexure (β=3.00)**	**Shear (β=3.25)**
Girders	α_{D1}	1.07	1.08
Deck, Sidewalk, Barriers	α_{D2}	1.14	1.16
Asphalt Surface	α_{D3}	1.35	1.4

The live load factor, α_L, is also dependent on the target reliability index. Furthermore, it is a function of analysis type and span length (CSA 2000). In the present case, it was deemed that a "simple" analysis could be carried out, and that all three spans of the Red Deer River Bridge could be classified in the

"other spans" category due to their lengths, which are longer than the "short spans" specified in CAN/CSA-S6-00 (CSA 2000). Different live load factors are also applied for different types of live loading, such as for various types of permit vehicles. In Saskatchewan, special live load factors which are not explicitly specified in CAN/CSA-S6-00 (CSA 2000) are typically applied for log trucks. These "timber haul factors," which are dependent upon the target reliability indices, were taken as 1.37 for flexure, and 1.43 for shear (EarthTech 2002).

4.2.4.2 Multiple Lane Loading Factor

In accordance with the bridge code provisions, the modification factor for multiple lane loading, R_L , was used to account for the probability of having more than one design vehicle travelling across a bridge simultaneously, side by side. The bridge in question consists of two design lanes, which, regardless of the intended travel direction of the design, may be considered to be carrying traffic in the same direction for evaluation purposes, due to the possibility of passing scenarios. In addition, the modification factor for multiple lane loading is a function of highway class and the number of loaded design lanes. Based on the criteria provided in CAN/CSA-S6-00 (CSA 2000), the Red Deer River Bridge is classified as class C, for bridges where the average daily traffic (ADT) per lane is between 100 and 1000 vehicles, and the average daily truck traffic (ADTT) per lane is between 50 and 250 trucks. As a result, the multiple lane loading factor was determined to be 0.85, reflecting a reduced probability of having two fully loaded design vehicles side by side (a multiple lane loading factor of 1.0 would suggest a full probability of having all lanes loaded simultaneously, which is typically applied only to single lane bridges).

4.2.4.3 Dynamic Load Allowance

The dynamic load allowance, I (see Eq. 2.2), is a factor which accounts for additional load effects created by vehicle dynamic effects, caused by bumps in the riding surface or expansion joints which cause impact forces, dynamic variation in axle loads due to roughness in the riding surface, and dynamic response of the longitudinal bridge components due to moving loads (CSA 2000).

The dynamic load allowance is given as a fraction of the static truck load, and thus is typically less than 1.0. In the as-designed analysis, the dynamic load allowance was taken as 0.25, which is specified in CAN/CSA-S6-00 for trucks with six or more axles. Furthermore, the dynamic load allowance is multiplied by another factor for permit vehicles, dependent upon the speed at which they typically cross the bridge. For permit vehicles travelling at speeds typically greater than 40 km/h, as on the Red Deer River Bridge, the dynamic load allowance is multiplied by 1.0, thus remaining unchanged from the value given above.

4.2.4.4 Distribution Factors

The total live load effect per design lane (denoted as M_T for bending moment and V_T for shear) at a given longitudinal location, as determined from the structural analysis of the bridge, described in Section 4.2.2.4, must be distributed laterally to the various girders in differing proportions, depending on a number of factors relating to the bridge configuration and loading characteristics. The procedures described in CAN/CSA-S6-00 (CSA 2000) to estimate lateral distribution factors for bending moment and shear are described separately below.

For bending moments, the average bending moment per girder, M_{gavg} (if the total load effect were evenly distributed among all girders) at a given section is first determined from the total design lane moments using the expression:

$$M_{gavg} = \frac{nM_T R_L}{N} \qquad [4.26]$$

where n is the number of design lanes (n=2 for the bridge in question), R_L is the multiple lane loading factor discussed in Section 4.2.4.2, and N is the total number of girders (here, N=3). This average load effect is then modified to obtain the design bending moment, M_g, for a specified girder according to the expression:

$$M_g = F_m M_{gavg} \qquad [4.27]$$

in which F_m is an amplification factor to account for the transverse variation in the bending moment intensity between the girders sharing the load effect. The amplification factor F_m is dependent on the configuration of the girders, the location of the section under consideration, and the sense of the bending moment, as follows:

$$F_m = \frac{SN}{F\left(1 + \frac{\mu C_f}{100}\right)} \geq 1.05 \qquad [4.28]$$

where S is the centre-to-centre girder spacing (S=2.74 m for the bridge in question),

$$\mu = \frac{W_e - 3.3}{0.6} \leq 1.0 \qquad [4.29]$$

in which the design lane width, W_e (m) is found from

$$W_e = \frac{W_c}{n} \qquad [4.30]$$

and W_c is the total deck width (W_c=8.02m for the bridge in question). Finally, the width parameter F (m), and the correction factor C_f (%), are determined based on the type of bridge deck, the span length L, the class of highway, the number of design lanes, as well as the location of the girder and bending moment in question. For example, expressions for the parameters F and C_f for slab-on-girder bridges are provided in Table 4.4, which summarizes all input parameters that are needed for the determination of distribution factors. Depending upon the continuity of the girder design, the span length is modified to account for positive and negative bending moment regions. The modified span length, L_m, is used in determining the parameters F and C_f.

Table 4.4. Variables for determination of lateral distribution factors (reproduced in part from CSA 2000).

Girder location	Type of moment	Highway class	Design lanes	Actual span length (m)	Modification of span length	F (m)	C_f(%)
external	positive, exterior span	C	2	30.92	80% of 30.92	6.4-3/L_m	5-15/L_m
external	positive interior, span	C	2	38.66	60% of 38.66	6.4-3/L_m	5-15/L_m
external	negative, support region	C	2	30.92, 38.66	25% of (30.92+38.66)	6.4-3/L_m	5-15/L_m
internal	positive, exterior span	C	2	30.92	80% of 30.92	7.2-14/L_m	5-15/L_m
internal	positive, interior span	C	2	38.66	60% of 38.66	7.2-14/L_m	5-15/L_m
internal	negative, support region	C	2	30.92, 38.66	25% of (30.92+38.66)	7.2-14/L_m	5-15/L_m

The distribution factors for bending moments for ultimate limit states can be described by the expression:

$$DF = \frac{M_g}{M_T} \qquad [4.31]$$

where M_g and M_T are determined as previously described. The resulting distribution factors for different bending moments and locations on the bridge in question are summarized in Table 4.5. The distribution factors are less than 1.0, indicating that no single girder can carry the entire live load.

Table 4.5. Lateral distribution factors for bending moment.

Girder location	Type of moment	DF
external	positive, exterior span	0.712
external	positive, interior span	0.713
external	negative, support region	0.719
internal	positive, exterior span	0.674
internal	positive, interior span	0.678
internal	negative, support region	0.700

Considering shear effects, the average shear per girder V_{gavg} (if the total load effect were distributed evenly across all girders) at a given section is determined in a manner similar to that of bending moments, using the expression:

$$V_{gavg} = \frac{nV_T R_L}{N} \qquad [4.32]$$

in which all the variables are the same as those described in Eq. 4.26. The average shear per girder is further modified by an amplification factor F_v:

$$V_g = F_V V_{gavg} \quad [4.33]$$

in which the amplification factor F_v, used to account for transverse variation in shear intensity between the girders, is dependent upon similar factors as F_m, which is used to modify the average bending moments:

$$F_V = \frac{SN}{F} \quad [4.34]$$

where S and N are the same variables used in the determination of F_m, and F is a width dimension to characterize the load distribution, and is dependent upon bridge type, number of design lanes, and highway class. For the bridge in question, F was taken as 6.10 as specified in Table A5.7.1.2.1 in CAN/CSA-S6-00 (CSA 2000).

The distribution factors for shear for at the ultimate limit state can be described by the expression:

$$DF = \frac{V_g}{V_T} \quad [4.35]$$

The resulting distribution factor for shear was determined to be 0.764 throughout, for both the interior and exterior girders.

4.2.4.5 Live Load Capacity Factor

The live load capacity factor, F, provides a means to determine the amount of live load that may be applied to a bridge. The live load capacity factor is typically the criteria by which allowable loading on a bridge is decided, and must have a value greater than 1.0 for the loading in question. Under ultimate limit states, the live load capacity factor is determined by:

$$F = \frac{U\phi R - \sum \alpha_D D - \sum \alpha_A A}{\alpha_L L(1+I)} \qquad [4.36]$$

where U is a resistance adjustment factor dependent on the construction material of the bridge and the load effect being considered; the values used in this study were taken from CAN/CSA-S6-00 (CSA 2000) and are summarized in Table 4.6. For bending moments in a reinforced concrete bridge, U depends on the ratio between the reinforcing ratio, ρ, and the balanced reinforcing ratio, ρ_b, where

$$\rho = \frac{A_s}{bd} \qquad [4.37]$$

and A_s is the cross-sectional area of the tensile reinforcing steel, b is the width of the girder, and d is the depth to the tensile bars. The balanced reinforcing ratio ρ_b occurs for the case where the extreme tensile bars yield simultaneously (at a strain of 0.002) with the crushing of the concrete in the extreme compressive fibre (at a strain of 0.0035). For the girders in question, the reinforcing ratios varied along the girder length, such that both values of U cited in Table 4.6 were encountered at some sections.

For shear, U is dependent on the amount of shear reinforcement provided relative to the minimum allowable amount, where the minimum shear reinforcement is defined in Cl. 8.9.2.3 of CAN/CSA-S6-00 (CSA 2000). For all locations analysed in this study, more than the minimum allowable amount of shear reinforcement was present.

Table 4.6. Resistance Adjustment Factors (reproduced in part from CSA 2000).

Load Effect	Amount of Steel	U
Bending Moment	$0.4\rho_b$ - $0.7\rho_b$	0.99
	< $0.4\rho_b$	1.06
Shear	< minimum	0.82
	> minimum	0.94

The term ϕR in Eq. 4.36 refers to the factored resistance, which was calculated as discussed in Sections 4.2.2.1 and 4.2.2.2. The second term in Equation 4.36, $\Sigma\alpha_D D$, is the sum of all the factored dead load effects, D1, D2, and D3, at the location under consideration, determined as discussed in Section 4.2.2.2. The third term, $\Sigma\alpha_A A$ refers to factored load effects caused by forces such as wind, creep, shrinkage, temperature, and differential settlement which were not considered in the analysis of the bridge in question.

In Eq. 4.36, the factored live load effect, $\alpha_L L$, at the location being considered is defined such that it includes the modification factor for multiple lane loading, R_L, and lateral live load distribution factors.

4.2.5 Mean Load Method Evaluation

Another approach to evaluating the live load capacity of a bridge is the mean load method (CSA 2000). Rather than using load and resistance factors in the analysis, the uncertainty in loading, resistance, and analysis methods are considered through the use of representative statistical parameters, defined by a bias coefficient, δ, and a coefficient of variation, V. The bias coefficient is defined as the ratio of the mean effect to the nominal effect, whereas the coefficient of variation is defined as the ratio of the standard deviation of the effect to its mean value. CAN/CSA-S6-00 (CSA 2000) lists some benefits of

using the mean load method as compared to the load and resistance factor method, including the following:

- The mean load method is simpler than adjusting load and resistance factors if the uncertainty in load, analysis method, or resistance is significantly different than assumed by the code.
- The reliability index, β, a measure of the risk associated with permitting passage of a load over a structure, may be determined directly.
- Greater accuracy may be achieved than by using load and resistance factors which represent approximations intended to cover a variety of situations.

4.2.5.1 Statistical Parameters

In applying the mean load method, statistical parameters (δ and V) for ten different variables were considered:

- Dead load effect of D1,
- Dead load effect of D2,
- Dead load effect of D3,
- Live load effect (bending moment or shear),
- Dynamic load allowance,
- Live load analysis method (live load distribution factors),
- Resistance (bending moment or shear),
- Dead load analysis method of D1 (dead load distribution factors),
- Dead load analysis method of D2, and
- Dead load analysis method of D3.

The statistical parameters developed for CAN/CSA-S6-00 (CSA 2000) were based on work completed by several researchers which can be found in the Canadian Highway Bridge Design Code Commentary (CSA 2000), and used to "calibrate" the factors used in the load and resistance factor method. As such,

the results of the mean load method should be comparable to those of the load and resistance factor method.

The statistical parameters used in this study for the ten variables described above are listed in Table 4.7. Statistical parameters for dead load effect remain unchanged for all bridge types and configurations, although they differ for each of the three dead load types. In the load and resistance factor evaluation, special timber haul factors assigned by Saskatchewan Highways and Transportation (EarthTech 2002) were used in place of CAN/CSA-S6-00 (CSA 2000) values, although no corresponding statistical parameters were given.

However, live load statistical parameters for the special timber haul factors were taken to be equal to a CAN/CSA-S6-00 (CSA 2000) permit truck from a truck with similar load factors. It was determined that the difference between live load factors for annual permit holders (PA type) in CAN/CSA-S6-00 (CSA 2000) and the special timber haul factors was only 0.56% on average, with a standard deviation of 3.89%. Therefore, the statistical parameters for annual permit traffic were considered to correspond to the special timber haul factors. It should be noted that the actual permit type using the Red Deer River Bridge is the bulk haul permit (PB type), which has been found to have better compliance with weight restrictions than annual permit holders (PA type) (CSA 2000). Due to the increased uncertainty associated with hauling logs however, the more conservative factors and their resulting statistical parameters have been adopted for this case by DHT.

The statistical parameters for dynamic load allowance were based on the "other" span length case (not a short span as specified in CAN/CSA-S6-00 (CSA 2000)) with two or more loaded lanes. For the purposes of selecting appropriate statistical parameters, the lateral live load distribution analysis methods discussed in Section 4.2.4.4 were considered to be "simplified analyses."

The statistical parameters for components of resistance depend on the type of construction of the bridge in question and, in the case of concrete bridges, the load effect being considered. For bending moment resistance, the statistical parameters depend on the reinforcing ratio relative to the balanced reinforcing ratio, while for shear, they depend on the amount of shear reinforcement relative to the minimum allowable amount of shear reinforcement, as specified in CAN/CSA-S6-00 (CSA 2000).

All statistical parameters in the table were taken from the CAN/CSA-S6-00 (CSA 2000), with the exception of the statistical parameters for the dead load analysis method (lateral distribution of dead load), which were taken from work done by Au et al. (2005), in which it was assumed that there was essentially no uncertainty in dead load distribution.

Table 4.7. Statistical parameters used with the mean load method.

Variable	Bias coefficient		Coefficient of variation	
	Notation	Value	Notation	Value
Dead load (D1) effect	δ_{D1}	1.03	V_{D1}	0.08
Dead load (D2) effect	δ_{D2}	1.05	V_{D2}	0.1
Dead load (D3) effect	δ_{D3}	1.03	V_{D3}	0.3
Live load effect	δ_L	1.06	V_L	0.0094
Dynamic load allowance	δ_I	0.4	V_I	0.8
Live load analysis method	δ_{AL}	0.93	V_{AL}	0.12
Resistance	δ_R	1.06 (shear)	V_R	0.14 (shear)
		1.04, (moment, $\rho<0.4\rho_b$)		0.08, (moment, $\rho<0.4\rho_b$)
		1.01, (moment, $0.4\rho_b< \rho<0.7\rho_b$)		0.12, (moment, $0.4\rho_b< \rho<0.7\rho_b$)
Dead load (D1) analysis method	δ_{AD1}	1	V_{AD1}	0
Dead load (D2) analysis method	δ_{AD2}	1	V_{AD2}	0
Dead load (D3) analysis method	δ_{AD3}	1	V_{AD3}	0

4.2.5.2 Determination of Live Load Capacity Factor

The primary use of the mean load method is to determine the live load capacity factor of the bridge in question, which is calculated as follows:

$$F = \frac{\overline{R}\exp\left[-\beta\left(V_R^2 + V_S^2\right)^{\frac{1}{2}}\right] - \Sigma\overline{D}}{\overline{L}} \qquad [4.38]$$

where $\overline{R}$ is the mean resistance, given by:

$$\overline{R} = \delta_R R \qquad [4.39]$$

Here, R is the nominal unfactored resistance at the section being analyzed, determined as described in Section 4.2.3 (assuming ϕ_c=ϕ_s=1.0). The target reliability index, β, is determined as discussed in Section 4.2.4.1, depending on the load effect being considered. The variable V_R in Eq. 4.38 is the coefficient of variation for the resistance, and V_S is the coefficient of variation of the total load effect, calculated by:

$$V_S = \frac{\left(S_{\Sigma\overline{D}}^2 + S_{\overline{L}}^2\right)^{\frac{1}{2}}}{\left(\Sigma\overline{D} + \overline{L}\right)} \qquad [4.40]$$

where $S_{\Sigma\overline{D}}$ is the standard deviation of the sum of the dead load effects, given by:

$$S_{\Sigma\overline{D}} = \sqrt{\left(V_{D1}^2 + V_{AD1}^2\right)\left(\delta_{D1}\delta_{AD1}D1\right)^2 + \left(V_{D2}^2 + V_{AD2}^2\right)\left(\delta_{D2}\delta_{AD2}D2\right)^2 + \left(V_{D3}^2 + V_{AD3}^2\right)\left(\delta_{D3}\delta_{AD3}D3\right)^2} \qquad [4.41]$$

In Eq. 4.41, D1, D2, and D3 are the nominal unfactored load effects of each of the three different dead loads, as discussed in Section 4.2.2.2, although the dead load factors are all taken as 1.0. The standard deviation of the live load effects, $S_{\overline{L}}$, is calculated by:

$$S_{\overline{L}} = \left[V_{AL}^2 + V_L^2 + \frac{\left(V_I\delta_I I\right)^2}{\left(1+\delta_I I\right)^2}\right]^{\frac{1}{2}}\overline{L} \qquad [4.42]$$

where $\overline{L}$ is the mean combined static and dynamic live load effect, given by:

$$\overline{L} = \delta_L \delta_{AL} L(1 + \delta_I I) \qquad [4.43]$$

in which I is the dynamic load allowance, determined using the methods described in Section 4.2.4.3, L is the nominal unfactored static live load effect, as discussed in Section 4.2.2.4, with the live load factor and the multiple lane loading factor each taken as 1.0, but including lateral live load distribution factors. Finally, $\Sigma\overline{D}$ is the sum of the mean dead load effects:

$$\Sigma\overline{D} = \delta_{D1}\delta_{AD1}D1 + \delta_{D2}\delta_{AD2}D2 + \delta_{D3}\delta_{AD3}D3 \qquad [4.44]$$

4.2.5.3 Determination of Reliability Index

As discussed in Section 4.2.5, one of the key benefits of the mean load method is that it may be used to determine the reliability index, β, in addition to the live load capacity factor, by rearranging Eq. 4.38:

$$\beta = \frac{-\ln\left(\frac{F\overline{L} + \Sigma\overline{D}}{\overline{R}}\right)}{\sqrt{V_R^2 + V_S^2}} \qquad [4.45]$$

In the rearranged Eq. 4.45, the live load capacity factor, F, was taken as the minimum allowable value of 1.0, such that the resulting value of β corresponds to the full allowable live load.

Reliability indices are a method commonly used in bridge management literature to describe the risk associated with allowing the passage of load over a structure. Reliability indices are related to probability of failure; however, they provide a more convenient measure of describing the risk. Table 4.8

(reproduced from CSA 2000) demonstrates the relationship between reliability index and probability of failure; it can be seen that the relationship is highly non-linear.

Table 4.8. Reliability indices and corresponding probability of failure (reproduced from CSA 2000).

Reliability index, β	Notional probability of failure, P_f
2	2.3×10^{-2} or 1:44
2.25	1.2×10^{-2} or 1:81
2.5	6.2×10^{-3} or 1:160
2.75	2.8×10^{-3} or 1:360
3	1.4×10^{-3} or 1:740
3.25	5.6×10^{-4} or 1:1800
3.5	2.3×10^{-4} or 1:4300
3.75	8.8×10^{-5} or 1:11000
4	3.2×10^{-5} or 1:31500
4.25	1.1×10^{-5} or 1:93500
4.5	3.4×10^{-6} or 1:294000

4.3 IN-SITU ANALYSIS

4.3.1 Overview

The “in-situ" analysis consisted of evaluating the bridge girders based on the mean load method outlined in CAN/CSA-S6-00 (CSA 2000). However, several variables in the evaluation were determined by measuring site-specific statistical parameters and substituting them for code-prescribed values. Only those variables involving live load effects were changed based on data collection; dead load effects were not measured and, therefore, remained unchanged from code-prescribed values. Data collected at the Red Deer River

Bridge was analysed to generate statistical parameters for a number of variables used in the evaluation, including:

- Dynamic load allowances,
- Bending moments at instrumented locations,
- Shear,
- Lateral load distribution factors,
- Bending moment resistance, and
- Shear resistance.

For this portion of the study, the analysis methods remained essentially the same as those used in the as-designed analysis; however, the effect of using site-specific parameters in the determination of the allowable loading for the bridge while maintaining the required level of reliability was considered. A key assumption in analysing the collected data to obtain the necessary statistical parameters was that all measured random variables featured normal probability distributions, a characteristic that appeared to be reasonable based on a visual examination of the results. By assuming normal distributions, the methodology remained the same as in the as-designed analysis, so that CAN/CSA-S6-00 (CSA 2000) methodology could still be used in the girder evaluation. From the statistical distributions generated for the variables described in the paragraph above, bias ratios and coefficients of variation were determined for use with the mean load method. For the in-situ analysis, only sections at the installed strain gauge locations were evaluated.

4.3.2 Geometry and Material Properties

Site specific characterization of the variables described in the previous section were determined based on strain measurements and rebound hammer test results. Several statistical parameters for geometric and material properties were obtained from published literature in cases where on-site measurements

would have been costly or difficult to determine. The statistical parameters for geometric and material properties taken from Nowak et al. (1994) are summarized in Table 4.9 below.

Table 4.9. Statistical parameters of variables taken from the literature.

Variable	Notation	Bias ratio	Coefficient of variation
Yield strength of reinforcing steel (internal)	f_{yi}	1.125	0.12
Yield strength of reinforcing steel (external)	f_{ye}	1.12	0.1
Modulus of elasticity reinforcing steel (internal and external)	E_s	1	0.06
Girder section height	h_g	1	$0.4/h_g$
Flange height	h_f	1	$0.4/h_f$
Cross-sectional area of reinforcing steel layer i (internal and external)	A_{si}	1	0.015
Effective depth to reinforcing steel layer i (internal and external)	d_{si}	1	$0.7/d_{si}$

4.3.3 Non-Destructive Evaluation

Rebound hammer tests were performed at the Red Deer River Bridge, from which rebound hammer numbers were obtained, as described in Section 3.3.3.2. Rebound hammers record the surface hardness of the measured

concrete, correlating the ultimate compressive strength of concrete to hardness. As a result, the accuracy of rebound hammer testing is limited; it was performed in this study to demonstrate the use of non-destructive evaluation results in a reliability analysis. The rebound hammer calibration testing was used to generate a graph relating the mean measured rebound hammer number to the ultimate compressive strength of concrete, a description of which can be found in Section 5.3.3. A "best fit" regression was fit through the 21 measured data points, and the expected hammer readings for 20 MPa – 50 MPa strength concrete were subsequently extrapolated from the derived relationship. Rebound hammer readings recorded on site were converted to ultimate compressive concrete strengths using calibration curve. Based on these values, statistical parameters of measured ultimate compressive strength were determined.

4.3.4 Measured Strain Data

4.3.4.1 Correcting and Filtering Data

The raw strain data consisted of measurements taken at a sampling rate of 3000 Hz. For the raw data measurements, no attempt was made to remove the initial static (DC) offset in the gauge reading, as shown in Fig. 4.5. Therefore, the recorded strain time-histories were first corrected to indicate the condition of the state in which no vehicles were present on the bridge deck. This correction was completed by subtracting the average of the first 100 strain readings, recorded before trucks were on the bridge, in the time-histories from each of the strain gauges from subsequent strain measurements in the time-histories.

The strain gauge readings also contained significant levels of measurement noise, resulting in high frequency fluctuations that created wide bands of strain (see Fig. 4.5) rather than smoothly varying plots. To attenuate

the influence of this noise, the strain time-histories were filtered by averaging sequential blocks of 100 strain readings, thereby reducing the effective sampling rate to 30 Hz. The resulting filtered strain time-histories were thought to be more representative of the actual strain variations occurring in the girders, as illustrated in Fig. 4.6. However, this averaging procedure also had the result of filtering out higher frequency responses along with the electrical noise.

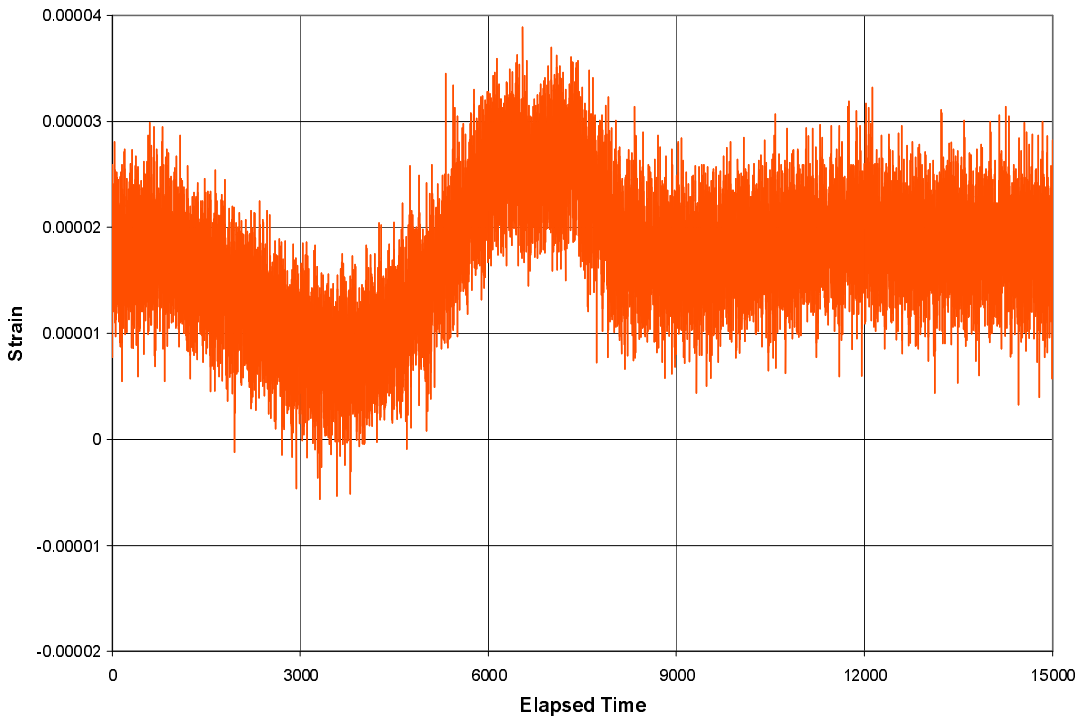

Figure 4.5. Example raw strain time-history (Gauge 2-3l, Sept 29 trial 1, static).

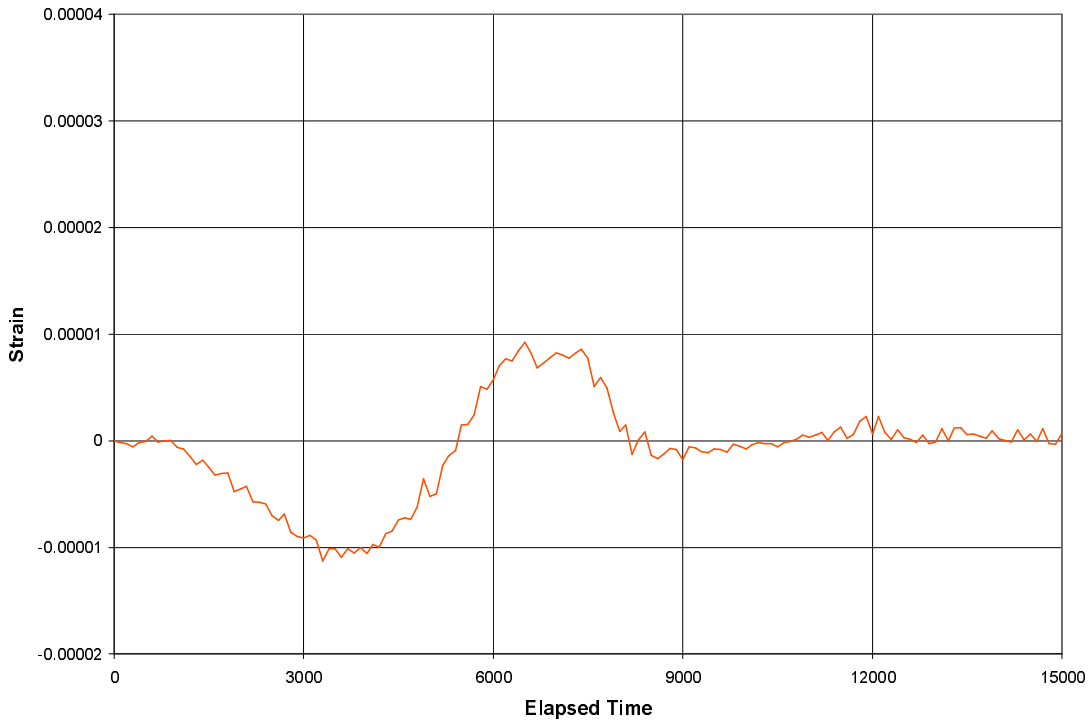

Figure 4.6. Example corrected and filtered strain time-history (Gauge 2-3l, Sept 29 trial 1, static).

4.3.4.2 Neutral Axis Location and Curvature

The corrected and filtered strains were used to determine the neutral axis locations, as well as the instantaneous curvature time histories, at each vertical line of strain gauges; both of these results were used in the determination of load effects. The neutral axis locations and curvature histories were determined for each measured truck pass, using a data analysis program written in the FORTRAN™ programming language (Sparling 2005). The FORTRAN™ program used the normalized and filtered strain data, along with information describing the girder and strain gauge geometry, to place best-fit lines, determined using a simple linear regression with the method of least squares, through the measured strains in each specified vertical line of strain gauges for each instant in the time-histories. The neutral axis location was determined as the point of intersection of the best-fit line and vertical axis,

measured from the bottom of the girder. Curvature was calculated as the tangent of the angle formed between this best-fit and a vertical line.

4.3.4.3 Critical Load Effects

For a given loading event, only extreme values of curvature and corresponding neutral axis locations and strain were of interest, as they corresponded to the most extreme load effects. "Extreme" was considered to be those instants in the time history where the curvature reached its absolute maximum value. Two different methods were used to define strain profiles at critical instants:

- Using measured maximum curvatures, and
- Using the measured neutral axis locations and strains in the lower strain gauges corresponding to the maximum curvatures.

Curvatures

Extreme values of curvature were extracted from the measured strain gauge data for each truck loading event considered. Due to the continuity of the girders, both positive and negative strains could be induced at a given location, depending on the location of the truck on the bridge. However, only the largest absolute values of strain were considered; in the negative bending moment regions, negative curvatures were used, while in the positive bending moment regions, positive curvatures were used.

After the extreme curvature values were extracted for each vertical line of strain gauges, the values were tested to ensure they were reasonable. In some cases, abnormal extreme curvatures were identified that were thought to result not from loading, but from some error in data acquisition. For this purpose, abnormal curvatures were considered to be those which lay more than

two standard deviations from the mean curvature. Curvatures identified as abnormal were rejected and not considered in subsequent evaluation.

Neutral Axis Locations

It was found that measured neutral axis locations varied significantly, depending on loading conditions, as a result of the presence of axial forces. In pure flexure, the neutral axis of an uncracked section is independent of loading in the elastic range; however, when axial forces are present, compression is added as a uniform stress throughout the girder section, as discussed in Section 4.3.5.2. Due to this added degree of compression in the section, the neutral axis location is no longer independent of loading.

In the current study, only those neutral axis locations under critical loading were considered to be of interest. In other words, the neutral axis locations corresponding to the instantaneous extreme curvatures extracted from the strain time-histories were considered in the subsequent analyses. Abnormal neutral axis locations were removed in a manner similar that discussed for curvature previously in this Section.

Strains in Lower Gauges

A second method of establishing strain profiles at critical instants was undertaken using the measured neutral axis locations and strains at the lowest gauge locations corresponding to the instants where the measured curvatures were maximum.

Only lower strain gauge measurements were used for this purpose as they typically generated the largest values of the three gauges in a vertical line; in several cases, the middle and upper strain gauges were located very close to the measured neutral axis locations; therefore, measured strains for these

gauges tended to be small. Furthermore, as discussed in Section 2.2.6, previous studies used only the lower strain gauges. Abnormally large or small strains (i.e. outliers) were removed systematically in a manner similar to that described previously in this Section.

4.3.5 Bending Moments

Bending moments induced at each evaluated location in the girders by log truck loading were determined using two different methods: the measured curvature, and the measured neutral axis location along with the measured strain in the lower gauge, all determined using the methods discussed in Section 4.3.4.

4.3.5.1 Bending Moments Based on Measured Curvature

In this first approach, the live load bending moment induced at a girder cross-section was determined on the basis of measured extreme curvature, which was defined in Section 4.3.4. Since unfactored results are used in the mean load method, all material resistance factors were set equal to unity.

Unlike conventional moment resistance calculations, in evaluating measured bending moments adjustments had to be made for the fact that ultimate conditions were not reached, so that the reinforcing steel did not yield and the concrete did not crush. In this case, the measured strain diagram was used to define the actual strains rather than using standard ultimate condition assumptions. Furthermore, code-specified Whitney stress block parameters used to approximate concrete compressive stresses for bending moment calculations (see Section 4.2.3.2) are based on the assumption that the concrete reaches the crushing strain of 0.0035; therefore, these parameters were modified for concrete at lower levels of strain. For this study, the method for determining Whitney stress block parameters at non-ultimate conditions

described in ISIS Canada's Reinforcing Concrete Structures with Fibre Reinforced Polymers Manual (ISIS 2001) was employed.

The ISIS (2001) method for determining Whitney stress block parameters at an arbitrary strain level is based on a table which provides the two parameters, α and β at non-ultimate conditions, for different concrete strengths and different ratios of concrete strain to the strain at f'_c. Based on these parameter values, the following equations were generated using a best-fit regression procedure:

$$\alpha = -0.262\left(\frac{\varepsilon_c}{\varepsilon_o}\right)^6 + 1.562\left(\frac{\varepsilon_c}{\varepsilon_o}\right)^5 - 3.173\left(\frac{\varepsilon_c}{\varepsilon_o}\right)^4 + 2.355\left(\frac{\varepsilon_c}{\varepsilon_o}\right)^3 - 0.751\left(\frac{\varepsilon_c}{\varepsilon_o}\right)^2 + 1.159\left(\frac{\varepsilon_c}{\varepsilon_o}\right) + 0.02 \qquad [4.46]$$

$$\beta = -0.037\left(\frac{\varepsilon_c}{\varepsilon_o}\right)^6 + 0.321\left(\frac{\varepsilon_c}{\varepsilon_o}\right)^5 - 1.134\left(\frac{\varepsilon_c}{\varepsilon_o}\right)^4 + 1.995\left(\frac{\varepsilon_c}{\varepsilon_o}\right)^3 - 1.654\left(\frac{\varepsilon_c}{\varepsilon_o}\right)^2 + 0.666\left(\frac{\varepsilon_c}{\varepsilon_o}\right) + 0.549 \qquad [4.47]$$

where ε_c is the measured strain in the concrete at the extreme compressive fibre, and ε_o is the concrete strain at f'_c. The concrete strain at f'_c, ε_o, is defined as:

$$\varepsilon_o = \frac{f'_c}{E_c}\frac{n}{n-1} \qquad [4.48]$$

where a curve-fitting factor, n, relates the actual parabolic concrete strain distribution to the linear Whitney strain distribution:

$$n = 0.8 + \frac{f'_c}{17} \qquad [4.49]$$

Here, the ultimate compressive strength of concrete, f'_c, must be in units of MPa.

As a first step in estimating bending moments the neutral axis location was determined by balancing the tensile and compressive forces within the girder cross-section. Although the curvature was known, the location of the flexural neutral axis was determined by shifting the neutral axis until the internal forces were balanced. The bending moment was then determined using the methods described in Section 4.2.3.2. It should be noted that the internal forces estimated in this manner included only those associated with the flexure-induced strain gradient over the height of the girder; the uniform strain component associated with axial loads was excluded in this approach.

Statistical distributions of bending moments were generated for each cross-section analysed. The statistical distributions represent the uncertainty of the multiple loading events (represented by curvature or neutral axis location and strain), as well as the uncertainty due to the variability in material and geometric properties. The mean bending moment was determined by using the mean values of all variables used in the bending moment analysis. The standard deviation of bending moment was determined using the following equation (Nowak and Collins 2000):

$$\sigma_M = \sqrt{\sum_{i=1}^{n} v_i^2 \left(\frac{\partial M}{\partial v_i} \right)^2} \qquad [4.50]$$

where v_i is the *i*th random variable in the bending moment analysis, and $\frac{\partial M}{\partial v_i}$ is the partial derivative of the bending moment with respect to the *i*th random variable in the bending moment analysis. Random variables in the analysis included:

- Yield strength of internal and external steel reinforcement,
- Cross-sectional area of internal and external steel reinforcement,
- Depth to each layer of steel reinforcement (internal and external),
- Modulus of elasticity of internal and external steel reinforcement, and

- Heights of girders and flanges.

4.3.5.2 Bending Moments Based on Neutral Axis Location and Lower Strain

The second method of determining bending moment was based on the instantaneous measured location of the neutral axis and the strain at the level of the lower strain gauge. As was the case when using curvature to determine bending moments, all sections were found to remain in the elastic response region; therefore, Eqs. 4.46 through 4.49 were used to describe the Whitney stress block parameters.

The measured strain distributions were in actuality a combination of bending moment and axial force, as shown in Fig. 4.8. Using the neutral axis location and the strain at the level of lower strain gauge, the internal tensile and compressive forces in a section could be determined. For all sections analysed, the internal compressive forces were larger than the internal tensile forces; thus, the neutral axes were shifted toward the compression region indicating that there were net compressive axial forces present in the sections in addition to the bending moments. The magnitude of bending moment was determined by artificially shifting the neutral axis location keeping the curvature unchanged, until a condition was reached in which the internal tensile and compressive forces associated with strains defined by the measured curvature and assumed neutral axis location were balanced. The excess strains, beyond those accounted for by the bending moment analysis, were then used to determine the net axial force.

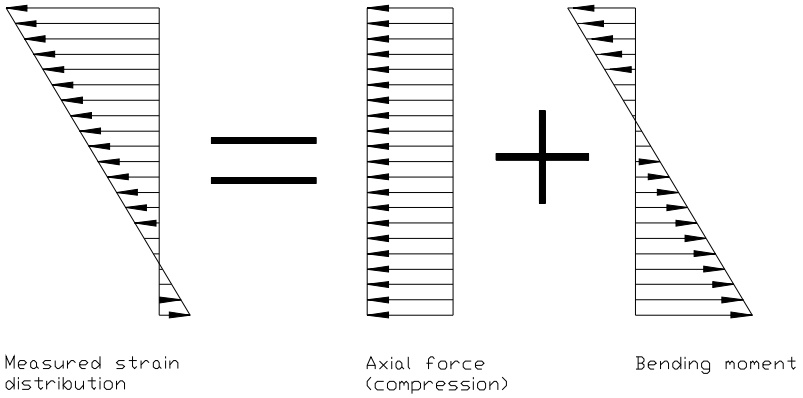

Figure 4.8. Axial force and bending moment components of measured strain distribution.

The net axial force was determined using the following equation:

$$P = \Delta\varepsilon E_s A_s + \Delta\varepsilon E_{se} A_{se} + \Delta\varepsilon E_c A_c \qquad [4.51]$$

where $\Delta\varepsilon$ is the uniform strain offset between the measured strain distribution and that used to determine the bending moment, which feature identical curvatures, but different neutral axis locations, and A_c is the net cross-sectional area of the concrete, defined as the gross cross-sectional area less the cross-sectional area of the reinforcing steel. The mean values of all variables in Eq. 4.51 were used to determine the mean axial force. The standard deviation of axial force was then determined in manner similar to that of bending moment:

$$\sigma_P = \sqrt{\sum_{i=1}^{n} v_i^2 \left(\frac{\partial P}{\partial v_i} \right)^2} \qquad [4.52]$$

where v_i is the *i*th random variable in the axial force analysis, and $\frac{\partial P}{\partial v_i}$ is the partial derivative of the axial force with respect to the *i*th random variable for axial force. All random variables noted previously were included.

Bending moment diagrams were generated for each of the girders, using both methods of evaluating bending moments. To define the moment diagrams a fifth order polynomial was fit through the calculated bending moments determined at the five strain gauge locations on each girder, such that the fitted line passed though each measured data point.

4.3.6 Shear

Shear induced into the girders by live loading was determined from the bending moment diagrams, which were generated as discussed in Section 4.3.5. Since shear may be expressed as the first derivative of bending moment with respect to position along the girders, the shear and bending moment diagrams are directly related. Furthermore, the area under the shear diagram between two points on a girder represents the change in the bending moment diagram between those points. Finally, points of maxima and minima on the bending moment diagrams represented locations of zero shear, thereby providing a starting point for generating the shear diagram. It should be noted that this is only a approximation of the instantaneous shear along the girders, as the peak moment events at the five instrument locations do not necessarily occur simultaneously. The measured bending moment diagram represents an envelope of maximum bending moments due to a moving load; the corresponding shear diagram may not identify the critical shear case at all instrument locations.

Using the technique described above, shear diagrams were generated for each of the girders, using the bending moment diagrams from each of the methods described in Section 4.3.5. Five hundred intervals, each 0.773 m in length, were used along the middle spans of the girders to develop the shear diagrams. Since nominal values for the random variables were described in Section 4.3.2 were used in generating the bending moment and shear diagrams, these diagrams represent the most likely, or mean load effects.

Representative standard deviations for the shear forces were determined based on the coefficients of variation derived for bending moments (i.e. the mean shear was multiplied by the coefficient of variation for bending).

4.3.7 Load Effect Factors

4.3.7.1 Distribution Factors

Distribution factors for both bending moments and shear forces were determined at each vertical line of strain gauges, using both of the two methods described in Section 4.3.5 for determining bending moments. The distribution factors at a given strain gauge location were determined directly from the load effects as follows (Nowak et. al. 2000):

$$DF_{Mi} = \frac{M_i}{\sum_{i=1}^{3} M_i} \qquad [4.53]$$

$$DF_{Vi} = \frac{V_i}{\sum_{i=1}^{3} V_i} \qquad [4.54]$$

where DF_{Mi} and DF_{Vi} are the distribution factors of the *i*th girder for bending moment and shear, respectively. The bending moment in the *i*th girder at the strain gauge location under consideration is denoted by M_i, while the corresponding shear is denoted by V_i. Since these equations represent the load effects associated with a single truck, corresponding distributions factors for the occurrence of multiple trucks in adjacent traffic lanes can be obtained by simply multiplying the values obtained from Equations 4.53 and 4.54 by the number of lanes present (Barnes et al., 2003). The mean distribution factors were determined using the mean values of M_i and V_i. The standard deviations of the distribution factors were determined using the following expression

(Nowak and Collins 2000), in which *i* refers to the lateral position of strain gauges, and j refers to the girder (see Section 3.3.1):

$$\sigma_{DFi} = \mu_{DFi}\left[\left(V_{ij}\right)^2 + \left(V_{\sum i}\right)^2\right] \qquad [4.55]$$

where μ_{DFi} is the mean distribution factor at the *i*th lateral location on the girders, determined using Eq. 4.53 or Eq. 4.54. The coefficient of variation of the load effect at the *i*th lateral location on the *j*th girder is given by V_{ij}. The variable $V_{\Sigma i}$ is the coefficient of variation of the sum of the load effects on all three girders at the *i*th lateral location. Eq. 4.55 can also be written as:

$$\sigma_{DFi} = \mu_{DFi}\left[\left(\frac{\sigma_{ij}}{\mu_{ij}}\right)^2 + \left(\frac{\sigma_{\sum i}}{\mu_{\sum i}}\right)^2\right] \qquad [4.56]$$

where σ_{ij} is the standard deviation of the load effect at the *i*th lateral location on the *j*th girder (for example, the middle strain gauge location on the second girder), and μ_{ij} is the mean load effect at the *i*th lateral location on the *j*th girder. The mean total load effect at the ith lateral location is given by:

$$\mu_{\sum i} = \sum_{j=1}^{3} \mu \qquad [4.57]$$

where μ is the mean load effect on the *j*th girder. The standard deviation of the total load effect at the *i*th lateral location is given by:

$$\sigma_{\sum i} = \sqrt{\sum_{j=1}^{3} \sigma^2} \qquad [4.58]$$

where σ is the standard deviation of the load effect on the *j*th girder. As the governing loading case on the Red Deer River Bridge is two trucks travelling

side by side in the two design lanes, distribution factors were all multiplied by two, in accordance with the requirements of CAN/CSA-S6-00 (CSA 2000).

4.3.7.2 Dynamic Load Allowance

The dynamic load allowance for the Red Deer River Bridge was determined from strain data obtained under controlled loading, using the following equation:

$$DLA = \frac{\varepsilon_{dyn}}{\varepsilon_{stat}} \qquad [4.59]$$

where ε_{dyn} is the measured peak strain under a truck pass at full speed, and ε_{stat} is the measured strain under a corresponding truck pass at crawl speed. All combinations of similar truck passes were considered for all different loading configurations shown in Table 3.4. The dynamic load allowance was determined using only the lower strain gauges in each vertical line of gauges, for the reasons discussed in Section 4.3.4.3. A single dynamic load allowance was determined for the entire bridge by averaging the measured peak DLA from each instrument location for all log truck events. Abnormal dynamic load allowance values were removed using the procedure described in Section 4.3.4.3.

4.3.8 Resistance

4.3.8.1 Bending Moment Resistance

Bending moment resistance was re-evaluated at the strain gauge locations for the in-situ analysis, using the statistical parameters of a number of variables which were taken from the literature, shown in Table 4.9, as well as the measured ultimate compressive strength of concrete from the rebound hammer testing, as discussed in Section 4.3.3. The mean bending moment

resistance was evaluated using the methods described in Section 4.2.3.2, although all material resistance factors were taken as 1.0 for the mean load method. The standard deviation of bending moment resistance was determined using Eq. 4.50.

4.3.8.2 Shear Resistance

Shear resistance was also re-evaluated for each strain gauge location for the in-situ analysis, using the statistical parameters from the literature and rebound hammer tests. In accordance with the modified compression field theory, however, shear resistance determined using the CAN/CSA-S6-00 (CSA 2000) method is also affected by the applied shear, bending moment, and axial force. The methods described in Section 4.2.3.3 were used to determine in-situ shear resistance, although all material resistance factors were taken as 1.0 for the mean load method. However, the term including the axial force, N_f, in Eq. 4.24 was included in the in-situ analysis, because axial force was measured at all locations. As determining the shear resistance is dependent on a manually selection of θ and β values from Table 4.1, the method outlined in Section 4.2.3.3 was modified such that the derivative, and therefore the standard deviation, could be determined, as described below.

As described in Section 4.2.3.3, shear resistance is the sum of V_c and V_s, defined by Eqs. 4.21 and 4.25, which include the parameters β and θ, determined from Table 4.1. As an intermediate step in determining the shear resistance, statistical distributions of β and θ were determined. A statistical distribution of longitudinal strain, ε_x, was first determined from Eq. 4.24. The mean of value of ε_x was determined by using the nominal values of all variables, while the standard deviation was determined using:

$$\sigma_{\varepsilon_x} = \sqrt{\sum_{i=1}^{n} v_i^2 \left(\frac{\partial \varepsilon_x}{\partial v_i} \right)^2} \qquad [4.60]$$

where v_i is the *i*th random variable in the longitudinal strain analysis, and $\frac{\partial \varepsilon_x}{\partial v_i}$ is the partial derivative of the strain with respect to the *i*th random variable. All random variables listed in Section 4.3.2 were included in this analysis.

An iterative procedure was used to determine an appropriate value of θ from Table 4.1. To facilitate the calculation of derivatives, interpolated values of θ and β were generated at longitudinal strain increments of 0.00005.

Using the standard deviations of longitudinal strains, the standard deviations of β and θ were estimated from the interpolated values described above. Using the statistical parameters of β and θ, along with the statistical parameters for other variables in the analysis, the standard deviations of shear resistance were determined by:

$$\sigma_V = \sqrt{\sum_{i=1}^{n} v_i^2 \left(\frac{\partial V}{\partial v_i} \right)^2} \qquad [4.61]$$

where v_i is the *i*th random variable in the shear resistance analysis, and $\frac{\partial V}{\partial v_i}$ is the partial derivative of the shear resistance with respect to the *i*th random variable for shear resistance. All random variables described in Section 4.3.2 were included.

4.3.9 Mean Load Method Evaluation

The mean load method was used with the measured variables to obtain estimates of the live load capacity factor and reliability index. The statistical parameters generated for the variables discussed in the previous sections were

converted to bias ratios and coefficients of variation for use in the mean load method, as described in the following sections. Contributing variables were assumed to be normally distributed, as has been done in previous research (Cheung and Li 2002, Ghosn et al. 1986, Kim and Nowak 1997). Furthermore, a visual examination of the parameters considered indicated that they do, in fact, exhibit the characteristics of normal probability distributions (i.e. cumulative probabilities plot as approximately straight lines on normal probability paper.)

4.3.9.1 Live Load Capacity Factor

The live load capacity factor was re-evaluated using the site-specific statistical parameters and the mean load method. The bias ratios required for use in the mean load method were determined using:

$$\delta = \frac{\mu_{meas}}{\mu_{nom}} \qquad [4.62]$$

where μ_{meas} is the measured mean value of the variable under consideration, determined using the methods described in Sections 4.3.5 through 4.3.8, and μ_{nom} is the nominal mean value of the variable under consideration (the unfactored value of the variable), determined using methods discussed in Section 4.2. The coefficients of variation for use in the mean load method were determined using:

$$V = \frac{\sigma_{meas}}{\mu_{meas}} \qquad [4.63]$$

where σ_{meas} is the measured standard deviation of the variable under consideration, determined using the methods described in Sections 4.3.5 through 4.3.8. It should be noted that the mean values of shear and bending moment were doubled to account for two-lane loading, in accordance with the

distribution factors. The coefficients of variation for shear and bending moment remained unchanged from single-lane loading.

Live load capacity factors were evaluated in the in-situ state using the resulting statistical distributions from bending moments determined using both methods discussed in Section 4.3.5. Furthermore, in-situ live load capacity factors were also determined for the girders under the proposed increased allowable truck loading of 110 t. One of the main assumptions in evaluating the live load capacity factors under the increased loading was that the coefficients of variation remained the same as those for the measured load effects. The in-situ live load capacity factors were determined using Eqs. 4.40 through 4.46.

4.3.9.2 Reliability Index

In addition to determining the in-situ live load capacity factors, the in-situ reliability indices were also determined, using Eq. 4.47. In-situ reliability indices were determined using statistical distributions resulting from evaluations of bending moments using both methods discussed in Section 4.3.5. As well, in-situ reliability indices were determined for the proposed increased loading of 110 t.

CHAPTER 5 RESULTS

5.1 INTRODUCTION

The results of the as-designed and the in-situ analyses of the Red Deer River Bridge are presented in this chapter. The intermediate results, including strain gauge and non-destructive evaluation results, load effects, and resistances are presented first, followed by the resulting reliability indices, and discussion of the results. The expected economic benefit associated with the use of the methodology is also discussed.

5.2 AS-DESIGNED ANALYSIS

5.2.1 Overview

The results of the as-designed analysis are presented for both the load and resistance factor method and the mean load method of evaluation. The load effects and resistances for all evaluated girder sections are presented first, followed by the live load capacity factors, and reliability indices, where applicable. Results are presented for the current allowable gross vehicle weight (GVW) of 62.5 t, as well as for the proposed allowable GVW of 110 t. Load effects are based on two design trucks travelling side by side, in each of the two design lanes. For the as-designed analysis, the resulting load effects are shown for the instrumented locations, as well as for other critical locations, which are discussed in Section 4.2.2.4.

The results presented in this section are representative of assessments that can be undertaken using only the original design information. The reliability indices resulting from the mean load method of analysis are more indicative of the actual possibility of failure than the live load capacity factor typically determined in bridge evaluations, as reliability indices are directly related to probability of failure.

5.2.2 Load and Resistance Factor Evaluation

5.2.2.1 Factored Load Effects

Factored load effects were determined using the finite element model of the girders and the methods discussed in Section 4.2.2. The resulting load effects are summarized in Figs. 5.1 and 5.2 (values are also tabulated in Table D.1 in Appendix D). Data points on the graphs represent the strain gauge locations and critical locations, as discussed in Section 3.2.2. It can be seen that factored bending moments were different for the interior and exterior girders, due to varying distribution factors. However, the factored shear forces were the same for all girders because the distribution factors for shear were the same for all locations.

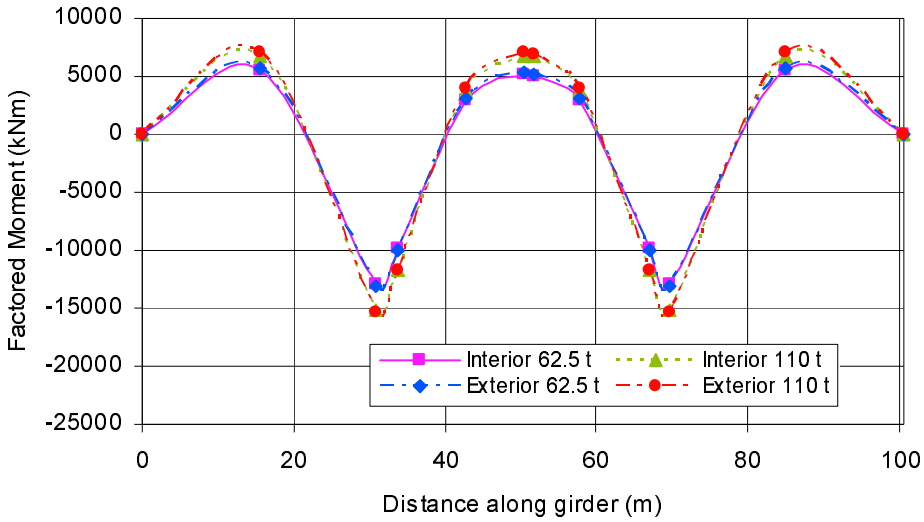

Figure 5.1. Estimated factored bending moments based on load and resistance factor method.

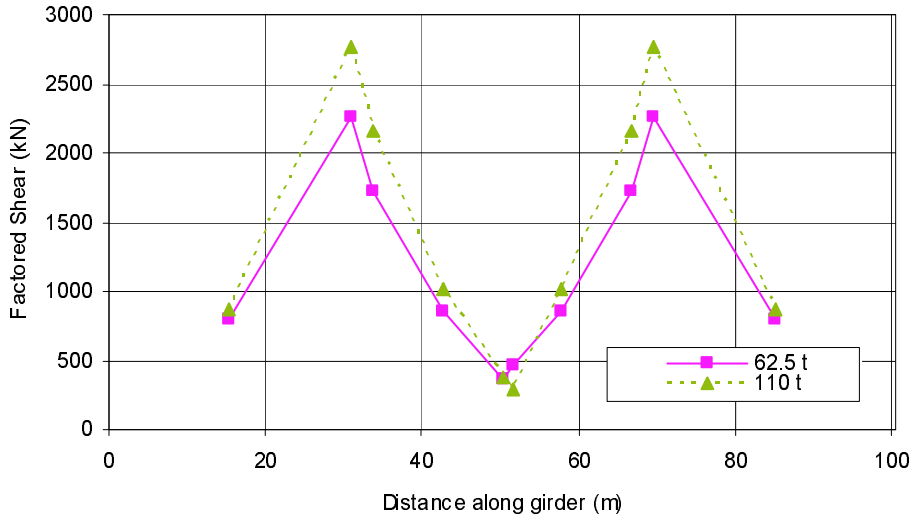

Figure 5.2. Estimated factored shear forces based on load and resistance factor method.

5.2.2.2 Factored Resistance

Factored resistances were determined for both bending moment and shear, and are presented graphically in Figs. 5.3 and 5.4, respectively, while the numerical values may be found in Table D.2 in Appendix D. Flexural resistances were determined using the methods described in Section 4.2.3.2,

while shear resistances were determined using the methods described in Section 4.2.3.3. Flexural resistances were determined to be different for interior and exterior girders, as the effective flange widths of the girder sections were different, resulting in different concrete cross-sectional areas, as well as different amounts of steel in some cases.

Because shear resistance was dependent not only on shear forces, but also bending moments, the shear resistance was also different for the interior and exterior girders. Furthermore, shear resistances at various girder cross-sections were different for 62.5 t truck loading and 110 t truck loading, due to the dependency of shear resistance on load effects.

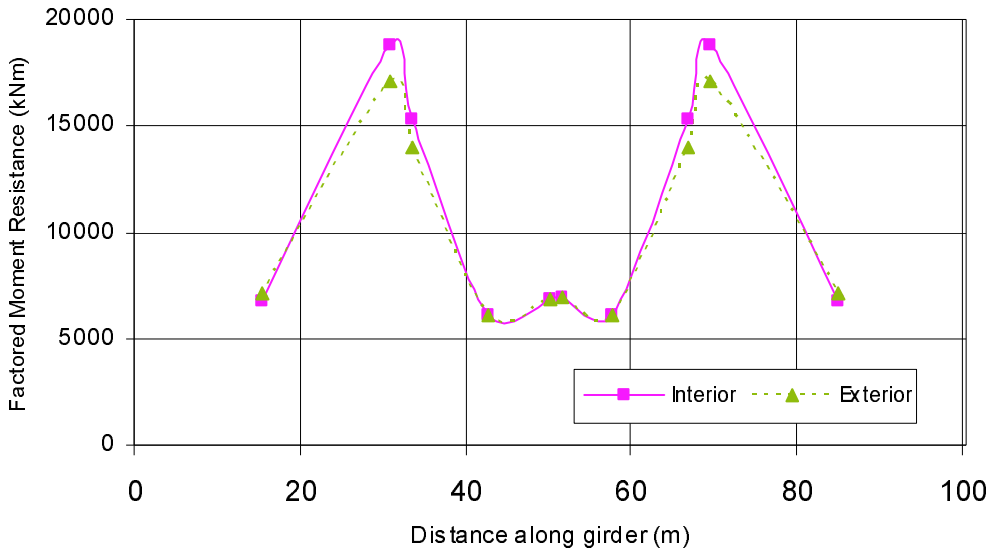

Figure 5.3. Estimated factored bending moment resistance based on load and resistance factor method.

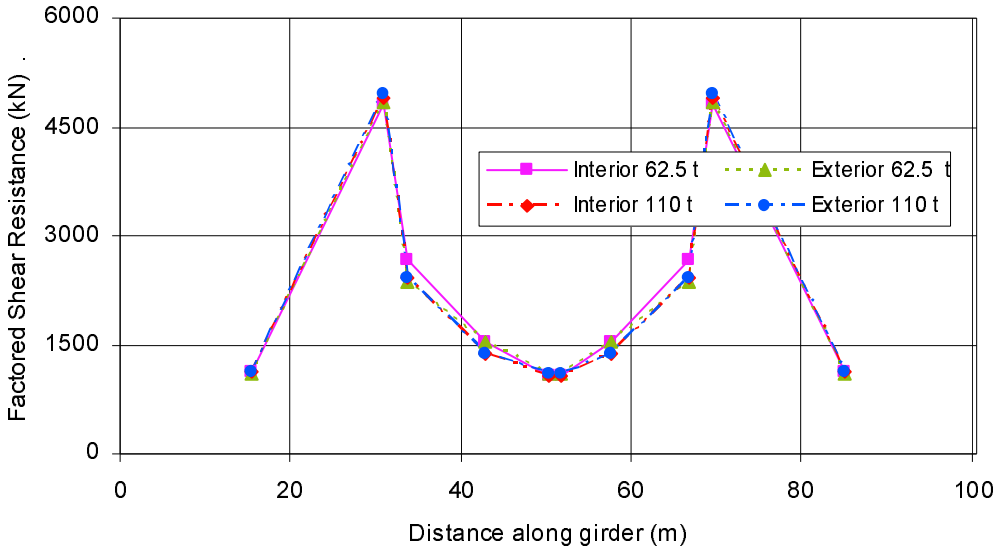

Figure 5.4. Estimated factored shear resistance based on load and resistance factor method.

5.2.2.3 Live Load Capacity Factor

Although the factored resistance of a girder section may be greater than the factored load effects, what ultimately determines the maximum allowable loading on a bridge for design purposes is the live load capacity factor, F, determined using the methods described in Section 4.2.4.5. As described earlier, the live load capacity factor represents the ratio of the live load that can be safely carried to some nominal design live load. The live load capacity factors for the as-designed analysis are presented in graphically in Figs. 5.5 and 5.6, for bending moment and shear, respectively, and for both 6.25 t and 110 t truck loading. The numerical results can be found in Table D.3 in Appendix D. Since the determination of the live load capacity factor requires that the nominal dead and live load effects be calculated separately, these values are summarized in Figs. 5.7 through 5.10.

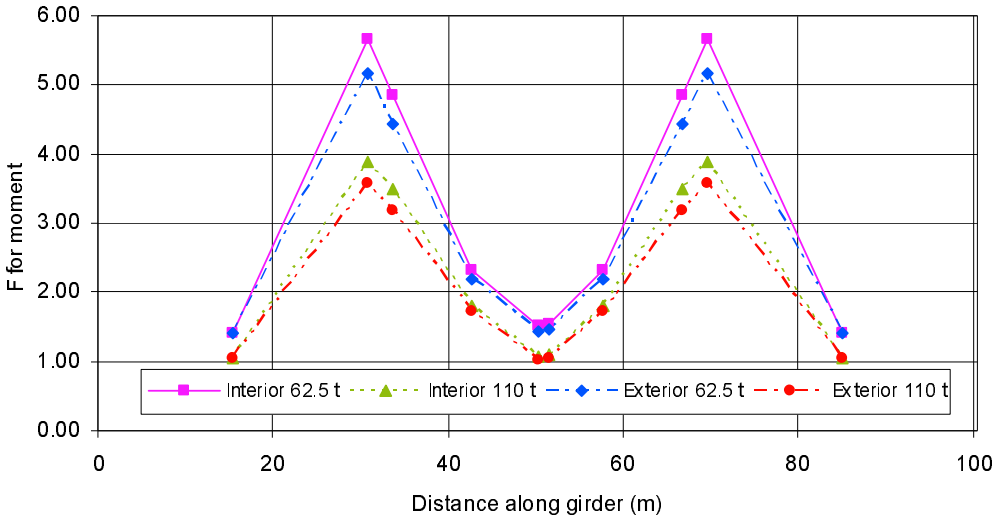

Figure 5.5. As-designed live load capacity factors for bending moments determined using load and resistance factor method.

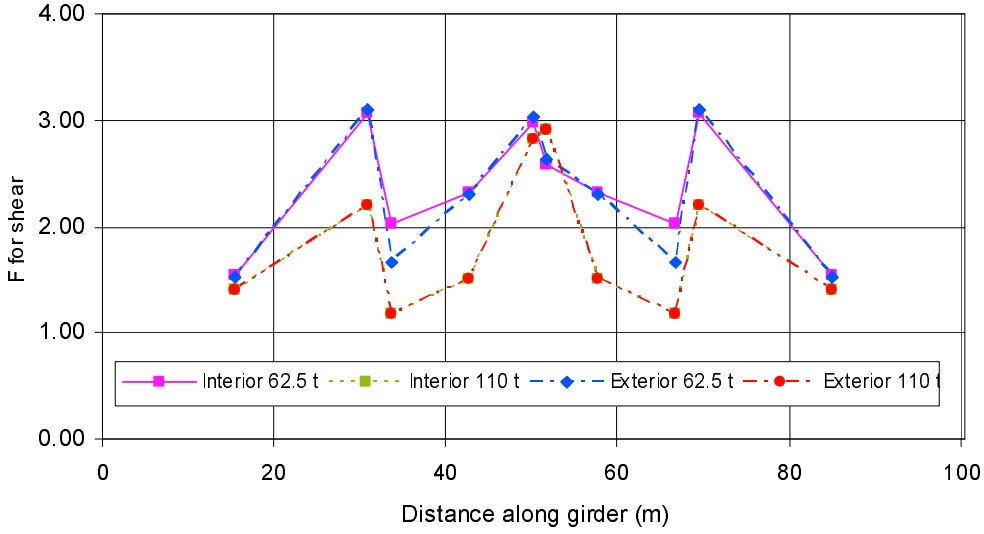

Figure 5.6. As-designed live load capacity factors for shear determined using load and resistance factor method.

The live load capacity factors determined based on the methods and assumptions adopted for this study indicate that the bridge safety would not be compromised, even if the allowable GVW was increased to 110 t. In terms of bending, the lowest values of F encountered occurred at the midspans of each span, not surprisingly, as bending is highest in the midspan regions.

Furthermore, the proposed strengthening would provide additional bending capacity in the positive moment regions, thus improving the situation further. For shear, the lowest values of F occurred at the piers, where shear is typically highest. The proposed strengthening would provide no additional shear capacity at the piers, although the live load capacity factor are sufficiently large that none should be required.

Although the bridge evaluation carried out by a private consultant found that live load capacity fell below the minimum 1.0 for the proposed 110 t GVW loading in bending (EarthTech 2002), the discrepancy is likely due to slightly different assumptions and interpretations of the bridge plans. Primarily, it is believed that the private consultant used different material resistance factors from those specified in CAN/CSA-S6-00 (CSA 2000).

5.2.3 Mean Load Method Evaluation

5.2.3.1 Nominal Load Effects

For use in the mean load method, the various nominal load effects were determined separately, using the methods described in Section 4.2.2. The nominal dead load bending moments and shear forces by dead load type are presented in Figs. 5.7 and 5.8, respectively, for the interior and exterior girders, while all nominal live load effects are presented in Figs. 5.9 (bending moment) and 5.10 (shear), for both 62.5 t and 110 t truck loading. Numerical results can be found in Tables D.4 through D.6 in Appendix D.

Although increasing the allowable GVW from 62.5 t to 110 t represents a 76% increase in live load, the results graphed in Figs. 5.9 and 5.10 show that the increases in load effects were considerably less. In flexure, the increase in load effects corresponding to the increased allowable loading was at most 45% (at the piers), while, in shear, the maximum increase was 49% (at the location

of the end strain gauges). In part, this may be attributed to the fact that the live load effects were somewhat mitigated by the configuration of the 110 t trucks, as there are more axles, and the overall length of the truck and trailer unit was substantially increased.

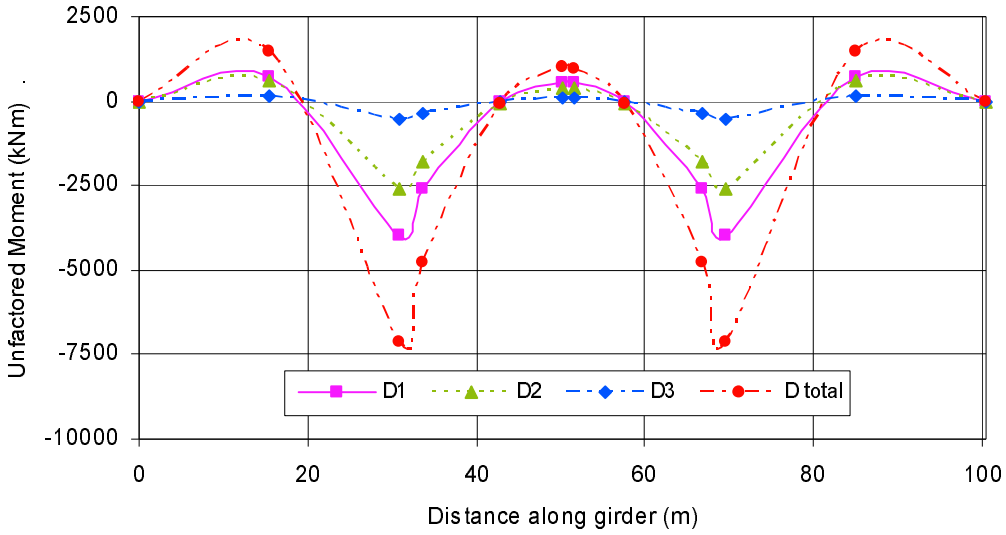

Figure 5.7. Nominal peak dead load bending moments for use in as-designed evaluations based on the mean load method.

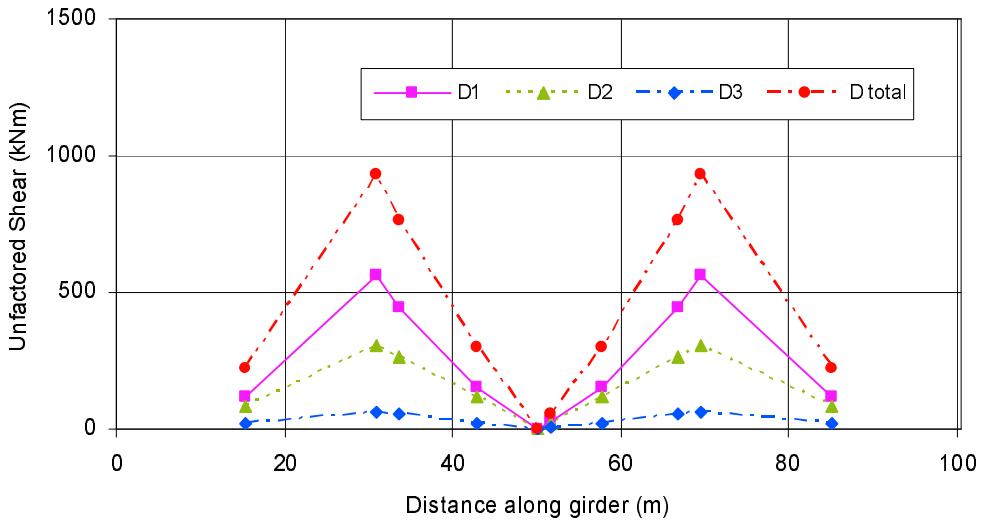

Figure 5.8. Nominal peak dead load shear forces for use in as-designed evaluations based on the mean load method.

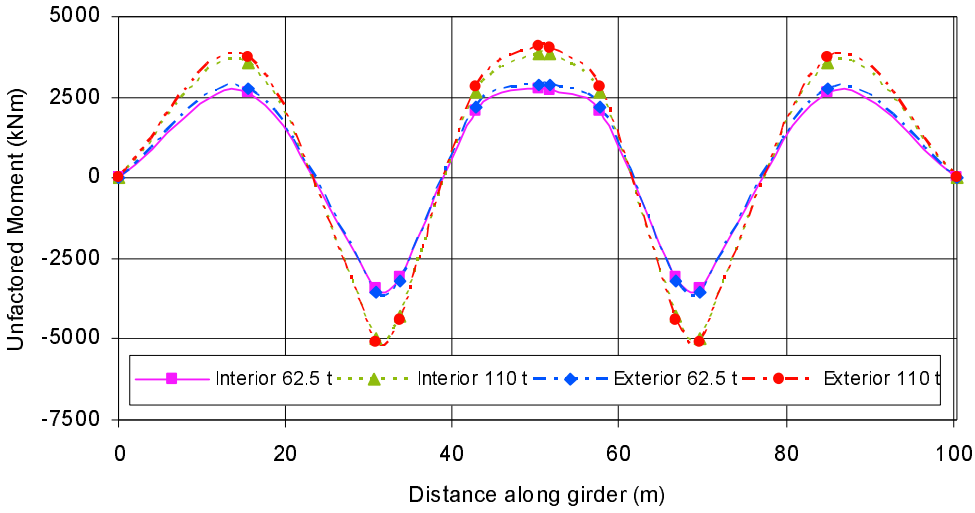

Figure 5.9. Nominal peak live load bending moments for use in as-designed evaluations based on the mean load method.

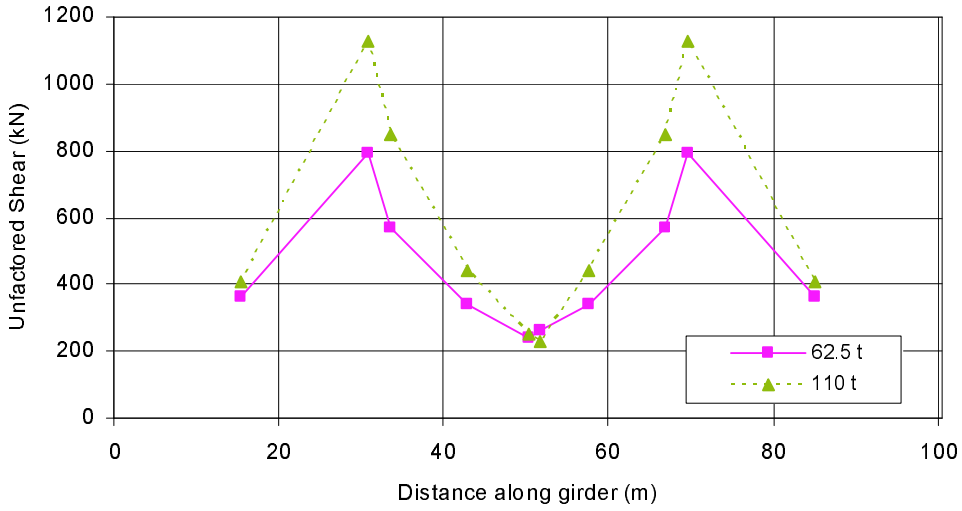

Figure 5.10. Nominal peak live load shear forces for use in as-designed evaluations based on the mean load method.

5.2.3.2 Nominal Resistance

The nominal resistance in flexure and shear were also determined for use in the mean load method, using the methodology described in Sections 4.2.3.2 and 4.2.3.3, respectively, and are presented in Figures 5.11 and 5.12.

The corresponding table can be found in Appendix D. It was observed that the nominal resistance was, on average, 13% and 36% higher than factored resistance in flexure and shear, respectively. Therefore, the "effective" resistance factor for bending was 0.89, while for shear it was 0.74.

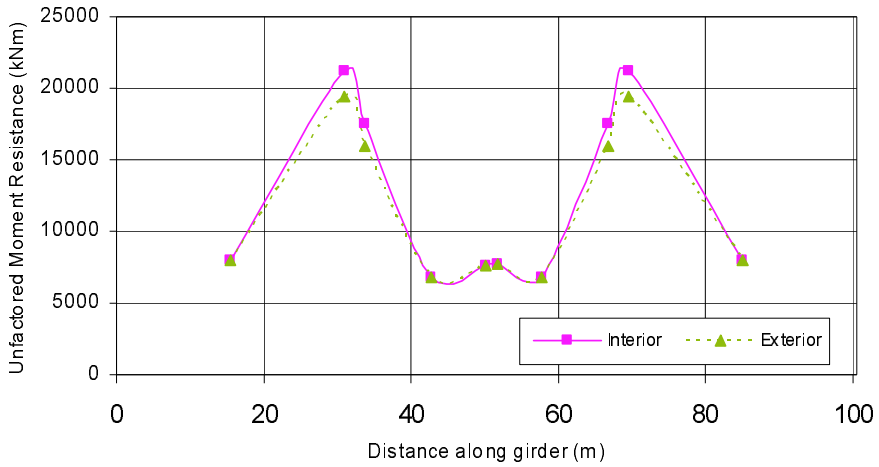

Figure 5.11. Nominal as-designed bending moment resistance for use in evaluations based on the mean load method.

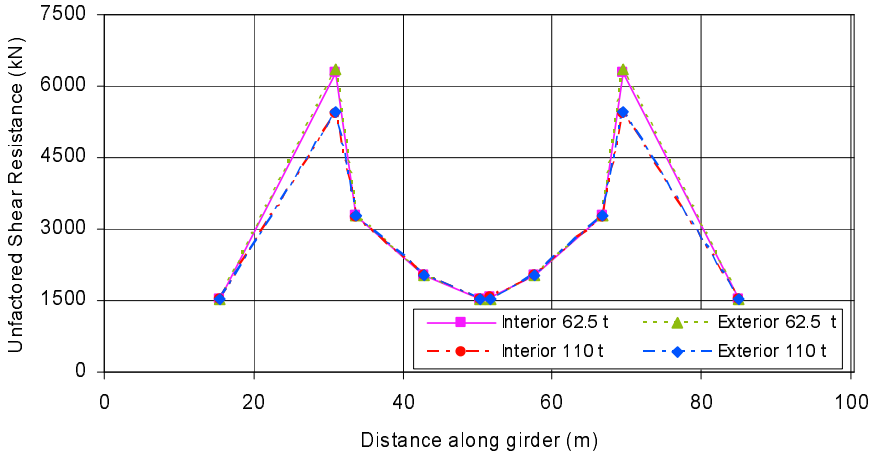

Figure 5.12. Nominal as-designed shear resistance for use in evaluations based on the mean load method.

5.2.3.3 Live Load Capacity Factors

Live load capacity factors were also determined using the mean load method, as described in Section 4.2.5.2. These are presented in Figs. 5.13 (for moment) and 5.14 (for shear) for the current and proposed design truck loading. The results are tabulated in Table D.8 in Appendix D. The resulting live load capacity factors show insufficient flexural capacity for the proposed 110 t GVW, and are also quite low near all midspan regions for bending moments. However, at the piers, the live load capacity factors are much higher, being over twice the minimum allowable value (1.00) for the worst case (110 t truck on an exterior girder).

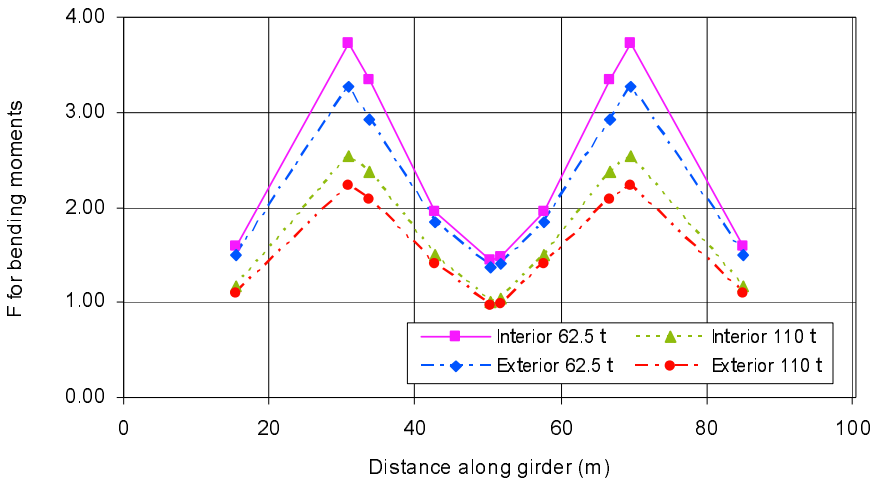

Figure 5.13. As-designed live load capacity factor for moment from the mean load method.

The live load capacity factors for shear show, to some extent, the opposite effects, being lower in the pier regions than in midspan regions, since the shear forces are highest at those locations. However, the lowest live load capacity factor occurs, not directly at the pier, but at the location of the end strain gauges. This is due to the fact that the shear forces at these locations are still relatively high, although the tapered girder section has been significantly reduced, and the stirrup spacing increased.

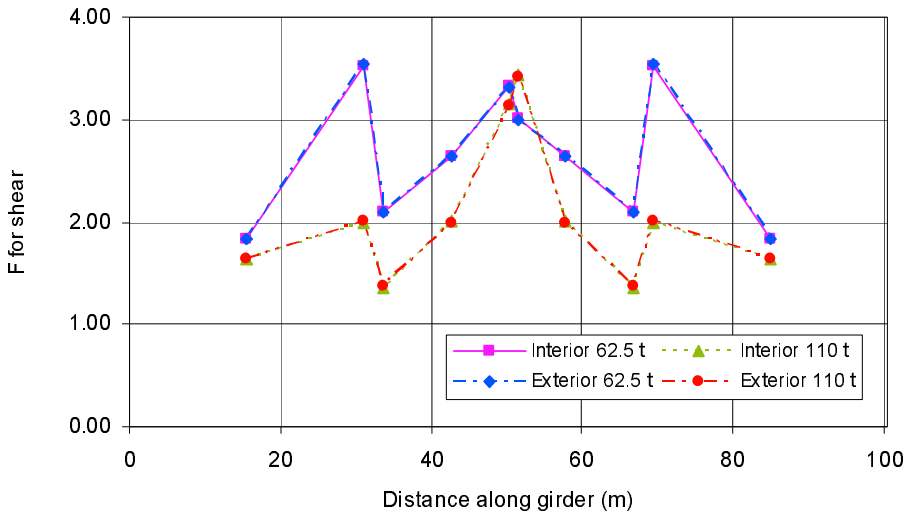

Figure 5.14. As-designed live load capacity factors for shear from the mean load method.

The minimum live load capacity factors near midspan of the exterior girders therefore fall below the minimum allowable value of 1.0, with the critical live load capacity factor being 0.96, a slight difference from the results of the load and resistance factor method (where the critical F was 1.02). The results indicate that the mean load method is somewhat more conservative than the load and resistance factor method, as comparisons of Figs. 5.13 and 5.5, and 5.14 and 5.6 show. As such, the results of the mean load method will be used in this study as the basis for comparison with the in-situ results.

As CAN/CSA-S6-00 (CSA 2000) specifies that the live load capacity factor must be at least 1.0, the as-designed mean load method analysis shows that the bridge cannot safely carry the proposed loading without remedial measures, a conclusion supported by the independent consultant's study (EarthTech 2002). Consequently, strengthening alternatives have been presented by a private consultant to increase the live load capacity factor to a value greater than 1.0 (EarthTech 2002).

5.2.3.4 Reliability Indices

Results from the mean load method of evaluation can also be used to indicate the reliability index of a bridge. For the bridge in question, the reliability indices were also determined using the methods described in Section 4.2.5.3; the results are shown in graphically in Figs. 5.15 for bending and 5.16 for shear, and are tabulated in Table D.9 in Appendix D. Minimum allowable reliability indices suggested by CAN/CSA-S6-00 (CSA 2000) for bending moment and shear are 3.0 and 3.25, respectively.

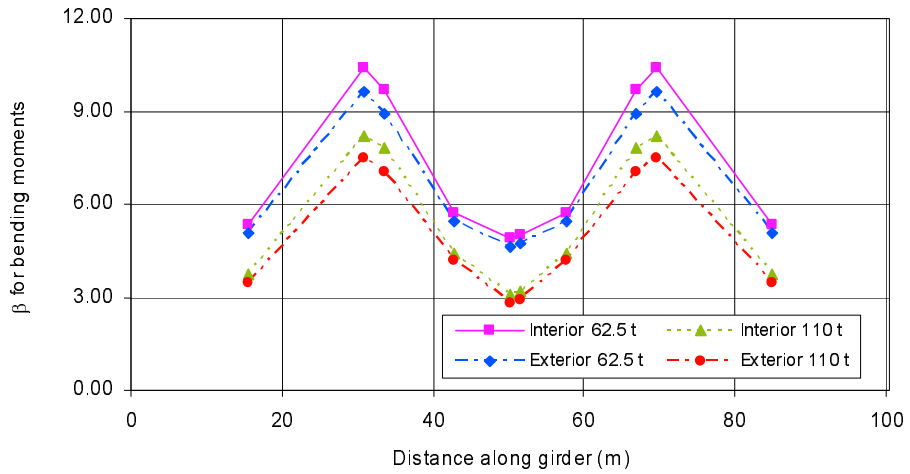

Figure 5.15. Reliability indices for bending moments based on the as-designed analysis.

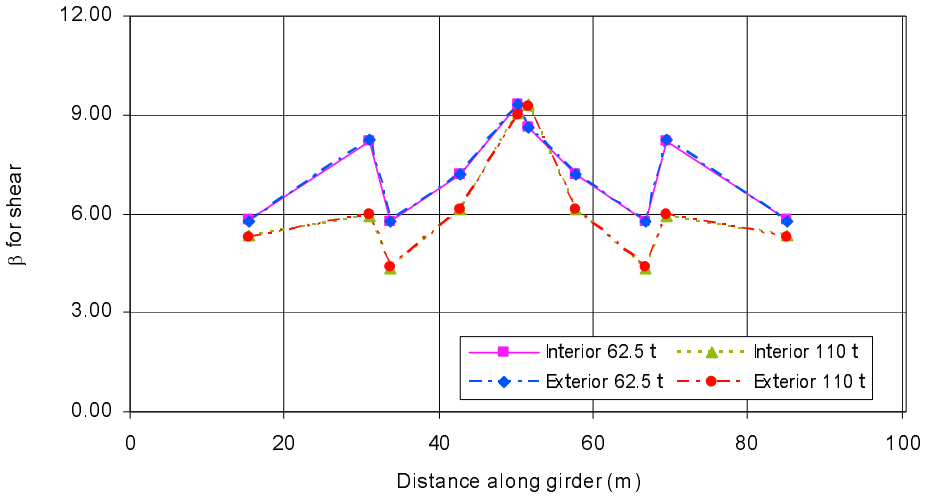

Figure 5.16. Reliability indices for shear based on the as-designed analysis.

As would be expected from the live load capacity factor results, the reliability index results also indicate that the Red Deer River Bridge will have insufficient flexural capacity to resist the moments induced by 110 t truck loading. The critical reliability index of 2.79 at midspan of the exterior girders falls below the minimum allowable, or target, reliability index of 3.0 in bending. This result also indicates that strengthening of selected girders in flexure is required to obtain an acceptable level of reliability prior to increasing GVWs.

In summary, the mean load method results were found to be more conservative than those of the load and resistance factor method in this study, although this is generally not expected to be the case since the load and resistance factor method is a simplified approach that should be more conservative. Although the bridge in question was determined to have sufficient structural capacity in shear to resist the load effect induced by the proposed truck GVW of 110 t, flexural capacity would be compromised in the midspan regions of the exterior girders in the central bridge span. The critical live load capacity factor under 110 t truck loading was found to be 0.96, less than the minimum allowable value of 1.0, with a corresponding reliability index of 2.79.

5.3 IN-SITU ANALYSIS

5.3.1 Overview

The results of the in-situ analysis, based on field measurements, are presented in the following sections. The intermediate results are presented first, followed by the resulting reliability indices, which were determined for the current allowable loading, as well as for the proposed increased loading. Similar to the as-designed analysis, in-situ evaluations were carried out for trucks travelling side by side. Results were determined for all instrument locations; however, the 1-3 gauge location was found to contain only one properly recording strain gauge, and as such, the results from this location were not used in subsequent analyses. The lower and middle gauges at the 1-3 gauge location were found to have recorded exceptionally high values of strains; it is believed that they were placed across a significant crack in the concrete, thereby measuring high local strains rather than the "average" strain in the girder at that location.

5.3.2 Measured Responses

5.3.2.1 Curvatures

The maximum measured curvatures were determined using the methods described in Section 4.3.4.3. Statistical parameters describing the curvature are presented in Table E.1 of Appendix E, while the corresponding graph is shown in Fig. 5.17. The statistical parameters are based on the peak curvatures measured for each log truck loading event, of which 28 were recorded, summarized in Table B.1 in Appendix B. From these 28 loading events, the mean and standard deviation of peak curvatures were determined for each strain gauge location on the girders. The plots show the mean curvatures at each of the strain gauge locations, represented by solid lines and

data points, while the dashed lines represent the mean curvature values, plus or minus one standard deviation.

Trends in the measured results show a generally good agreement between the three girders in magnitude. The only exception to this was seen at the gauge locations near midspan, where the 1-3 gauge location did not record any usable data; furthermore, the results from the remaining gauges near the midspan location were highly dissimilar, with girder 2 showing over seven times the measured strain as that recorded in girder 3. The results therefore generally indicated that load was well distributed among the three girders. Although variance in the data was similar in each girder, there was significant variance in the measured curvatures, with an average coefficient of variation of 0.542.

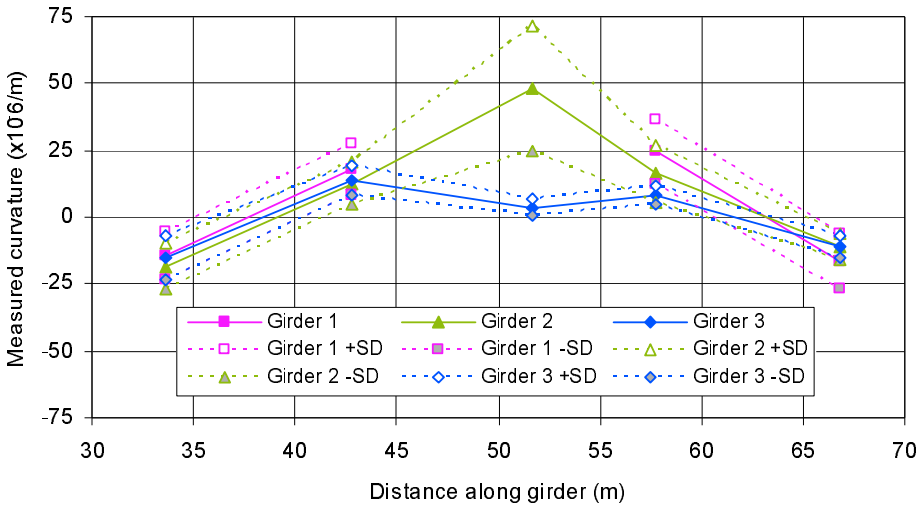

Figure 5.17. Measured curvatures in the central span girders (where SD = standard deviation).

5.3.2.2 Neutral Axis Locations

The neutral axis locations corresponding to the maximum measured curvatures were determined using the methods described in Section 4.3.4.3. Fig. 5.18 shows the height of the mean measured neutral axis location as a percentage of the girder height at that location (neutral axis height / girder

height), as well as the mean plus or minus one standard deviation, in order to illustrate the variability in the measurements. The corresponding numerical statistical parameters describing these locations, based on the 28 log truck loading events described in the previous section, are presented in Table E.2 in Appendix E.

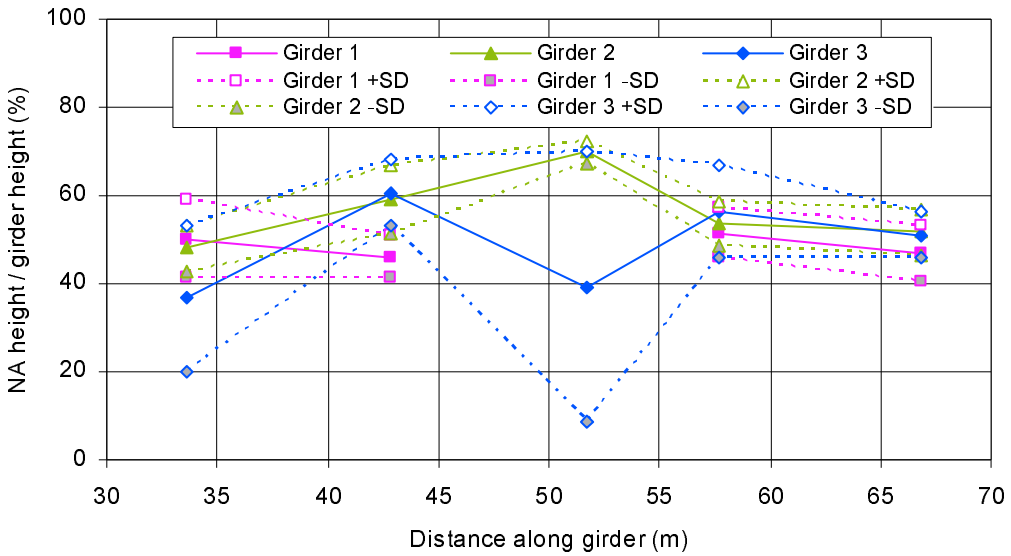

Figure 5.18. Measured neutral axis locations in the central span girders as a percentage of girder height (where SD = standard deviation).

The neutral axis locations generally showed good agreement between girders 1 and 2, although the results of Girder 3 were inconsistent with the other two girders, an indication of different load distributions between the girders. Between girders 1 and 2, there was only 6.8% difference in the average mean values, while between all three girders, there was an average difference of 10.2%. Unlike the curvature results, there was little variation in the measured neutral axis locations, with an average coefficient of variation of 0.12. This result was not unexpected, due to the fact that the neutral axis should remain relatively stationary in the service load region.

5.3.2.3 Strains

The maximum strains were determined for the bottom strain gauges at each vertical line of sensors using the methods described in Section 4.3.4.3; the results are presented in Fig. 5.19 below, and tabulated in Table E.3 of Appendix E. The statistical parameters of measured peak strains were based on 28 log truck loading events, as described in Section 5.3.2.1. The results show that the strains induced in the girders under the applied log truck loadings were very small. For all locations, the measured strains on the bottom face of the concrete were less than 2% of the strain required to yield the internal steel (nominally 0.00138), and much lower than that required to crush the concrete (nominally 0.0035). The measured strains for each girder followed a similar pattern, as shown in Fig. 5.19, although the agreement between girders was not as good as for the neutral axis location or curvature, with an average difference of 80% between the three girders. The measured variance was substantial, with an average coefficient of variation of 0.574 at the instrumented locations.

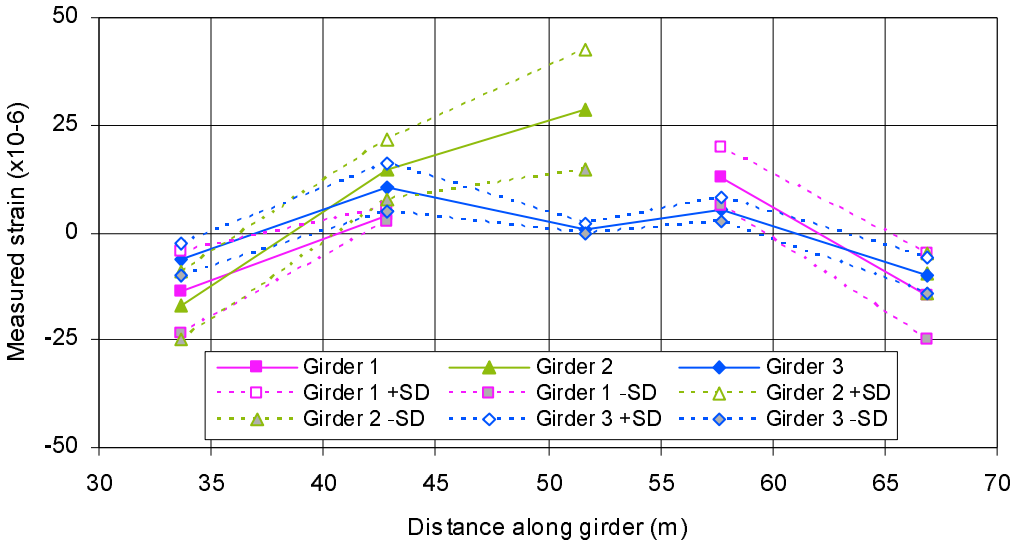

Figure 5.19. Measured strains in the lower strain gauges in the central span girders (where SD = standard deviation).

5.3.3 In-Situ Concrete Properties

The ultimate compressive strength of the concrete, f'_c, in the Red Deer River Bridge deck was determined using the rebound hammer test results. It was assumed that concrete strength in bridge girders was similar. As part of this evaluation, a calibration procedure for the rebound hammer was carried out, as described in Section 4.3.3. The results of the rebound hammer calibration are shown in Fig. 5.20. The discrete data points on this plot represent the measured values of ultimate concrete strength versus the average rebound hammer number reading for each cylinder tested. The thicker solid line represents the best-fit extrapolated line corresponding to the measured data points, which was subsequently used in determining the ultimate concrete strength at the bridge site. Also included for comparison are curves determined in another study (Lee 1978), as well as the curve provided by the manufacturer of the rebound hammer. It is evident that there is little correlation between the published manufacturer's curve and the measured data, demonstrating the need for careful, project specific calibration. The measured curve does, however, correlate well with those curves determined in the previous study by Lee (1978).

Based on the best-fit curve in Fig. 5.20, the ultimate compressive strengths of concrete in the bridge in question were determined from rebound hammer readings taken on site, as discussed in Section 3.3.3. It was determined that the in-situ ultimate compressive strength of concrete in the bridge deck had an average measured value of 41.7 MPa, with a standard deviation of 4.4 MPa, over twice that specified on the design drawings of the bridge, which was 20.7 MPa (3000 psi). It should be noted that the standard deviation of the ultimate compressive strength represents the scatter in the measured results only, and does not include the variability from the calibration process.

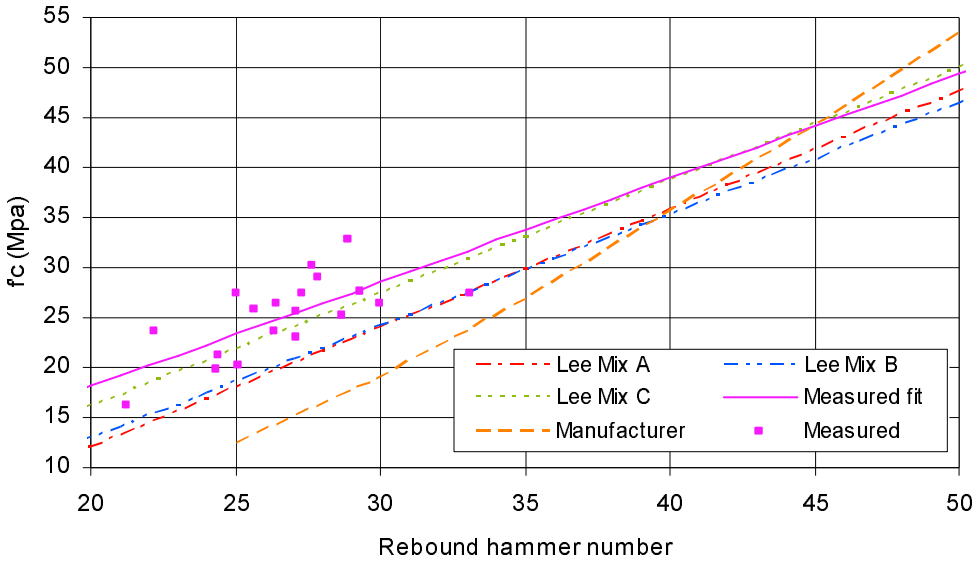

Figure 5.20. Rebound hammer calibration.

5.3.4 Load Effects Determined from Field Measurements

5.3.4.1 Bending Moments and Axial Forces

Measured bending moments were determined by two methods: using the measured extreme curvatures, as described in Section 4.3.5.1, and using the measured instantaneous neutral axis locations along with the corresponding measured strain in the lower gauges, as described in Section 4.3.5.2. Use of the latter method also allowed for the determination of axial forces within the girders.

Bending Moment Based on Measured Curvatures

The bending moments determined from the measured curvatures were found to be very small, relative to results predicted based on a flexural analysis of the girders (see Section 5.2.3.1). The measured statistical parameters of bending moments determined from measured curvatures are presented in Table 5.1. It should be noted that the mean values and standard deviations of

bending moments presented in the first three columns of Table 5.1 were found for one truck only; therefore, corresponding mean values for two lane loading are also presented in the right-most column of the table. The mean results for two lane loading were very small, ranging from 1% to 29% of the unfactored bending moments determined in the as-designed analysis, as presented in Fig. 5.9 (and tabulated in Table D.6). However, the variation in measured bending moments was high, with an average coefficient of variation of 0.398, due to variation of the variables contributing to the bending moment analysis described in Section 5.3.2, although the measured curvature contributed the most variability.

Table 5.1. Estimated in-situ bending moments based on measured curvatures.

Girder	SG Location	Mean Moment (kNm)	Standard Deviation of Moment (kNm)	Coefficient of Variation	Mean 2xMoment (kNm)
1	1-1	-336.6	222.4	0.661	-673.2
	1-2	101.4	29.3	0.289	202.8
	1-3	240	112.6	0.469	480
	1-4	136.9	37.8	0.276	273.8
	1-5	-384.6	250.1	0.650	-769.2
2	2-1	-453.5	210.6	0.464	-907
	2-2	117.1	33.4	0.285	234.2
	2-3	234.5	59.6	0.254	469
	2-4	94.2	33	0.350	188.4
	2-5	-293.1	132.7	0.453	-586.2
3	3-1	-355.4	206.4	0.581	-710.8
	3-2	80.1	17.5	0.218	160.2
	3-3	20.5	8.1	0.395	41
	3-4	47.2	10.6	0.225	94.4
	3-5	-274.2	110.7	0.404	-548.4

Bending moment diagrams were generated for each girder by placing best-fit lines through the measured bending moment data points for two lane loading at the strain gauge locations. The diagrams for bending moments determined by curvatures are shown in Fig. 5.21, with the measured bending moments shown as discrete data points on the graph. The agreement between

bending moments in the three girders at the strain gauge locations can be clearly seen on Fig. 5.21, although the middle strain gauge location on Girder 3 shows some discrepancy, as the bending moments in Girder 1 and 2 are over ten times that of Girder 3.

Fig. 5.22 shows the theoretical bending moments for two trucks for the central span girders, based on flexural behaviour. It can be seen that the bending moments determined from the measured strains were much smaller than those determined theoretically in the as-designed analysis. Using girder 1 as an example, the ratio between the theoretical and measured bending moments was over 27 at the middle strain gauges (where the positive moment is near maximum), and over 18 at the end north end strain gauges (where the negative moment is near the maximum). Also noteworthy is the fact that the magnitudes of positive and negative theoretical bending are similar. However, the magnitudes of the measured positive bending moments are much smaller than the negative bending moments (less than one-third the magnitude for girders 1 and 2), suggesting that some other mechanism besides pure bending may be at work.

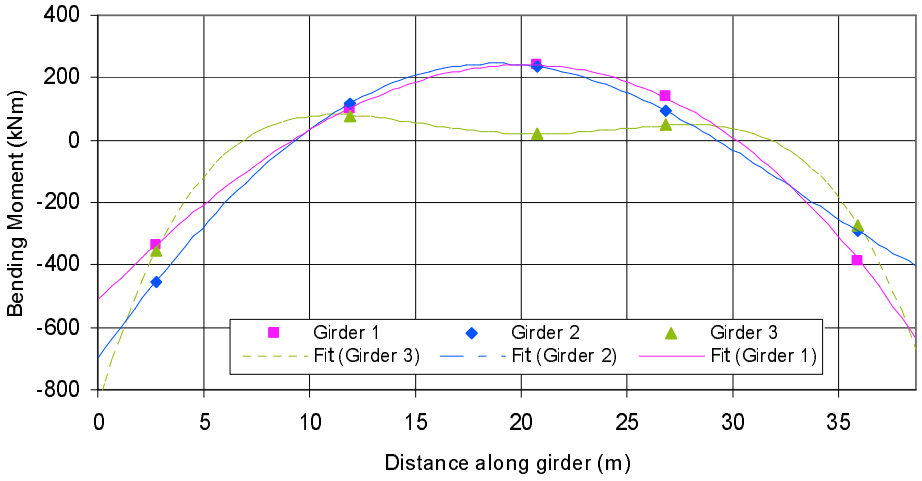

Figure 5.21. Bending moment distribution in the girders of the central span derived from measured curvatures.

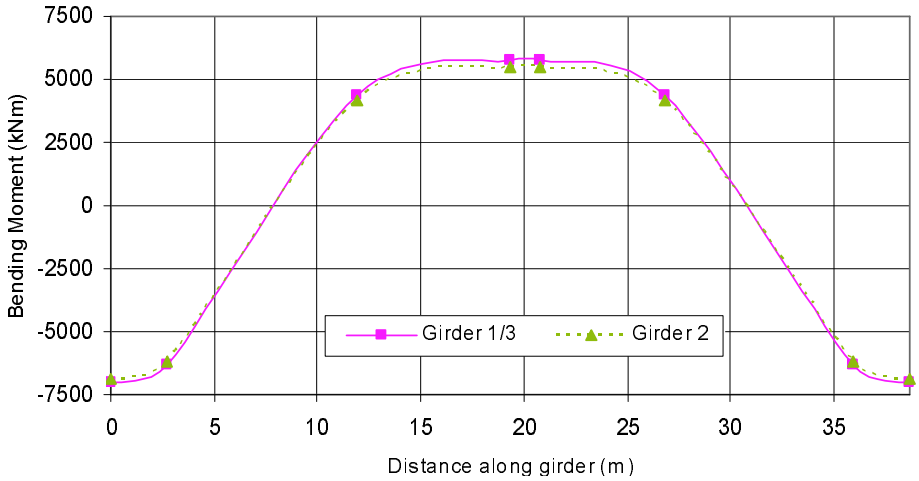

Figure 5.22. Bending moment distribution in the girders of the central span determined in the as-designed analysis.

The distribution of maximum bending moments along girder 3 suggests that arching action, rather than flexure, may be the dominant mechanism of load transfer. This is clearly illustrated in Fig, 5.23, which shows the bending moment distribution in a circular arch subjected to uniform loads, generated using a finite element computer program. The arch was pinned at the center, as the pinned analogy provided a better representation of the observed in-situ behavior, disallowing moment transfer across the pin. Positive bending (tension at bottom) is shown as a solid area, while negative bending is shown as broken segments. Particularly striking is the similarity between the bending moments in the arch and the distribution seen for girder 3 in Fig. 5.21.

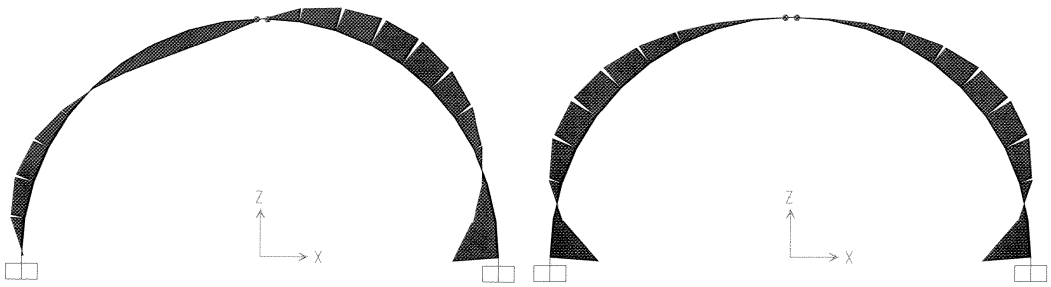

Figure 5.23. Bending moment distribution in an arch subjected to uniform vertical loads: a) load on one side of arch (left), and b) load over entire arch.

Bending Moment Based on Measured Neutral Axis Locations and Strains

The bending moments determined using the measured neutral axis locations and the measured strains (see Section 4.3.5.2), are summarized in Table 5.2. In general, the values were found to be comparable to those determined using the measured curvatures, but were 12% lower on average. As with the curvature-based values, the measured bending moments for two lane loading ranged from 1% to 30% of the unfactored bending moments determined from the as-designed analysis. The average coefficient of variation for the measured bending moments was 0.578, also comparable to that determined using the measured curvatures. Differences between the bending moments determined by the two different methods may be attributed in part, to the filtering process, as described in Section 4.3.4.1. Although the filtering methodology was the same, outlying values (outside of two standard deviations) may have been different for curvatures than for neutral axis locations.

Table 5.2. Estimated bending moments based on measured neutral axis locations and strains.

Girder	SG Location	Mean Moment (kNm)	Standard Deviation of Moment (kNm)	Coefficient of Variation	Mean 2xMoment (kNm)
1	1-1	-340.9	196	0.575	-681.8
	1-2	48.7	21	0.431	97.4
	1-3	207.7	106.3	0.512	415.4
	1-4	128	63.6	0.497	256
	1-5	-385.8	210	0.544	-771.6
2	2-1	-464.1	169.5	0.365	-928.2
	2-2	121.1	56.8	0.469	242.2
	2-3	179.5	75.7	0.422	359
	2-4	43.1	18.1	0.420	86.2
	2-5	-262.3	109.8	0.419	-524.6
3	3-1	-248.7	188.6	0.758	-497.4
	3-2	85.8	43.8	0.510	171.6
	3-3	18.7	34.5	1.845	37.4
	3-4	49.8	26.7	0.536	99.6
	3-5	-253.7	94	0.371	-507.4

The estimated two-lane loading bending moment distributions determined using measured neutral axis locations and strains at the lowest gauge are shown in Fig. 5.24. The diagrams are similar to those determined using curvatures, as shown in Fig. 5.21. Once again, near-zero bending moments near midspan in girder 3 can also be observed.

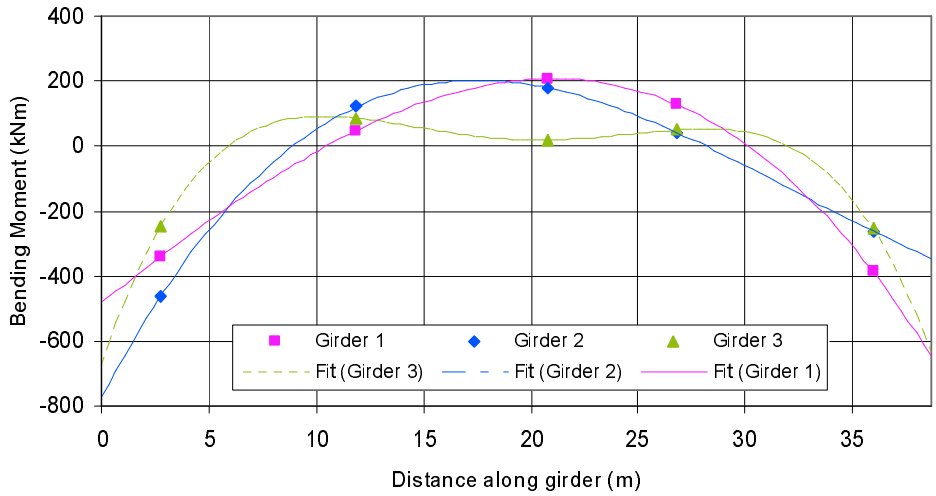

Figure 5.24. Bending moment distributions in the girders of the central span derived from measured neutral axis locations and strains

Resultant Axial Forces

Resultant axial forces in the girders, shown in Table 5.3, were also calculated when the neutral axis location and strain in the bottom strain gauge were used to estimate the measured bending moments, as described in Section 4.3.5.2. The measured axial forces in the girders were significant (as large as 875 kN for single truck loading), as can be seen from Table 5.3, which also shows the estimated axial forces for the two-lane loading case. Although the axial forces were not perfectly symmetrical about the midspan of the central span, there was a general trend of increasing axial forces nearer to the supports, shown in Fig. 5.25. Although axial force should increase near supports as the physical shape of the girder becomes inclined to a steeper angle, the horizontal component should remain constant. Although the

magnitudes of the resultant forces in girders were significant, the measured forces for the two-truck load case were on average only 3.6% of the axial load if the sections were under uniform compression at crushing, values for which are shown in the rightmost column of Table 5.3. It should be noted, though, that in this study the three strain gauges at each instrumentation location were installed along a vertical line, rather than perpendicular to the curved centroidal axis of the girders. Thus, the measured axial force is an approximation of the actual axial force occurring.

Use of conventional flexural theory, on the other hand, effectively precludes the existence of significant axial forces if the supports are truly pinned, as typically assumed. Obviously, this was not borne out by the measured responses, casting doubt on the strict applicability of the flexural model in this case.

Table 5.3. Axial forces derived from measured neutral axis locations and strains.

Girder	SG Location	Mean Axial Load (kN)	Standard Deviation of Axial Load (kN)	Coefficient of Variation	Mean 2xAxial Load (kN)	Axial Load at Crushing (kN)
1	1-1	-816	361	0.442	-1632	-35077
	1-2	-280	130.9	0.468	-560	-22946
	1-3	-417.9	189.9	0.454	-835.8	-19913
	1-4	-641.1	336.7	0.525	-1282.2	-22946
	1-5	-811.9	310.5	0.382	-1623.8	-35077
2	2-1	-874.7	225.9	0.258	-1749.4	-35286
	2-2	-508	278.1	0.547	-1016	-23207
	2-3	-419.8	120.6	0.287	-839.6	-20173
	2-4	-463.5	167.7	0.362	-927	-23207
	2-5	-617.5	218.7	0.354	-1235	-35286
3	3-1	-402.6	189.9	0.472	-805.2	-35077
	3-2	-348.4	204.2	0.586	-696.8	-22946
	3-3	-97	218.9	2.257	-194	-19913
	3-4	-229.1	153.7	0.671	-458.2	-22946
	3-5	-649.1	202.7	0.312	-1298.2	-35077

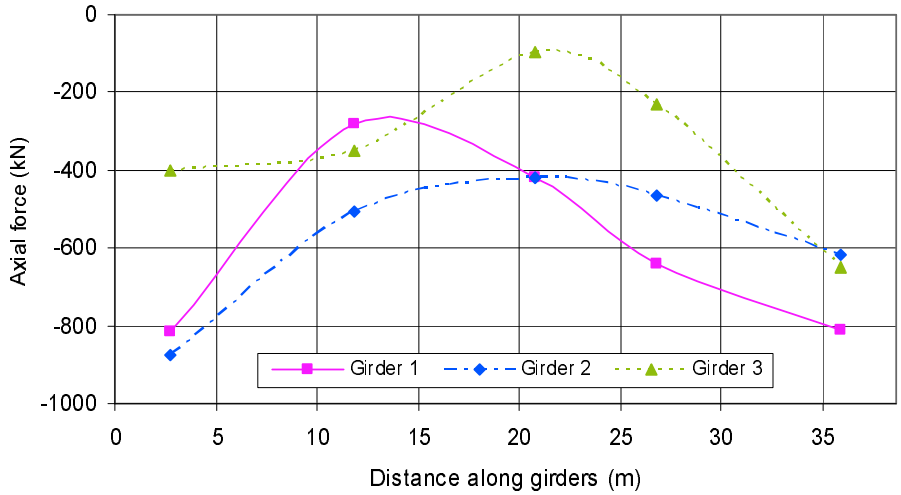

Figure 5.25. Axial force distributions in the girders of the central span derived from measured neutral axis locations and strains.

The arching action suggested by the axial forces present in the girders can develop only if there is some form of horizontal restraint at the girder supports. Although the bearings on the bridge in question were designed to allow free movement horizontally, it is possible that some amount of corrosion or other environmental factor (such as an accumulation of debris) has caused full or partial bearing seizure over the lifetime of the bridge, thereby restricting lateral translation. Alternatively, the necessary horizontal restraint may have developed through tension-tie action of the internal and external reinforcing along the bottom face of the girders. Furthermore, the girders are physically tapered into an arched form, further encouraging the development of arching forces.

The apparent arching action would increase the potential capacity of the girders substantially by providing an alternate mechanism to flexural behaviour for load transfer. Since the flexural capacity has been cited as the limiting factor restricting an increase in allowable loads, the results of this study suggest that the need for flexural reinforcing may not be as great as suggested by conventional analysis techniques.

5.3.4.2 Shear

Shear Based on Measured Curvatures

In addition to bending moments and axial forces in the girders, peak shear forces were also determined, using the methods described in Section 4.3.6. The shear forces determined from measured curvatures are presented in Table 5.4. The measured shear forces were significantly smaller than those determined in the as-designed analysis, shown in Table D.6 in Appendix D, ranging from less than 1% to 32% of the theoretical shear forces for two-lane loading. The variability of these results, however, was high, with an average coefficient of variation of 0.4. The shear force diagrams derived from measured curvatures are shown in Fig. 5.26; here, the shear forces at instrument locations are shown as discrete data points, while the associated lines show the shear diagrams developed on the basis of the bending moment diagrams presented in Section 5.3.4.1.

Although the distribution of peak shear force in girders 1 and 2 is relatively linear, as expected based on flexural theory, the observed results for girder 3 were distinctly non-linear. Once again, this is likely due to the apparent arching action discussed previously.

Table 5.4. Estimated peak shear force based on measured curvatures.

Girder	SG Location	Mean Shear (kN)	Standard Deviation of Shear (kN)	Coefficient of Variation	Mean 2xShear (kN)
1	1-1	61.2	40.5	0.662	122.4
	1-2	32.9	9.5	0.289	65.8
	1-3	-2.99	1.4	0.468	-5.98
	1-4	-32.1	8.85	0.276	-64.2
	1-5	-83.5	54.3	0.650	-167
2	2-1	84.4	39.2	0.464	168.8
	2-2	38.9	11.1	0.285	77.8
	2-3	-8.72	2.22	0.255	-17.44
	2-4	-31.3	11	0.351	-62.6
	2-5	-36.1	16.3	0.452	-72.2
3	3-1	135.8	78.9	0.581	271.6
	3-2	-3.74	0.82	0.219	-7.48
	3-3	0.19	0.07	0.368	0.38
	3-4	3.13	0.7	0.224	6.26
	3-5	-109.5	44.2	0.404	-219

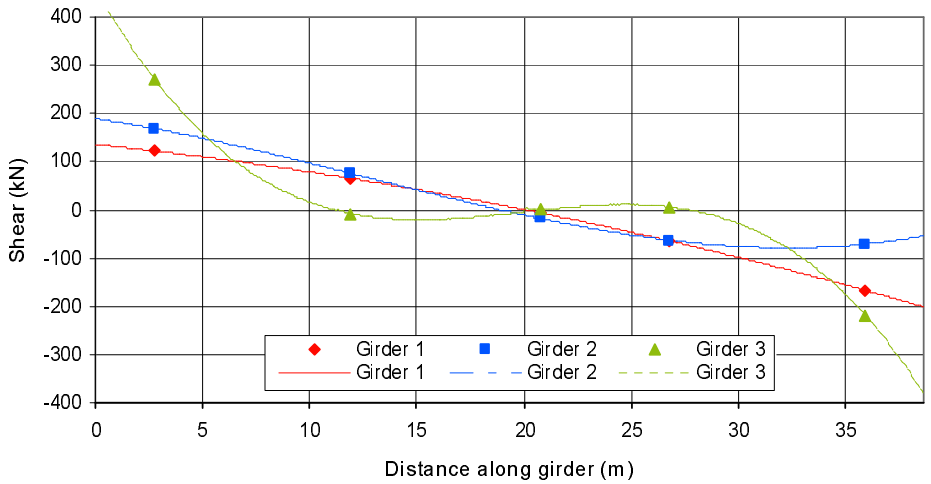

Figure 5.26. Estimated shear distributions based on measured curvatures.

Shear Based on Measured Neutral Axis Locations and Strains

The shear forces determined using the neutral axis locations and the strains at the bottom gauge, as presented in Table 5.5, were comparable to those determined using curvatures, with less than 10% difference on average for two-lane loading. The shear distributions generated using neutral axis locations and strains in the bottom gauge are shown in Fig. 5.27. Although there was significant variation, with an average coefficient of variation of 0.59, the shear forces were small, ranging from 1% to 27% of those determined in the as-designed analysis.

Table 5.5. Estimated shear forces based on measured neutral axis locations and strains.

Girder	SG Location	Mean Shear (kN)	Standard Deviation of Shear (kN)	Coefficient of Variation	Mean 2xShear (kN)
1	1-1	50	30.6	0.612	100
	1-2	32.6	14.2	0.436	65.2
	1-3	0.97	0.5	0.515	1.94
	1-4	-28.6	14.5	0.507	-57.2
	1-5	-86.5	50.3	0.582	-173
2	2-1	101.3	39.8	0.393	202.6
	2-2	30.5	14.5	0.475	61
	2-3	-13.5	5.7	0.422	-27
	2-4	-29.7	12.5	0.421	-59.4
	2-5	-33.1	14.6	0.441	-66.2
3	3-1	114.3	86.7	0.759	228.6
	3-2	-7.05	3.6	0.511	-14.1
	3-3	2.5	4.61	1.844	5
	3-4	8.38	4.49	0.536	16.76
	3-5	-94.7	35.1	0.371	-189.4

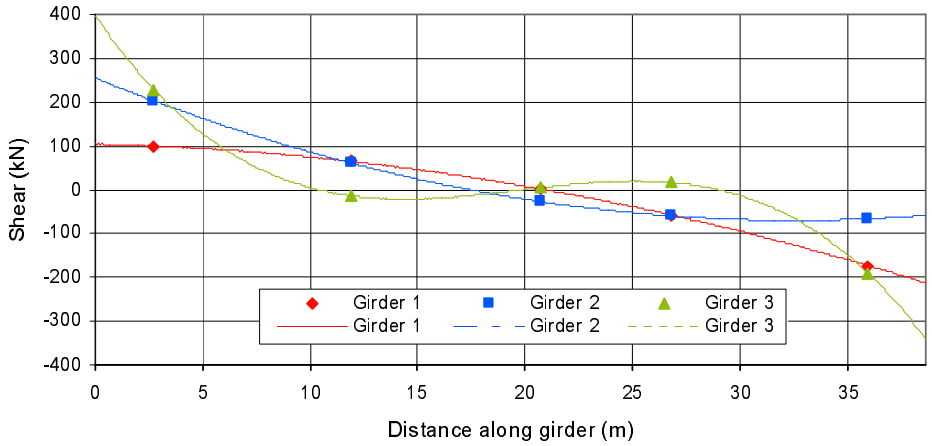

Figure 5.27. Estimated shear distributions based on measured neutral axis locations and strains.

5.3.5 Factors Determined from Field Measurements

5.3.5.1 Distribution Factors

Distribution Factors for Bending Moments

Distribution factors, describing how flexural load effects are shared between the girders, were determined for flexure based on both measured curvatures and neutral axis locations in conjunction with strains in the bottom strain gauges, using the methodology presented in Section 4.3.7.1. The distribution factors for bending moments determined using curvatures are presented in Fig. 5.28 (corresponding to Table E.4 in Appendix E), while those determined using neutral axis locations and strains in the bottom gauges are presented in Fig. 5.29 (corresponding to Table E.5 in Appendix E). The distribution factors shown are for two-lane loading; in addition, the factors determined in the as-designed analysis using CAN/CSA-S6-00 (CSA 2000) are shown for comparison.

The results of both flexural distribution factor analyses show that the measured distribution factors were considerably different than those determined in the as-designed analysis. There was little consistency along the lengths of the girders; the amount of load apparently carried by each girder varied significantly along its length. Furthermore, there is inconsistency between the resulting distribution factors determined using the measured curvatures, and those determined using the measured neutral axis locations and strains in the bottom strain gauges. The apparent inconsistencies in distribution factors may be due to the low levels of flexural response measured relative to the corresponding level of variability. It should be noted, though, that the distribution factor concept inherently presumes that flexure is the dominant load carrying mechanism. For cases with significant arching action, the flexural distribution factors are no longer an accurate indication of load distribution between girders.

Only two trends may be noted from the results: girder 3 carried very little load in flexure near midspan as a result of the previously discussed arching action, and the distribution factors are the most similar in the negative bending moment regions at the end strain gauge locations (they would be equal if all three girders shared the load evenly). The sum of all measured distribution factors must total 1.0 for single lane loading (2.0 for two-lane loading); thus, each distribution factor across the three girders at a given longitudinal location indicates the fraction of load carried by that girder at a particular location. It should be noted, however, that it would be impossible to measure distribution factors that were precisely consistent with those determined in the as-designed analysis, as the sum of the code-specified values is greater than 2.0 for two-lane loading.

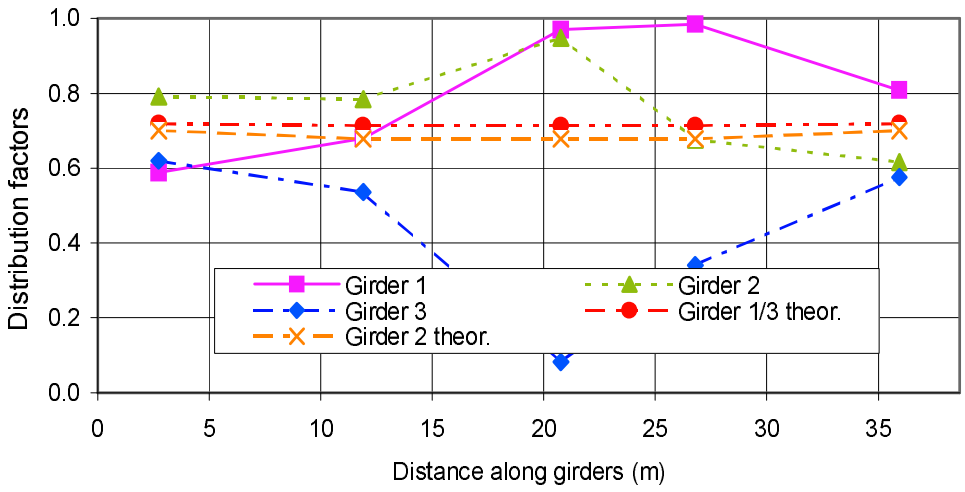

Figure 5.28. Approximate bending moment distribution factors based on measured curvatures.

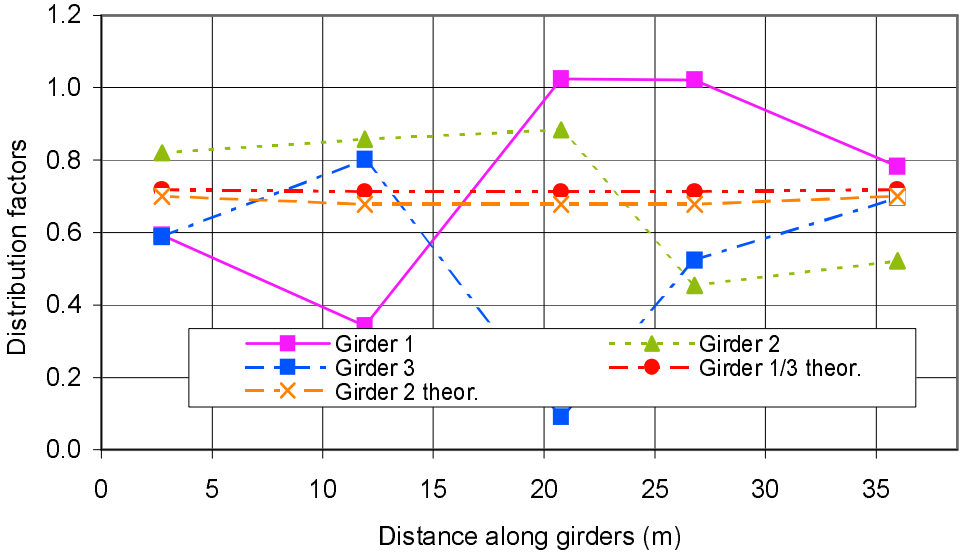

Figure 5.29. Approximate bending moment distribution factors based on measured neutral axis locations and strains.

Distribution Factors for Shear

Distribution factors were also determined for shear, using both measured curvatures and measured neutral axis locations with strains from the bottom gauges, based on the methods described in Section 4.3.7.1. The distribution

factors for shear determined using measured curvatures are presented in Fig. 5.30 (tabulated in Table E.6 in Appendix E), while those determined using measured neutral axis locations and strains in the bottom gauges are presented in Fig. 5.31 (tabulated in Table E.7 in Appendix E). The shear distribution factors resulting from both analyses were very different than the two-lane value of 0.719 determined in the as-designed analysis at nearly every location. The distribution factors from measured values at the middle strain gauge location on the girder 2 was very large, having a magnitude of approximately 1.5, or about twice that determined theoretically. As a result, the middle strain gauge locations on the remaining two girders were considerably smaller (recall that the sum must be 2.0 for two lane loading). However, as with bending moment, it should be noted that the theoretical distribution factors represent envelopes of possible values totalling greater than 2.0 and, therefore, cannot be exactly replicated using field measurements.

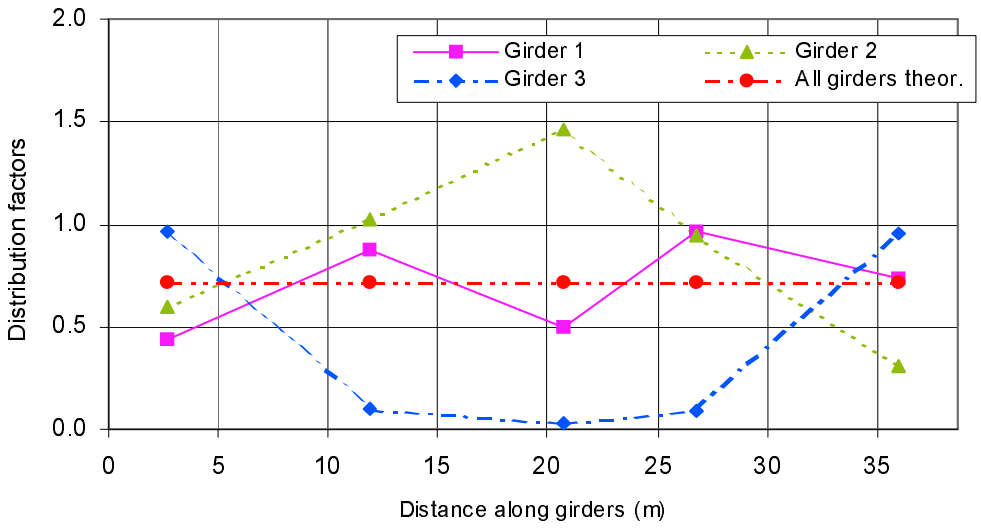

Figure 5.30. Approximate shear distribution factors based on measured curvatures.

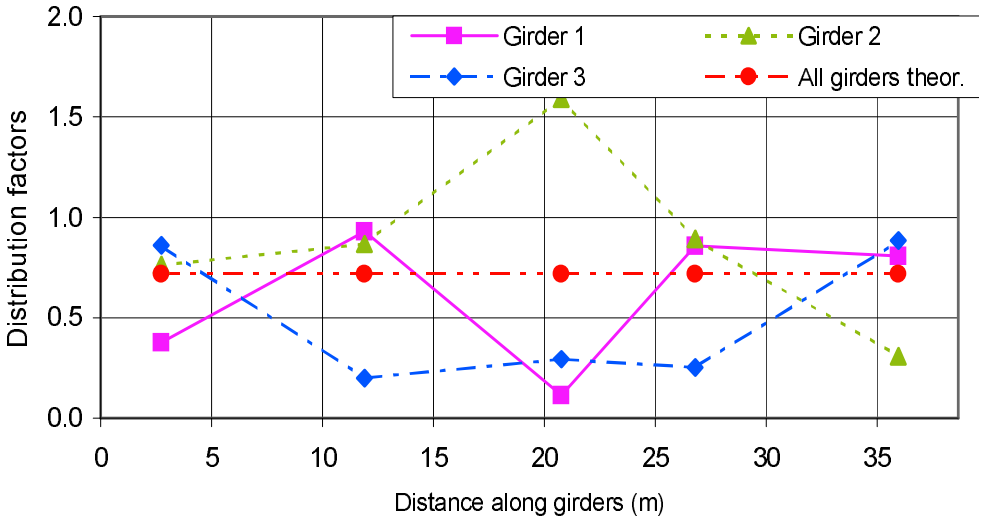

Figure 5.31. Approximate in-situ shear distribution factors determined using measured neutral axis locations and strains.

The distribution factors determined using measured data for both flexure and shear clearly demonstrate that load is shared much differently among bridge girders than is predicted by the distribution factors determined using CAN/CSA-S6-00 (CSA 2000). The estimates of distribution factors in this study were found to be both higher and lower than the code-predicted values, indicating the necessity for more accurate site-specific data when potential increased loading is being considered. However, the use of distribution factors implies that flexure is the dominant load carrying mechanism, whereas arching appears to be more important in this case.

5.3.5.2 Dynamic Load Allowance

The measured dynamic load allowance (DLA) for the bridge was determined using the methods described in Section 4.3.7.2. Statistical parameters for the DLA were estimated based on the peak strains measured in the bottom strain gauges for the 28 log truck loading events summarized in Table B.1 in Appendix B. Measurements from all the lower strain gauge locations for all the loading events were then used collectively to estimate a

single DLA for the bridge, rather than estimating it at each instrumentation location.

The average measured ratio of dynamic to static loading at the 13 measurement locations (locations 1-3 and 2-4 were excluded as they were not functioning correctly) was found to be 0.925, for a DLA of -0.075, significantly less than the CAN/CSA-S6-00-prescribed value of 0.25 (CSA 2000); individual measured ratios of dynamic to static loading ranged from -0.21 to 15.58, and ranged from -0.21 to 8.25 after outlying values were removed. A negative DLA signifies that the bridge response induced by a load applied dynamically was actually less than that induced by comparable pseudo-static (slowly applied) loading. Although the coefficient of variation was 0.619, it was still considerably lower than the value of 0.8 used in the as-designed analysis; however, both measured and code values reflect the considerable uncertainty in this variable.

The negative measured DLA was contradictory to what is generally understood of dynamic load effects, which are commonly found to induce a greater response than similar static load effects. One possible theory for a negative DLA is that the effective pulse time, or the time over which the fast moving truck load acts on the bridge, is very small. Although the log trucks were on the bridge for a considerable length of time, the time at a critical location for a given load effect was very short. The influence of a short impulse is illustrated in Fig. 5.32, which shows the relationship between the dynamic load factor (DLF) (ratio of dynamic to static response) and the ratio of impulse duration, t_p, to the fundamental period of the structure, T_o; in this context, DLA = DLF-1. The fundamental frequency of the bridge in question was measured to be 2.48 Hz in a related study carried out by Alwash et al. (2005). Thus, a pulse time of approximately 0.06 s would be expected to generate the observed DLA of -0.075.

For fundamental frequencies in the range of 2.5 Hz to 4.5 Hz, CAN/CSA-S6-00 (CSA 2000) suggests that the DLA is typically at its highest value of 0.4

(see Fig. 5.33). Cantieni (1984) reached similar conclusions, stating that bridges with fundamental frequencies between 2.5 Hz and 4 Hz will have DLA's up to 0.8.

Although it was found that dynamic load effects were smaller than the corresponding static load effects, there remains the possibility that trucks could stop, or slow to a crawl speed on the bridge in question, resulting in higher than measured load effects. Thus, a more conservative DLA value of 0.0 was assumed for subsequent analyses, although the measured coefficient of variation was utilized. It should be noted that the DLA is significantly influenced by factors such as road roughness and vehicle dynamics, and is therefore subject to change with driving conditions and different vehicles. Dynamic load effects are investigated further numerically in Section 5.3.8.2.

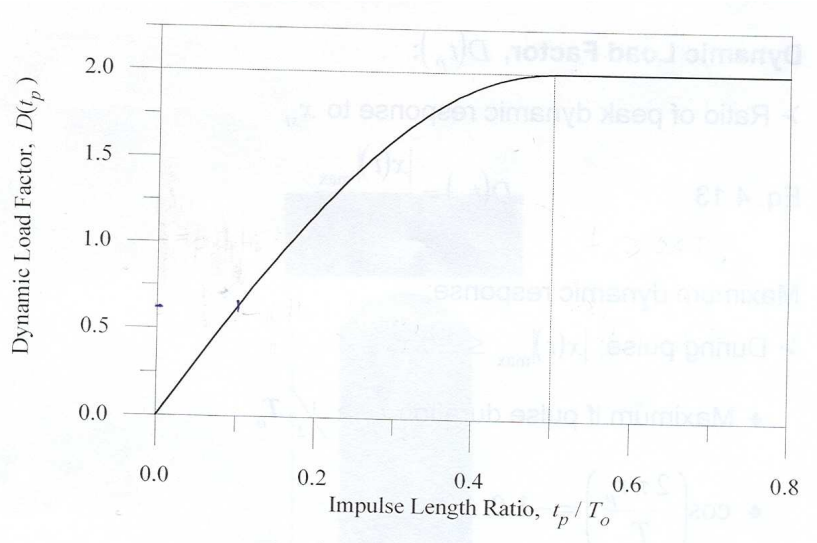

Figure 5.32. Dynamic amplification of impulse load response as a function of impulse time and fundamental period (taken from Sparling 2005).

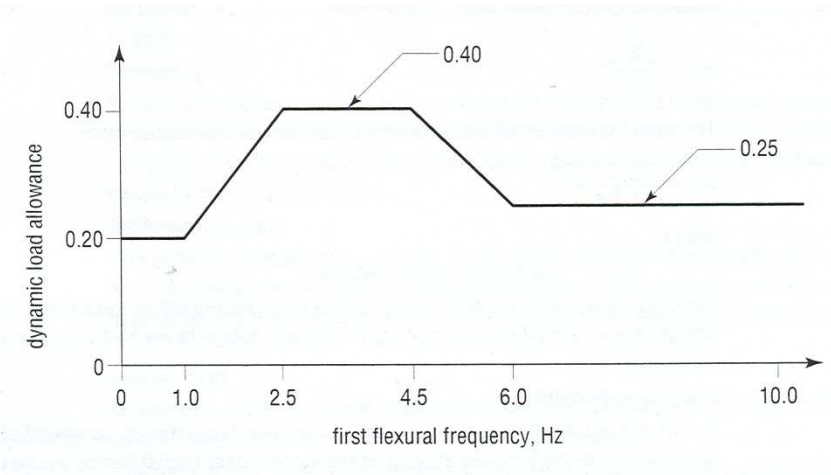

Figure 5.33. Dynamic load allowance vs. frequency relationship (taken from CSA 2000).

5.3.6 Resistance Determined using Field Measurements

5.3.6.1 Bending Moment Resistance

In order to provide an improved estimate of actual bending moment resistance, a conventional theoretical analysis (see Section 4.2.3.2), based on strain compatibility and rectangular Whitney stress block parameters was carried out using the measured ultimate compressive strength of concrete, as well as statistical parameters representative of in-situ material and sectional properties (see Section 4.2.5.1). Estimated bending moment resistance values, M_r, calculated on this basis are provided in Fig. 5.34, which also shows the bending moment resistances determined in the as-designed analysis for comparison purposes. Corresponding numerical values can be found in Table E.8 in Appendix E.

In-situ flexural resistance estimates were considerably increased over the as-designed resistance estimates, with observed increases ranging from 18% (at the end strain gauge location) to 37% (at the second strain gauge location). The measured coefficients of variation remained the same, on

average, as those assumed in the as-designed analysis (0.12), for cases where the reinforcing ratio was high (over 70% of the balanced reinforcing ratio). Where the reinforcing ratio was lower (see Section 4.2.4.5), the as-designed coefficients of variation were smaller than the average measured value.

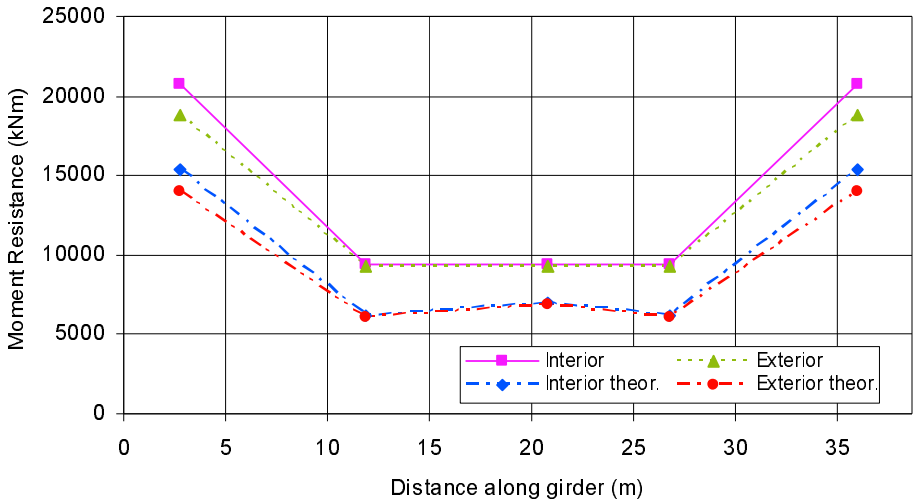

Figure 5.34. Estimated in-situ bending moment resistances using site-specific parameters.

5.3.6.2 Shear Resistance

Shear resistance was also re-evaluated using the site-specific data along with the statistical distributions obtained from the literature, based on the methods described in Section 4.3.8.2. As shear resistance is dependent upon the load effects, different shear resistances were obtained for the current allowable loading and the proposed increased loading, as shown in Figs. 5.35 and 5.36, respectively (tabulated results are available in Tables E.9 and E.10 in Appendix E). Also shown on the graphs are the shear resistances determined in the as-designed analysis. Furthermore, the shear resistances were found to change somewhat depending upon whether curvatures or neutral axis locations along with strains were used to determine load effects. However, for this purpose, shear resistance was determined based on the load effects from

neutral axis location and strain analysis only, as that analysis indicated the axial force present in the sections along with flexural response.

In-situ shear resistance estimates were also increased over the as-designed resistance estimates, which can be seen in the figures below. For the current allowable GVW of 62.5 t, the improvements in shear resistance ranged from 26% to 45%, with the largest increase seen at strain gauge location 3-5, while the smallest increase was noted at strain gauge location 1-4. For the proposed allowable GVW of 110 t, the improvements ranged from just 10% (at location 3-2) up to 43%. (at location 3-3). As shear resistance determined by the compression field theory in CAN/CSA-S6-00 (CSA 2000) is dependent upon the shear, bending, and axial force in the section, the load effects determined from measured values played a large role in the resulting increases in shear resistance, as inspection of Figs. 5.24, 5.25, and 5.27 will show. Furthermore, the coefficient of variation in the shear resistance was also reduced from the as-designed analysis, to an average of 0.091 from 0.14.

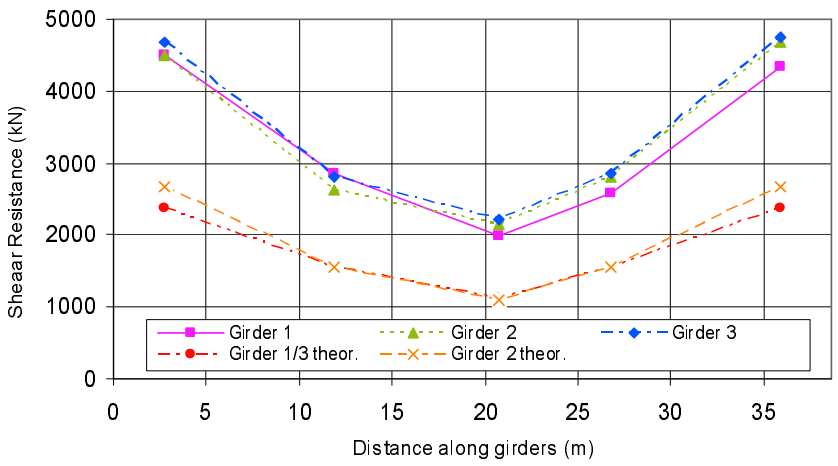

Figure 5.35. Estimated in-situ shear resistances using site-specific parameters for 62.5 t truck loading.

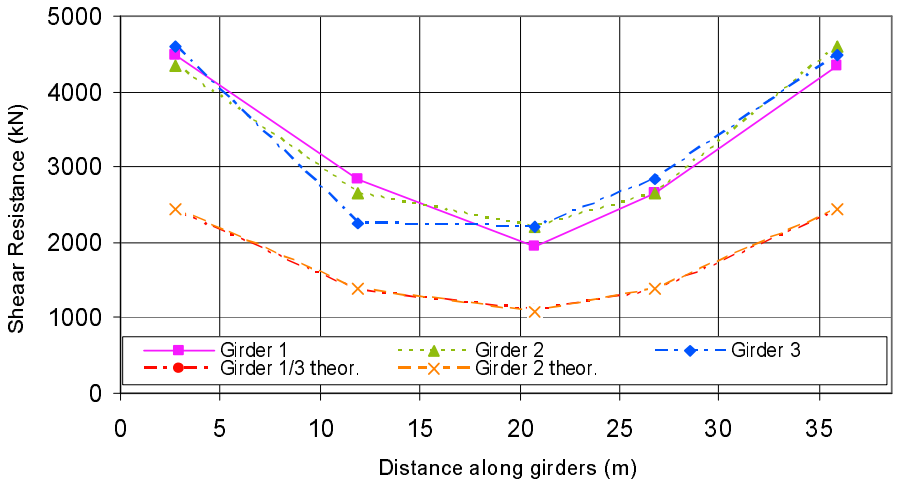

Figure 5.36. Estimated in-situ shear resistances using site-specific parameters for 110 t truck loading.

In summary, due to higher than specified measured concrete strengths, reduced variability in material and section properties, and lower than expected load effects, the estimated resistance of the bridge in question to flexure and shear was increased. The results of this section demonstrate that not only can load effects be better estimated from field measurements, but that estimates of resistance can also be improved.

5.3.7 Reliability Assessment

Incorporating the site-specific response and resistance data in the mean load method, the girders were re-evaluated to determine the live load capacity factor and reliability index, using the methodology described in Section 4.3.9. Bias ratios for all relevant variables required for the application of the mean load method are summarized in Tables E.11 through E.14 in Appendix E, while corresponding coefficients of variation have been presented previously in the appropriate sections in this chapter. Although the instrumentation at location 1-3 was not functioning properly, load effects at that location were nonetheless estimated based on the best-fit lines generated using data from the remaining four strain gauge locations which were functioning.

In an attempt to re-evaluate the reliability of the girders, eight different combinations of allowable loading, load effects, and evaluation methods were considered, as summarized in Table 5.6. A key assumption in the evaluation of reliability for the proposed increased GVW was that the statistical parameters (bias ratio and coefficient of variation for the loading parameters), remained the same as those determined for the current allowable loading.

Table 5.6. In-situ mean load method evaluation scenarios.

Load Effect	Allowable Load	Method of Evaluation
Bending Moment	62.5 t Truck	Curvature
		Neutral Axis and Strain
	110 t Truck	Curvature
		Neutral Axis and Strain
Shear	62.5 t Truck	Curvature
		Neutral Axis and Strain
	110 t Truck	Curvature
		Neutral Axis and Strain

The bridge reliability was re-evaluated at all instrument locations for the eight scenarios summarized in Table 5.6. The resulting live load capacity factors and reliability indices are presented in Appendix E, in Tables E.15 through E.18; reliability indices, as a more direct indication of bridge reliability are discussed in detail in the following sections. Recall that reliability indices are related to the estimated probability of failure, with higher reliability indices signifying lower failure probability. Plots of reliability indices include six separate curves: three curves represent the reliability indices for each girder determined in the as-designed analysis (theoretical), and three curves represent the reliability index estimates from the in-situ analysis. In addition, the minimum allowable reliability index for the load effect in question is included on each graph to facilitate evaluations of reliability.

5.3.7.1 Bending Moment Reliability Indices

For the current allowable loading, reliability indices for bending moment evaluated by both the curvature and neutral axis location-strain methods are shown in Figs. 5.37 and 5.38, respectively. As shown in these Figures, the results of both methods of evaluation show comparable results, with an average difference of 1%, and a maximum difference of 25% (occurring at the 1-4 location). The large difference at that location is due to the filtering process of the measured data, described in Section 4.3.4.1. It can be seen that the reliability estimates were generally significantly improved over those determined in the as-designed analysis, although they were actually reduced at the instrumented locations nearest to the piers; even at these locations, however, the reliability indices still remained well above the code-specified minimum value of 3.0.

Figs. 5.37 and 5.38 show girder 3 typically having the highest reliability indices, reflecting the fact that it was found to carry the least load in flexure of the three girders, as demonstrated by the measured distribution factors in Section 5.3.5.1. The in-situ reliability indices were generally lowest near midspan and near the piers, where the positive and negative bending moments were highest, respectively. At the second instrument locations (lateral locations 2 and 4, located approximately 11.89 m from either pier), the reliability indices were high (greater than 13.0), as the gauges were near inflection points in the measured bending moment distribution.

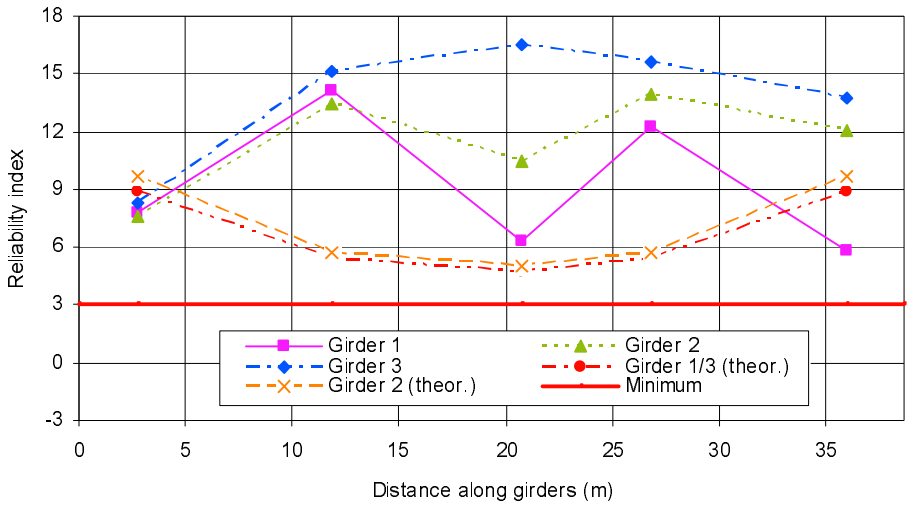

Figure 5.37. In-situ bending moment reliability indices for 62.5 t truck loading analysed based on measured curvatures.

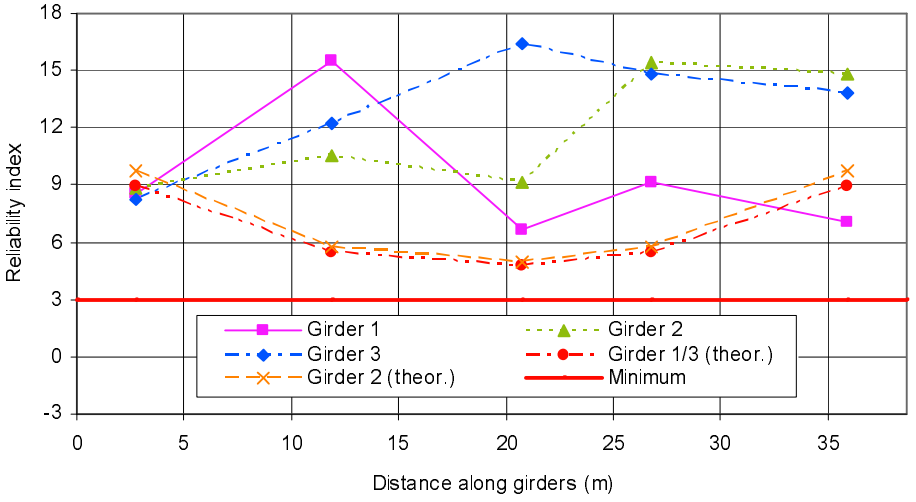

Figure 5.38. In-situ bending moment reliability indices for 62.5 t truck loading analysed based on measured neutral axis locations and strains.

For the proposed increased truck loading, the reliability indices for flexure evaluated on the basis of both the curvature and neutral axis location-strain data are shown in Figs. 5.39 and 5.40, respectively. These results suggest the same trends as those determined for the current allowable loading discussed previously. The average percentage difference between the

reliability indices determined by curvature and by neutral axis location and strain was only 0.3%, although the maximum difference was 30%, again occurring at the 1-4 location. Where the reliability indices fell below the values computed based on the as-designed analysis, in-situ reliability estimates were nevertheless still well above code-specified minimum acceptable levels. Considering only flexure, therefore, it appears that that the bridge in question has sufficient reliability to allow the passage of 110 t trucks based on the results of the present study.

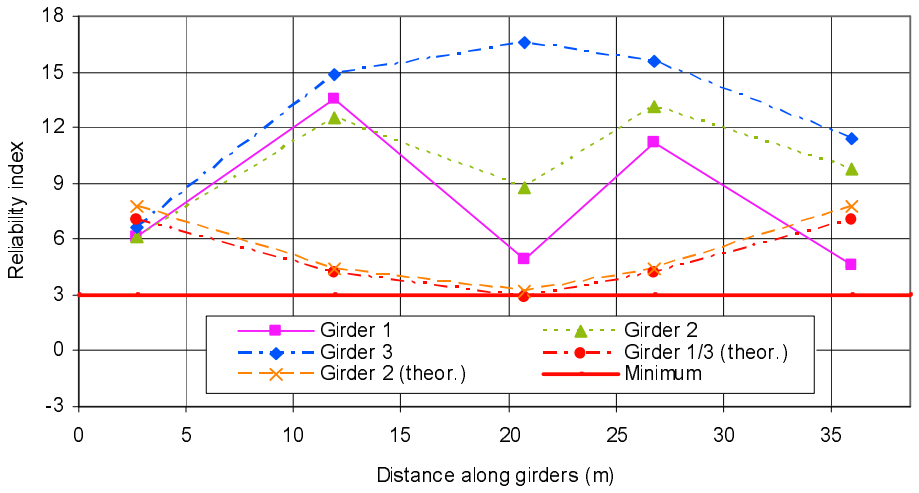

Figure 5.39. In-situ bending moment reliability indices for 110 t truck loading analysed based on measured curvatures.

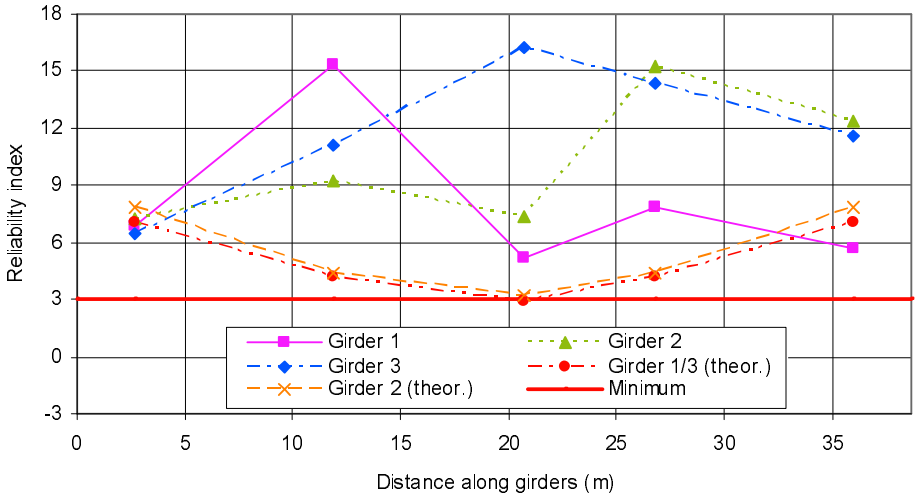

Figure 5.40. In-situ bending moment reliability indices for 110 t truck loading analysed based on measured neutral axis locations and strains.

5.3.7.2 Shear Reliability Indices

For the current allowable loading (62.5 t), the reliability indices for shear evaluated on the basis of both curvature and neutral axis location-strain data are shown in Figs. 5.41 and 5.42, respectively. The different methods of evaluation showed comparable results, although the average percentage difference between the methods was 10%, with the neutral axis location-strain data more often resulting in higher reliability indices. The maximum difference was 96% at the 2-3 location although, here, the large difference can be attributed primarily to the very low measured shear values, which can easily result in large percent differences (for example, the measured values of 9 and 13.5 result in a 50% difference, although the effects of either of these magnitudes of shear are minimal). As in flexure, the reliability estimates considering shear effects were typically significantly improved over those determined in the as-designed analysis, with only one location (3-1) showing a reduced reliability estimate (down to 5.32 from 5.77), due primarily to significant variation in the measured data.

From the shear reliability plots, it was not as evident as it was in flexure that Girder 3 carries the least flexural load of the three girders, as the reliability for that girder is not consistently the highest. The main reason for this seeming inconsistency appeared to be the higher uncertainty at some instrument locations than others, resulting in reduced estimates of reliability. However, there was a general trend of reliability indices being higher nearer to midspan, mainly as a result of the low levels of apparent shear forces at those locations.

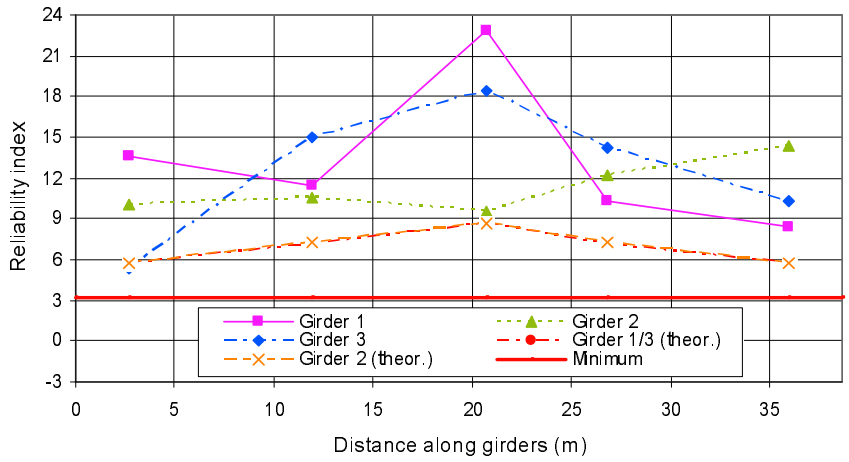

Figure 5.41. In-situ shear reliability indices for 62.5 t truck loading analysed based on measured curvatures.

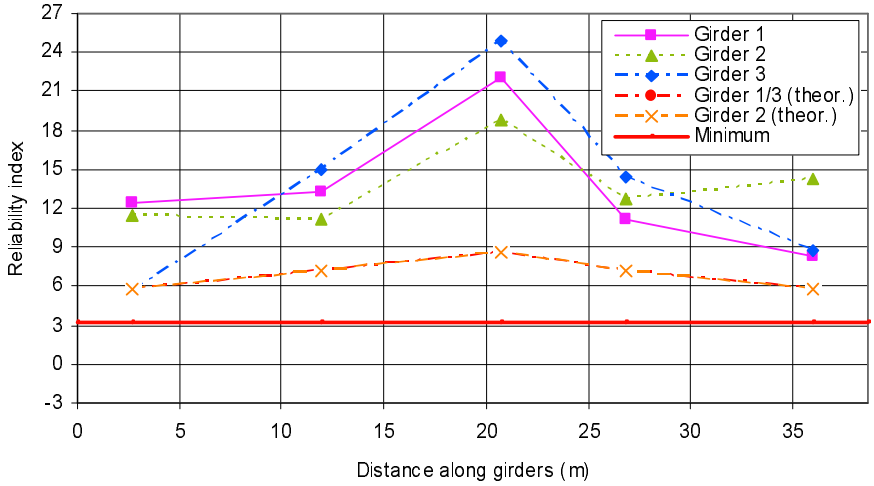

Figure 5.42. In-situ shear reliability indices for 62.5 t truck loading analysed based on measured neutral axis locations and strains.

For the proposed increased truck loading of 110 t, the shear reliability indices evaluated on the basis of both curvature and neutral axis and strain are shown in Figs. 5.43 and 5.44, respectively. The resulting reliability indices for the proposed increased loading displayed similar trends to those determined for the current allowable loading. They tended to be higher near midspan due to the very low shear levels in this region. Furthermore, the differences between the results of the two methods were similar to those determined for the current allowable loading; the average difference was 9.4% (as opposed to 10.3% for 62.5 t trucks), and the maximum difference, occurring at the same 2-3 location, was 73%, compared with 96% for the current loading condition. Based on shear reliability indices from the current study, therefore, it also appears that the bridge in question has sufficient reliability to allow the passage of 110 t trucks, as was the case for flexure.

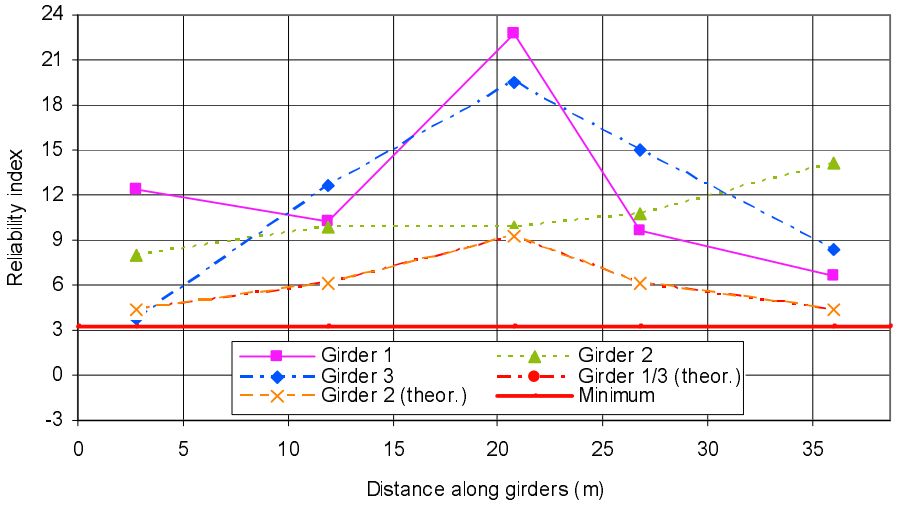

Figure 5.43. In-situ shear reliability indices for 110 t truck loading analysed based on measured curvatures.

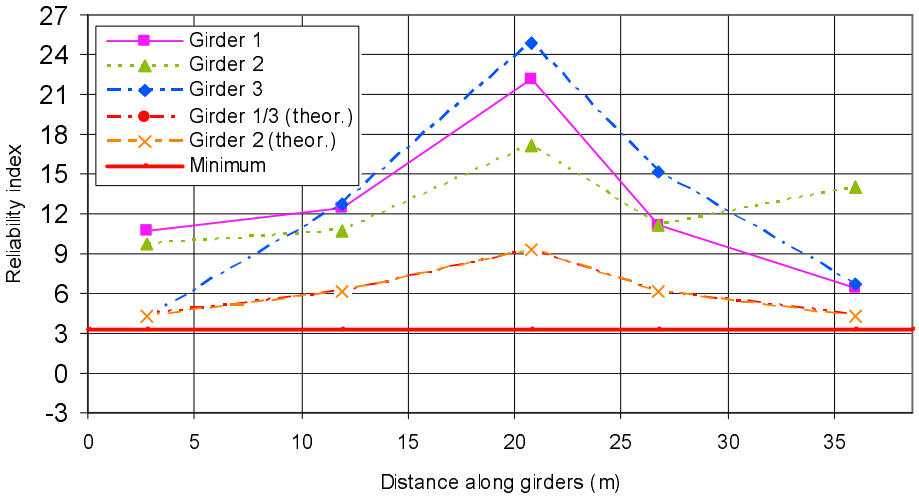

Figure 5.44. In-situ shear reliability indices for 110 t truck loading analysed based on measured neutral axis locations and strains.

5.3.7.3 Summary of Reliability

Critical reliability indices determined for the proposed increased loading, as well as for the current allowable loading, are discussed further in this section. The critical result is that which governs the design for the bridge in question (ie. the lowest value), and indicates the likely probability of failure; this critical reliability index can then be compared with the target values outlined in CAN/CSA-S6-00 (CSA 2000). The critical reliability index was taken as the lowest reliability index determined for the bridge in either bending or shear, from either method of evaluation, at any one location.

The critical reliability index for the current allowable GVW of 62.5 t was found to be 5.32, which corresponded to shear effects at instrument location 3-1 (see Table 3.1 for exact location), estimated on the basis of measured curvatures. The governing reliability index for the proposed increased GVW of 110 t was 3.81, corresponding to the same location, load effect, and method of analysis. The overall results of the in-situ analysis therefore indicate that the Red Deer River Bridge is adequate in its current configuration to safely handle the passage of 110 t trucks, as the computed reliability indices were found to be

greater than the minimum allowable values of 3.25 for shear and 3.0 for bending moment.

Several factors contributed to the improved estimates of reliability. The main reason was that the measured bending moments and shear forces were significantly lower than those determined in the as-designed analysis, due to the apparent prevalence of arching action, as opposed to the purely flexural behaviour assumed in the as-designed analysis. Measured bending moments were consistently less than 30% of those determined in the as-designed analysis, while measured shear forces were no more than 32% of the theoretical values. However, other factors also contributed to improving reliability estimates. The measured dynamic effects were found to be 74% of those assumed for the as-designed analysis; also, the observed variability in this factor was reduced by 23% compared to tabulated values. In addition, resistance estimates in bending and shear were increased up to 37% and 45%, respectively, as a result of increased estimates of material strengths above nominal values, while the variation in those estimates was also reduced somewhat. Furthermore, at some locations, the measured distribution factors were lower than the theoretical values, thereby indicating a more equitable sharing of load effects and the lowering the estimated load carried by certain members.

On the other hand, several mitigating factors were also found that tended to reduce the reliability estimates relative to those determined in the as-designed analysis. Best estimates of uncertainty in most of the variables used in the mean load method were increased significantly from those used in the as-designed analysis, with the exception of those few previously discussed. Furthermore, the distribution factors at several locations suggested considerably higher load effects in particular members as compared to those obtained from the theoretical analysis.

5.3.8 Numerical Simulations

5.3.8.1 Bearing Restraint

As summarized in Section 5.3.7.3, the estimates of bridge reliability were significantly increased using site-specific data. Furthermore, it was determined that a primary cause for these increases was the lower than anticipated flexural load effects due to significant arching action in the girders. In order to generate this arching action, though, some degree of horizontal restraint is required at the girder supports to resist the thrust forces developed in a potential arch. One possible source of this horizontal restraint would arise from unintended fixidity in the bridge bearings. If this is, in fact, the case for the bridge in question, the beneficial arching behaviour would be dependent, to some extent, on the operational condition of the bearings which is subject to change with maintenance. A numerical study was therefore undertaken to investigate the influence of support fixidity on the load resisting mechanisms of the girders.

The Red Deer River Bridge bearings, shown in Fig. 5.45, are constructed of steel. As such, they may have experienced some corrosion over time, causing the roller bearing to seize to the bearing plate. Other reasons for restraint can be due to friction between the roller bearing and the bearing plate, or freezing of the bearings during winter months (Chajes et al. 1997). Relying on this restraint, however, is highly uncertain as there is the possibility of a decrease in the bearing restraint as a result of maintenance and repairs. As the bearing condition can very easily change in a short period of time, it was necessary to understand the effect of bearing restraint on the resulting bridge reliability.

Figure 5.45. Red Deer River Bridge bearing.

A three-dimensional finite element model of the Red Deer River Bridge, created using Adina™ version 8.0 software, was used to determine the effect of bearing restraint on load effects in the girders. The model was created for a separate dynamic study of the Red Deer River Bridge, being undertaken by Alwash et al. (2005, 2006) at the time of writing, although the analysis for this study was carried out independently. As the model was generated using three-dimensional solid elements, axial forces could be developed and monitored. The model was "calibrated" to the physical bridge based on dynamic results measured at the bridge. Apparent bearing restraint, modelled by the use of fictitious horizontal springs, along with bridge material properties, were adjusted until the natural frequencies and mode shapes of the model were comparable to those which were measured on-site using accelerometer data. It was then assumed that the calibrated model provided a good representation of the Red Deer River Bridge in its current state; as such, the model was used to study the effects varying degrees of bearing restraint on the intensity of load effects in the girders.

Two bounds on possible horizontal bearing restraint were considered: zero restraint, in which the bearings were free to move horizontally; and full restraint, in which the bearings were not permitted any horizontal translation. In

both cases, rotation of the bearing was allowed to occur freely. In the following discussion, the measured in-situ results will be referred to as the measured case.

For the comparative study, a unit load was applied to the model centered on the central bridge span in both the longitudinal and lateral directions. At locations corresponding to instruments on the actual bridge, the strains at the top face and the bottom face of each girder section were extracted from model results. Bending moments and axial forces were then determined using the methods described in Section 4.3.5. Ratios of the results from the free case to the measured case in the calibrated model, and the fixed case to the measured case in the calibrated model were applied to the measured bending moments, from which measured shear forces were developed, using the methodology of Section 4.3.5.2. For example, if the ratio of bending moments for the fixed case to the measured case in the calibrated model was 2, then the measured bending moments would be multiplied by 2 to obtain values for the fixed case at the actual bridge. The intermediate results for the two bearing restraint cases, including bending moments, shear forces, and distribution factors, are presented in Tables E.19 through E.22 in Appendix E. In these analyses, variability of the contributing parameters was assumed to remain the same as those from the measured analyses.

Bearing Restraint Effects on Bending Moments

Based on the numerical analysis results for the two bearing restraint cases, reliability indices were determined for flexure; these are shown graphically for each girder separately in Figs. 5.46 through 5.48 for the case of proposed increased loading (110 t GVW), which were analysed using the method of curvatures (see Section 4.3.5.1). Similar results were determined for current truck load levels (62.5 t GVW) and for the neutral axis and strain

method of analysis (see Section 4.3.5.2); these results are presented in tables in Appendix E (Tables E.23 and E.24).

Figs. 5.46 to 5.48 show the current in-situ reliability indices, along with the reliability indices for each of the fictitious bearing restraint cases. The minimum allowable reliability indices are also shown on the plots.

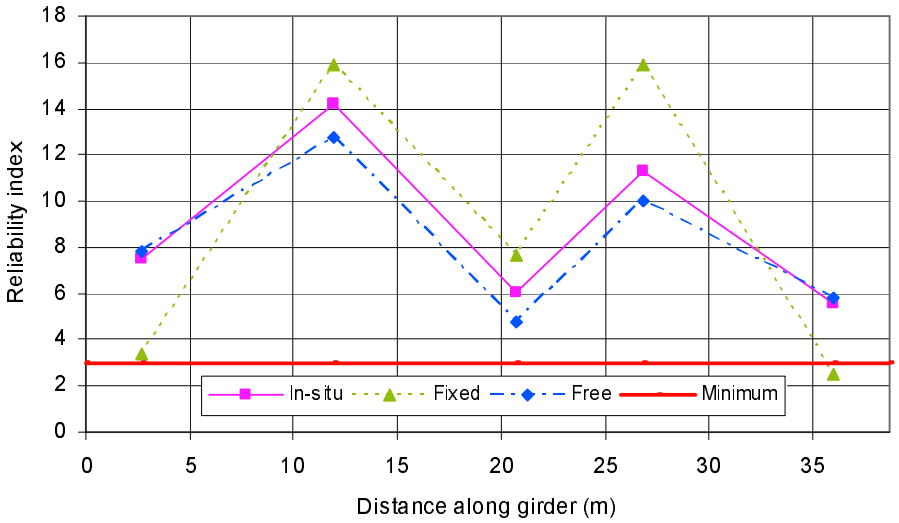

Figure 5.46. In–situ bending moment reliability indices for 110 t truck loading for girder 1 with different degrees of bearing restraint (using curvature).

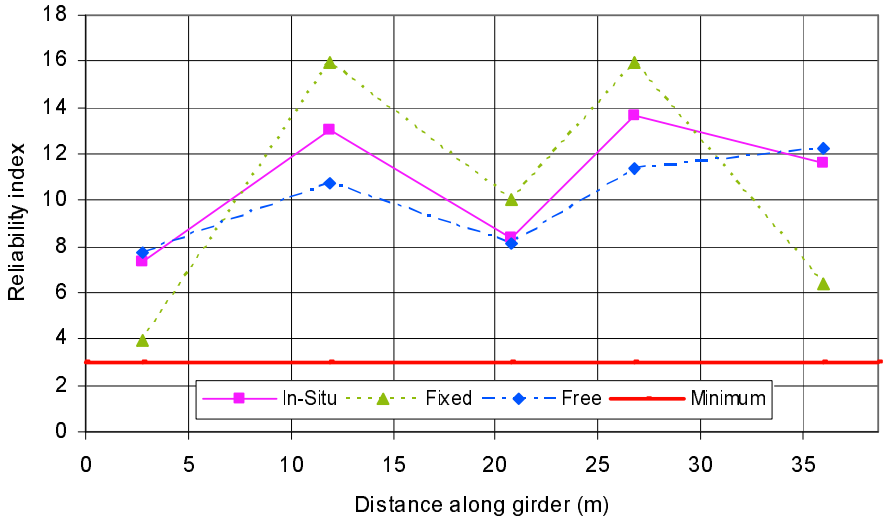

Figure 5.47. In-situ bending moment reliability indices for 110 t truck loading for girder 2 with different degrees of bearing restraint (using curvature).

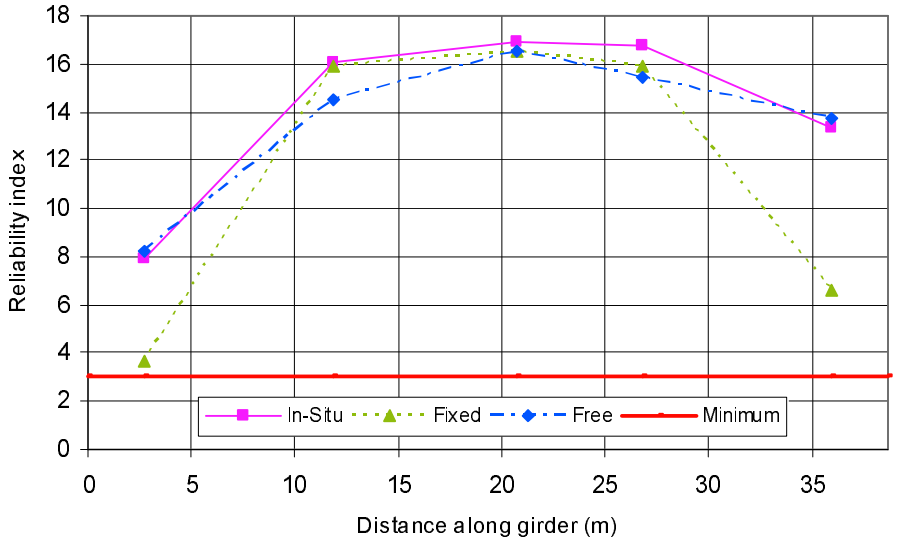

Figure 5.48. In-situ bending moment reliability indices for 110 t truck loading for girder 3 with different degrees of bearing restraint (using curvature).

Figs. 5.46 to 5.48 show that the degree of assumed bearing restraint had significant effects on the calculated reliability indices. Generally, although reliability was increased in the positive bending moment regions when the bearings were fully fixed, it was reduced in the negative bending moment regions. The opposite effect, however, was observed for the case with perfectly free bearings. The variation in flexural reliability occurred as a result of a shift in the moment diagram for different restraint conditions, as shown in Fig. 5.49 for girder 1. It can also be observed from the bending moment diagrams in Fig. 5.49 that the current bearing restraint case appears to be closer to the free case than to the fixed case.

An examination of Figs. 5.46 to 5.48 suggests that the flexural behaviour of the current in-situ condition fell somewhere between the fixed and free restraint cases, but was found consistently to be more similar to the free bearings case (with no lateral restraint) than the completely fixed case. This suggests that the estimates of the bridge reliability found in this study are not unduly sensitive to the actual condition of the bearing, particularly in the

midspan region that is of most interest. Furthermore, the existence of arching action in the model with no external lateral support constraint suggests that the restraint is provided by some other mechanism, likely a combination of internal tension ties formed by the bottom steel reinforcement, and some degree of bearing restraint.

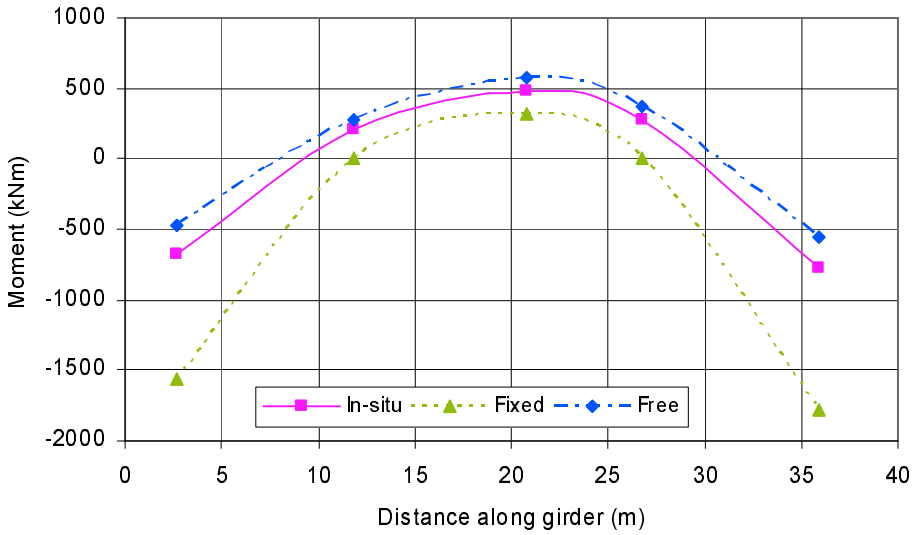

Figure 5.49. In-situ bending moment diagrams in girder 1 for different bearing restraint cases, analysed using curvatures, for the 62.5 t GVW load case.

Considering only flexural effects, it was found that the reliability estimates were reduced sufficiently by the imposition of fixed bearings, implying that bridge safety would fall lower than the minimum allowable level near the supports if such a degree of restraint occurred in conjunction with an increase in the allowable loading to 110 t GVW. Although the neutral axis location and strain method of analysis indicated that reliability would acceptable even with full fixity, the curvature analysis provided the most conservative reliability estimates and is therefore used here. For fixed bearings, assuming the current allowable loading, the governing reliability index was found to be 3.16, at location 1-5, which is above the minimum acceptable value of 3.0. For the proposed increased loading, however, the governing reliability index was 2.50 at the same location. Flexural reliability indices for the free bearing case, on the

other hand, exceeded code specified minimum values everywhere on the center span. This suggests that proper maintenance of the bearings is an important factor for optimizing bridge performance.

Bearing Restraint Effects on Shear

Reliability indices were also determined for shear in the girders under the two different bearing restraint cases. These results are shown graphically for each girder separately in Figs. 5.50 through 5.52 for the case of the proposed increased loading analysed using measured neutral axis locations and strains. The remaining scenarios for shear described in Table 5.6 are presented in Appendix E (Tables E.25 and E.26).

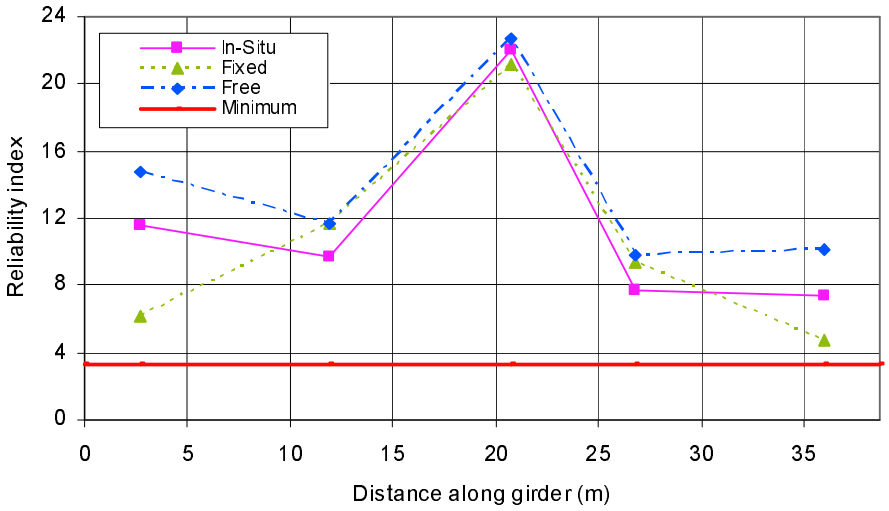

Figure 5.50. In-situ shear reliability indices for 110 t truck loading for girder 1 with different degrees of bearing restraint (using neutral axis locations and strains).

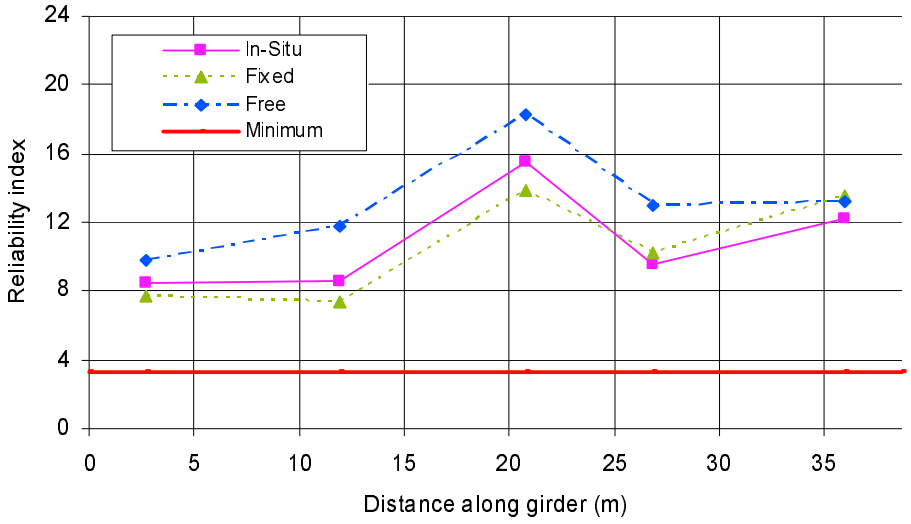

Figure 5.51. In-situ shear reliability indices for 110 t truck loading for girder 2 with different degrees of bearing restraint (using neutral axis locations and strains).

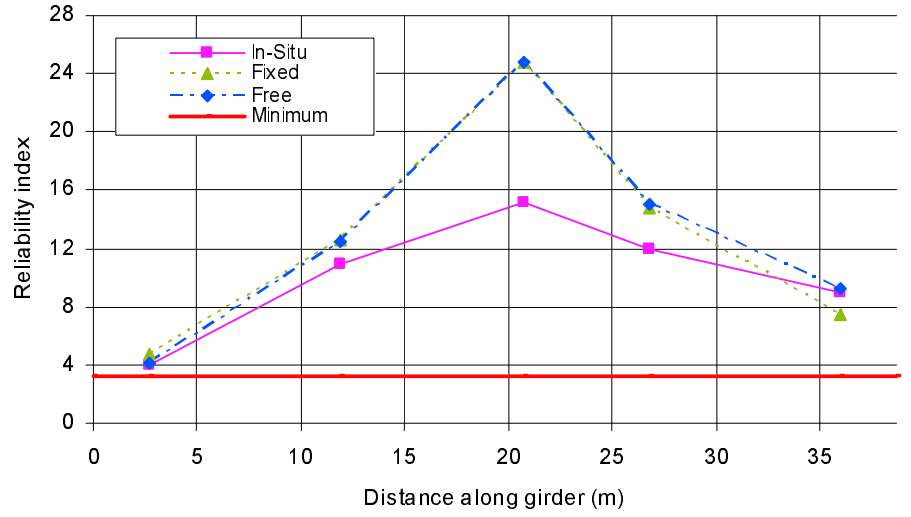

Figure 5.52. In-situ shear reliability indices for 110 t truck loading for girder 3 with different degrees of bearing restraint (using neutral axis locations and strains).

It can be seen that the degree of imposed horizontal bearing restraint had significant effects on the shear reliability estimates. Trends similar to those seen in the flexural reliability estimates were apparent, with reliability indices

generally increasing in the positive bending moment regions for the fixed case, relative to the in-situ case, and decreasing in the negative bending moment regions, with the opposite trends occurring for free bearings. These effects resulted from shifts in the shear diagrams for the various restraint cases, as can be seen in Fig. 5.53. As in the bending moment results, Fig. 5.53 suggests that in-situ bearing restraint case was closer to the free restraint case than to the fixed case. However, that was not necessarily true for the reliability indices at all locations, as illustrated in Figs. 5.50 through 5.52.

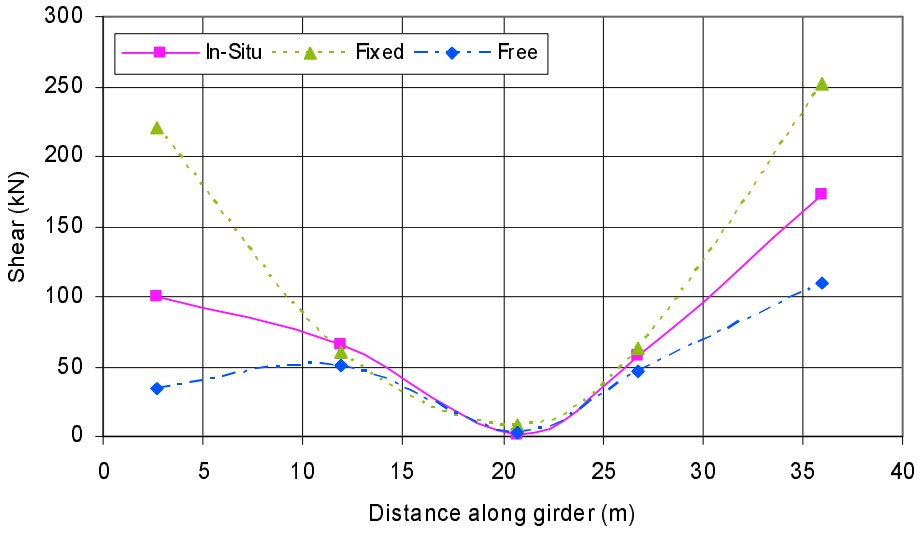

Figure 5.53. In-situ shear diagrams for girder 1 with different bearing restraint cases, analysed using curvatures, for the 62.5 t GVW load case.

Considering only shear effects, it was found that the case of fixed horizontal restraint in the bearings generally produced the lowest reliability ratings, with some values even falling below the minimum allowable reliability index of 3.25 for the proposed increased loading of 110 t trucks. As was the case for bending moments, the neutral axis location and strain analysis did not show that safety would be compromised by increasing allowable loading to 110 t, although the analysis using curvatures did. The governing reliability index for shear based on the current allowable loading was 4.53 at location 3-1, while it was 3.20 for the proposed increased loading at the same location.

Bearing Restraint Summary

The results of the bearing restraint analysis using a finite element model suggests that bridge safety would be adversely affected if the allowable loading was increased to a GVW of 110 t and the bearings were to become fixed against horizontal translation, as a result of deterioration or environmental conditions. Bending moments could become unacceptably high at location 1-5, where the governing reliability index for the fixed bearing case was 2.50, well below the minimum allowable value of 3.00 for flexure, or at location 3-1, where the reliability index for shear of 3.20 falls below the minimum allowable value of 3.25 for shear. There were no sub-standard results for bearings allowed free horizontal translation, indicating the need for proper maintenance to ensure that the bearing do not reach a critical degree of fixidity. However, the results indicate that apparent arching action in the girders is not primarily due to external restraint at the bearings caused by seizure, but likely by internal tension ties provided by the bottom reinforcing steel layers acting to restrain the horizontal spread at the girder supports.

5.3.8.2 Dynamic Load Allowance

In the in-situ analysis, it was determined that the DLA was negative, signifying that the dynamic effects were less severe than static under comparable load intensities, an observation that is contradictory to the requirements of CAN/CSA-S6-00 (CSA 2000), as well as to the generally accepted understanding of dynamic loading of bridges. Therefore, a finite element study was performed to analyse the dynamic effects of moving trucks on the bridge in question. A different finite element model was used than that used for the bearing restraint effects study, although the two models were similar in essential characteristics. The model was created with the finite element modelling software ANSYS^{TM} 9.0 for use in the study by Alwash et al. (2005, 2006), and an independent analysis was performed for the purposes of

this study. As the model was "calibrated" to the actual dynamic effects measured at the bridge, using an approach similar to that employed for the previously described model, it was assumed to provide an accurate representation of the bridge. The model did not include potential dynamic effects induced by factors such as road roughness, vehicle and suspension dynamics, and vehicle-bridge interaction.

The numerical model used for the DLA investigation was designed to simulate moving truck loads in a realistic manner. The test truck configuration described in Section 3.3.2.2 was used as the basis for the simulated truck loading. Two truck speeds were considered in the DLA study: 54 kph and 82 kph. In addition, a pseudo-static load case featuring the test truck travelling at 7.2 kph was considered for the purposes of comparison. The DLA was determined at locations on the bridge girders corresponding to the actual instrumentation locations on the bridge, at a rate of 30 readings per second; the same effective rate at which data was collected at the bridge, once filtering was complete. Statistical parameters were based on the peak DLA recorded at each instrumentation location, as in the in-situ study.

At the 54 kph truck speed, the numerically determined DLA was found to be -0.047, with a coefficient of variation of 0.054. Similarly, at 82 kph, the DLA was found to be -0.043, with a coefficient of variation of 0.055. Although these numerically generated dynamic load effects were greater than those determined in the in-situ analysis (-0.075), they were still less than the corresponding static load effects. This finding suggests that the in-situ measurements were, in fact, reasonable. It should be noted, however, that the numerical study did not consider any vertical motion of the truck due to road roughness or other factors. This suggests, perhaps, that the condition of the bridge surface was fairly smooth at the time of the field study.

5.4 ANALYSIS OF RELATIVE COSTS

The research described in this thesis provides a method of evaluating existing bridges using site-specific data to provide a better estimate of the true load rating which, in turn, may allow the passage of larger loads, as was the case for the bridge in question. The proposed alternative to employing the suggested research methodology was strengthening, such that larger GVWs may confidently be allowed over the stronger bridge without any need for improved knowledge of the bridge's actual performance. To this end, two strengthening methods were proposed for the Red Deer River Bridge: steel plates and fibre-reinforced polymer (FRP) sheets, both of which are discussed in Section 3.2.2. Both alternatives involve fixing the material to the bottom faces of the girders in the positive bending moment regions, providing sufficient capacity to allow the passage of 110 t trucks based on the perceived requirements obtained from the equivalent of the "as-designed" approach described herein. In the summer of 2006, the girders were strengthened using the steel-plate option at a cost of $258,000 (SHT 2007).

The research methodology described in this study demonstrates the economic value of improved information, which may be considered as an alternative strategy to the implementation of the strengthening alternatives. The research methodology of the study when applied to other bridges may not necessarily result in the load rating of the bridge in question being improved; however, the information in itself provides value. Placing structural health monitoring on a bridge will not increase structural capacity, although it will provide information indicating whether or the not that bridge has additional capacity, rather than simply making educated judgements of capacity based on a design code alone. As a general rule, If there is a significant probability of substantial economic benefit (i.e., an expected benefit clearly greater than the corresponding cost of an effective monitoring program), then the research methodology employed herein should at least be given due consideration.

Hence, while the outcome of monitoring may not prove favourable (since probabilities can fall either way), the additional information obtained, in and of itself, provides value to decision-makers since it helps by reducing uncertainty and hereby provides clearer direction. In this case, the load rating was increased by employing the methodology of the research. A post-monitoring economic evaluation was therefore carried out to roughly compare the costs and benefits of the monitoring program against considered strengthening options. User costs such as additional fuel and lost time incurred as a result of bridge closure or detours were not included in the economic model.

The costs of the strengthening alternatives were first evaluated. The strengthening designs were completed by a private consultant in 2002 (Earth Tech 2002), determining that either of the two proposed alternatives would provide the structural capacity for the increased loading at approximately the same cost. The total cost of the strengthening paid by SHT in 2006 did not include engineering fees. It was assumed that engineering costs were 8% of the total estimated project cost (estimated at $204,000 in 2002). Thus, the total cost of the strengthening alternative was $274,000.

The cost of implementing the research methodology was considered next. Assumptions for many variables were made based on the author's experience with implementing the methodology. The costs of the method as used in this study are summarized in Table 5.8. Instrumentation installation was assumed to be completed by a crew of four tradespersons over four-eight hour days, being billed out at $75/hour. Instrumentation installation also included the costs of hiring the bridge inspection truck shown in Fig. 3.10. Data collection was assumed to take place over two eight-hour days, using a crew of three: one engineer and two technologists, billing out at $110/hour and $90/hour, respectively. Expenses included travel, lodging, and meals in Hudson Bay, Saskatchewan. It was assumed that analysing the data was completed by the engineer billing out at $110/hour, who would take

approximately three months to complete the task. The costs of the research methodology are summarized in Table 5.7 below.

Table 5.7. Cost estimate of applying the proposed SHM methodology to the Red Deer River Bridge.

Task	Item	Item Cost (CAN $)	Totals (CAN $)
Instrumenting Bridge	Strain Gauges	45 @ 100/ea	4500
	Heavy Gauge Wire	1500	1500
	Adhesive	500	500
Installation Crew	Labour	128 hrs @ 75/hr	9600
	Expenses	2600	2600
Bridge Inspection Truck	Truck Rental	5000	5000
	Expenses	1500	1500
Traffic Control	Traffic Control	5000	5000
Data Collection	Computer/DAQ/Software	51500	51500
	Engineer	1x16 hrs @ 110/hr	1760
	Technicians	2x16 hrs @ 90/hr	2880
	Expenses	1250	1250
Analysis	Engineer	520 hrs @ 110/hr	57200
Contingency	Contingency	10% of total cost	14459
GST	GST	7% of total cost	11133
Total (CAN $)			**170182**

The annual cost of hauling logs using 62.5 t trucks, as well as using the proposed 110 t trucks, were determined based on the assumptions summarized in Table 5.9. For the 62.5 t units, Kenworth T600 trucks were assumed, costing $130,000, and pulling a logging trailer costing $65,000. The 110 t unit was assumed to be pulled by a Kenworth C500, valued at $225,000, pulling "super-logger" trailers costing $112,000. Truck costs were provided by GreatWest Kenworth in Calgary, AB (GreatWest Kenworth 2007), while trailer costs were provided by Manac in Edmonton, AB (Manac 2007), who specialize in logging transport trailers.

Benefits were quantified as a reduction in haul costs, calculated based on the difference between the costs of using 62.5 t trucks and using 110 t trucks. Fuel consumption was assumed to be approximately 0.44 L/km (6.5

mpg) for the 62.5 t unit, and 0.71 L/km (4 mpg) for the 110 t unit (GreatWest Kenworth 2007). The amount of t-km required to be hauled to be beneficial were determined for three hauling options: leaving the bridge as-is and continuing to haul using 62.5 t trucks, strengthening the bridge to haul with 110 t trucks, and finally, using the research methodology to increase allowable loading to 110 t trucks. Table 5.8 summarizes the assumptions used in the analysis; based on hauling scenarios at the time of research, it was assumed that up to 1500 t of logs were hauled per day. As such, twelve 62.5 t trucks, or seven 110 t trucks, hauling two loads per day, would be required for full haul capacity. Although the initial costs of the 110 t truck units are higher than the 62.5 t units, the reduced haul costs per t-km for the 110 t units makes the purchase of the units increasingly beneficial over time.

Table 5.8. Estimates in determining total hauling costs.

Gross Vehicle Weight		**62.5 t**	**110 t**
General	Round trip haul (km)	100	100
	Max. hauls/truck/day	2	2
	Max. tonnage/day	1500	1500
Trucks	Trucks required	12	7
	Payload (t)	40	80
	Truck cost (CAN $)	130000	225000
	Trailer cost (CAN $)	65000	112000
Fuel	Cost (CAN $/L)	1.25	1.25
	Consumption (L/km)	0.44	0.71
Labour	Hours/trip (hr)	4	4
	Wage (CAN $/hr)	25	25
Maintenance	Cost/truck (% of truck/trailer cost)	10	10

The required t-km hauled to cover the costs of the larger trucks, the research methodology, or the strengthening can be determined using the following:

$$C_{t\_62.5} + C_{m\_62.5} + C_{f\_62.5}tkm + C_{l\_62.5}tkm - \left(C_{t\_110} + C_{m\_110} + C_{f\_110}tkm + C_{l\_110}tkm\right) = C_o \qquad [5.1]$$

where $C_{t\_62.5}$ and C_{t_110} are the costs of the truck and trailer combinations for the indicated GVWs, $C_{m\_62.5}$ and C_{m_110} are the maintenance costs, $C_{f\_62.5}$ and C_{f_110} are the fuel costs per t-km, given by:

$$C_{f\_i} = \frac{(fuel\_\cos t)(fuel\_consumption)}{payload} \quad [5.2]$$

where C_{f_i} is the fuel cost per t-km for GVW *i*, and fuel cost, fuel consumption, and payload are given in Table 5.8 $C_{l\_62.5}$ and C_{l_110} in Eq. 5.1 are the labour costs per t-km, given by:

$$C_{l\_i} = \frac{(hours\_per\_trip)(wage)}{(haul\_dist)(payload)} \quad [5.3]$$

where C_{l_i} is the labour cost per t-km for GVW *i*, and hours per trip, wage, haul distance, and payload are given in Table 5.8. The final variable in Eq.5.1, C_o, is the cost of either increasing to 110 t trucks, \$0, the cost of the research methodology, \$171,000, or the cost of strengthening, \$274,000. Rearranging Eq. 5.1 and solving for t-km gives the required t-km to cover the costs of upgrading to 110 t truck, implementing the research methodology, or strengthening.

The cost of using 110 t trucks is paid for after hauling approximately 2,380,000 t-km. Assuming full hauling capacity, this would occur in less 11 haul days with 110 t trucks. After approximately 17,000,000 t-km, the cost of implementing the research methodology would be recovered. At full hauling capacity, this would occur in approximately 76 haul days with 110 t trucks. By comparison, it requires approximately 29,300,000 t-km to cover the costs of strengthening (occurring in approximately 131 haul days at full hauling capacity with 110 t trucks). Application of the research methodology is approximately

$108,000 less than the strengthening alternative, and the benefits become apparent after a relatively short time period.

There are also other benefits of implementing the research methodology, aside from the value of new information, which are more difficult to quantify in an economic sense. Strengthening the girders and re-evaluating with no new information shows that the bridge has sufficient capacity to carry 110 t trucks; however, little additional load beyond the 110 t configuration can be resisted by the strengthened bridge (EarthTech 2002). However, the use of site-specific data showed that the girders had very high reliability indices at most locations (many of which could be further improved through more extensive testing which would likely reduce the variability in the data), allowing trucks heavier than 110 t passage over the bridge. Furthermore, the research methodology provides a monitoring system from which data may be collected at any time after installation and used in re-evaluation. Therefore, any changes which may have occurred in the bridge behaviour over time would be accounted for, reducing inherent uncertainty regarding future performance. Additionally, with the instrumentation in place, the bridge itself can be used as a weight-in-motion system, as described in the literature (Au et al. 2005). The recorded data may be calibrated to known truck weights, from which future data could be used to estimate GVW with a reasonable degree of certainty.

5.5 SUMMARY

This chapter included discussion of the results of the as-designed (code-based) and in-situ (measurement-based) analyses. Intermediate results, including bending moments, shear forces, resistance, distribution factors, and dynamic load allowance, were presented, along with the resulting reliability estimates. Probable effects of varying the degree of bearing restraint were discussed, and a cost-benefit analysis outlining the most economical option for

managing truck loading over the bridge in question was introduced. Results were presented for two methods of analysis to estimate flexural load effects: using measured curvatures, and using measured neutral axis locations along with strains recorded in the lower strain gauges. In addition to the analysis of the measured results for the currently permitted 62.5 t truck loading, reliability indices were also estimated for the proposed increased 110 t GVW. In these analyses, each instrumented location was considered separately.

In the as-designed analysis, two methods of evaluation described by CAN/CSA-S6-00 (CSA 2000) were used: the load and resistance factor method, and the mean load method. The methods provided somewhat different results, with the mean load method found to be more conservative, although this is generally not expected to be the case. While the load and resistance factor method showed the girders to have sufficient capacity even under the proposed increased loading, the mean load method results showed that reliability would be compromised in flexure if the allowable GVW was increased to 110 t; in that case the critical reliability index of 2.79 (at midspan of the center span in an exterior girder) was found to fall below the target value of 3.0 for flexure. These results indicate that loading on the Red Deer River Bridge should likely not be increased without improving the reliability estimate.

The reliability estimates determined in the in-situ (measurement-based) analysis were significantly higher than those determined in the as-designed (code-based) analysis, indicating that the girders had sufficient capacity to resist the load effects which would be induced by 110 t trucks. The improved estimates of reliability occurred as a result of several factors, although they were mainly due to a change in the assessment of the dominant load carrying mechanism as compared to that assumed initially. Axial forces in the girders caused by arching action allowed for a reduction in the bending moments and shear forces induced in the girders. However, increased resistance, reduced dynamic load allowance, and in some cases more favourable distribution

factors also contributed to increasing in-situ reliability estimates. Based on the measurements taken as part of this study, the critical, or governing reliability index of the Red Deer River Bridge for the proposed increased loading was found to be 3.81 for shear at the girder supports, which is nevertheless significantly higher than the target value of 3.25 for shear. For flexure, estimated resulting reliability indices were even less critical, with the governing value of 4.60 at location 1-5 (in a negative bending moment region) being significantly greater than the minimum allowable reliability index of 3.25 for flexure.

The influence of horizontal bearing restraint at the bridge bearings and dynamic load effects were investigated numerically with finite element models dynamically "calibrated" to the measured behaviour of the Red Deer River Bridge. The effects of bearing restraint were checked for two cases: with the bearings completely fixed against horizontal translation, and perfectly free to move horizontally. It was found that the degree of bearing restraint significantly influenced the resulting reliability of the bridge girders. Fixed bearings generally resulted in substantially reduced reliability indices near the ends of the girders, where the negative bending moments and shear forces were greatest, with the critical reliability index of 2.50 in flexure falling well below the target value. Bearings assumed to provide no horizontal restraint, on the other hand, had no detrimental effects on resulting reliability indices relative to measured behaviour, actually increasing reliability estimates in the critical end regions. In general, numerical results based on the assumption of free bearings (no horizontal restraint) were consistently more similar to measured values than those assuming fixed conditions.

Another finite element model used to study the potential DLA provided results that were consistent with those measured on site. In both the field and numerical studies, negative DLA values were found, showing dynamic load effects to be less severe than comparable static load effects.

The analysis of relative costs was used to determine potential economic benefits of using site-specific data to aid in the management of bridge loading. Two methods of obtaining improved reliability estimates were considered: strengthening and the research methodology. The current hauling situation was also analysed for comparative purposes. It was determined that the proposed research methodology employing structural health monitoring provided the most economical means of improving reliability estimates for hauling increased loads, costing $108,000 less than the strengthening alternative.

CHAPTER 6 CONCLUSIONS AND RECOMMENDATIONS

6.1 SUMMARY

The primary objective of this research was to develop and apply a methodology for assessing safe levels of allowable loading on a bridge using information obtained from on-site instrumentation based on a reliability-based evaluation. The study involved two distinct analyses of the Red Deer River Bridge: the as-designed analysis and the in-situ analysis. In the as-designed analysis, the evaluation was carried out using the two reliability-based methods outlined in the Canadian Highway Bridge Design Code CAN/CSA-S6-00 (CSA 2000) based on information derived from design drawings and specifications. In the in-situ analysis, a re-evaluation was performed using site-specific parameters and factors measured as part of a field study.

The as-designed analysis involved the evaluation of the bridge girders by the load and resistance factor method and the mean load method. Evaluations were completed for the current allowable loading condition, as well as for a proposed increased allowable loading condition. The live load capacity factors resulting from each method were compared to determine the differences; in addition, reliability indices were determined using results from the mean load method. The reliability indices provided a base-line for which the in-situ reliability indices could be compared.

In the in-situ analysis, the bridge girders were re-evaluated using the mean load method. Several of the variables used in the mean load method were determined from field testing carried out at the bridge. Non-destructive evaluations were used to determine material properties, and strain gauges were installed on the girders to measure load effects. Loading was provided by trucks, both in a controlled setting and a normal traffic setting. From the field measurements and variables taken from the literature, site-specific statistical parameters were generated for bending moments, shear forces, distribution factors, the dynamic load allowance, bending moment resistance, and shear resistance. Site-specific reliability indices were determined using the generated statistical parameters.

Finite element models were used to verify and check the results of the in-situ analysis. The measured dynamic load allowance was compared with that determined using a finite element model with simulated truck loading conditions. In addition, the effects of varying degrees of bearing restraint on reliability were checked using a model.

A cost-benefit analysis was performed to determine the economic feasibility of using the research methodology as a means of managing bridge loading. The costs of the research methodology were compared with the proposed strengthening alternatives, as well as leaving the bridge in the current state.

6.2 CONCLUSIONS

The following sections summarize the conclusions which were drawn from the results of the as-designed analysis and the in-situ analysis.

6.2.1 *As-Designed Analysis*

1. The mean load method gave more conservative results than those determined by the load and resistance factor method in this study, although, in general, the load and resistance factor is more conservative. Although the load and resistance factor method provided results indicating that the bridge would have sufficient live load capacity to accommodate the proposed allowable loading of 110 t trucks, with a live load capacity factor of 1.02, the mean load method results indicated that the live load capacity would fall below the minimum allowable value of 1.00, at 0.96. Bending moments at midspan of the central span of the bridge, in the exterior girders, were found to be the critical load effect.

6.2.2 *In-Situ Analysis*

2. The use of site-specific statistical parameters in the determination of bending moments, shear forces, distribution factors, dynamic load allowance, bending moment resistances, and shear resistances was found to significantly increase the computed structural reliability for both bending moments and shear forces at nearly all strain gauge locations.

   Increases in structural reliability can be primarily attributed to measured load effects and material properties which were more favourable than those determined based on CAN/CSA-S6-00 (CSA 2000). The measured ultimate compressive strength of concrete was found to be 41.7 MPa, over twice that which was specified in the design (20.7 MPa), increasing resistance. Bending moments derived from strain gauge measurements were found to be, at most, only 30% of those determined in the as-designed analysis. Similarly, measured shear forces were at their maximum only 32% of those determined in the as-designed analysis.

The critical reliability index for the bridge was increased from 2.90 in the as-designed analysis (bending moment at the middle gauge location on an exterior center span girder), to 3.81 based on in-situ data (shear at the end strain gauges on an exterior center span girder), higher than the minimum allowable reliability index of 3.25 for shear. This represents a significant improvement in reliability; on this basis, the bridge was found to have sufficient capacity to carry the proposed increased allowable loading.

3. Actual flexural load effects were determined to be significantly smaller than those predicted in the as-designed analysis, due to large axial forces in the girders, indicating that the applied load was being carried, to some degree, by arching action. As a significant portion of the applied load appears to be carried axially in the girders, bending moments are correspondingly reduced, thereby increasing the reliability.

   The manner in which flexural load effects were shared amongst the girders was, in most cases, very different, and often less severe, than would be suggested by code-prescribed distribution factors. Approximately half of the measured distribution factors were less than those determined based on CAN/CSA-S6-00 (CSA 2000) for bending moment and shear, contributing to higher reliability indices at those locations.

   The measured dynamic load allowance (DLA) was determined to be negative (ie. dynamic loading was less severe than static), with a value of -0.075, and a coefficient of variation of 0.62. For the purposes of reliability calculations, however, the DLA was taken as 0.00 due to possibility of stopped or slow-moving trucks on the bridge. These values compared very favourably with the code-specified DLA of 0.3 and coefficient of variation of 0.8 from a structural reliability perspective.

Furthermore, the results from the numerical bearing restraint portion of the study suggested that, although structural reliability would become unacceptably low if the bridge bearings were to become fixed against lateral translation, well maintained bearings approaching ideal roller support behaviour would further increase the reliability index to 4.05 (governed by the same conditions as those described above).

The combination of these improvements contributed to increased overall reliability estimates.

4. The research methodology (ie. structural monitoring and the use of site specific data) provided the most economical option for safely increasing the allowable loading on the Red Deer River Bridge. The research methodology was found to be more economical than the proposed strengthening alternatives, as well as the option of leaving the bridge in it's current condition. Implementing the research methodology with the result that improved reliability estimates would enable the passage of increased truck loading would result in savings of approximately $206 000 in the first year compared with applying either of the strengthening alternative, and a savings of approximately $850 000 in the first year compared with leaving the bridge in the current state and continuing to haul with the current allowable truck GVW.

6.3 RECOMMENDATIONS FOR FUTURE RESEARCH

There are several areas in which future research should be performed in order to obtain more reliable results.

In this study, a small number of truck passes were recorded due to time and cost restrictions. However, a large number of truck passes should be used to ensure that a representative distribution of all trucks travelling over the bridge

is obtained. Furthermore, using a substantial number of truck passes would greatly decrease the variability in the resulting distributions of load effects, thereby increasing the reliability of the resulting evaluations. The most desirable method of obtaining strain data for a large number of truck passes is by installing a continuous monitoring system, in which the data acquisition remains unmanned, having sensors to record when trucks enter and exit the bridge. In a study by Au et al. (2005), a data acquisition system was used which recorded only the maximum and minimum strains over an extended period of time, resulting in a small amount of data. The setup in this study could remain essentially the same as was discussed in Chapter 3; however, the system would need to be triggered by certain strain amplitudes to notify the system when loaded trucks were present. In addition, the data processing routines could be modified to reduce the large amounts of data typically collected.

The data used in this study was measured over a two-day period in the autumn. It would be useful to record strain data in different seasons, as the weight of logs and the bridge response characteristics may vary depending on the weather. The logging trucks are loaded in the logging area "by eye," and as such, are often overloaded. In a wet season, the problem may be even more pronounced. Au et al. (2005) discussed the need for selecting the season and period of measurements to capture the most critical loading on a bridge, and, in particular, the importance of doing so in the forestry industry. Chajes et al. (1997) found that the loading characteristics and occurrence of loading events change in different weeks of the year, different days of the week, and even throughout the day.

In addition to obtaining more ambient truck traffic data, more controlled data should be collected. A large number of recordings for similar passes should be collected to minimize the variation in the measured dynamic load

allowance; in addition, several different speeds should be used to determine the dynamic load effects at speeds other than full highway speed.

Strain gauges should be installed at several other locations on the bridge girders to ensure that locations other than those used in this study do not govern the reliability indices of the bridge. Strain gauges should be placed on all three spans of the three girders, and at potentially critical locations, including as close to the piers and midspans as possible.

REFERENCES

AASHTO (a). 1994. *Guide Specifications for Distribution of Loads for Highway Bridges*, American Association of State Highway and Transportation Officials, Washington, D.C.

AASHTO (b). 1994. *LRFD Highway Bridge Design Specifications, 1st ed.*, American Association of State Highway and Transportation Officials, Washington, D.C.

AASHTO. 1998. *LRFD Highway Bridge Design Specifications, 2nd ed.*, American Association of State Highway and Transportation Officials, Washington, D.C.

AASHTO. 1983. *Standard Specification for Highway Bridges*, American Association of State Highway and Transportation Officials, Washington, D.C.

AASHTO. 1989. *Standard Specification for Highway Bridges*, American Association of State Highway and Transportation Officials, Washington, D.C.

AASHTO. 1992. *Standard Specifications for Highway Bridges*, American Association of State Highway and Transportation Officials, Washington, D.C.

AASHTO. 1996. *Standard Specification for Highway Bridges, 16th ed.*, American Association of State Highway and Transportation Officials, Washington, D.C.

Agarwal, C.A, and M.S. Cheung. 1987. Development of loading-truck model and live-load factor for the Canadian Standards Association CSA-S6 Code, *Canadian Journal of Civil Engineering*, Vol. 14, pp. 58-67.

Akgul, F., and D.M. Frangopol. 2004. Bridge Rating and Reliability Correlation: Comprehensive Study for Different Bridge Types, *Journal of Structural Engineering*, Vol. 130, No. 7, pp. 1063-1074.

Akgul, Ferhat, and D.M. Frangopol. 2003. Rating and Reliability of Existing Bridges in Network, *Journal of Bridge Engineering,* Vol. 8, No. 6, pp. 383-393.

Alwash, M., Sparling, B.F., and Wegner, L.D. 2005. Excitation sources for vibration-based damage detection on the Red Deer River Bridge. Proceedings of the 1st CSCE Specialty Conference on

InfrastructureTechnologies, Management and Policy, Toronto, ON, June 2-4, Canadian Society for Civil Engineering, Paper FR-124, on CD.

Alwash, M., Sparling, B.F., and Wegner, L.D. 2006. Influence of the Excitation Source on Modal Parameter Estimation for the Red Deer River Bridge. Proceedings of the 1st International Structural Specialty Conference, Calgary, AB, May 23-26, Canadian Society for Civil Engineering, Paper ST-28, on CD.

Asantey, S.B.A, and F.M. Bartlett. 2005. Impact of Posted Load Limits on Highway Bridge Reliability, *Journal of Bridge Engineering*, Vol. 10, No. 3, pp. 321-330.

ASTM. 2002. *Standard Test Method for Pulse Velocity Through Concrete: C597-02*, American Society of Testing and Materials.

ASTM. 2002. *Standard Test Method for Rebound Number of Hardened Concrete: C805-02*, American Society of Testing and Materials.

Au, A., C. Lam, A.C. Agarwal, and B. Tharmababla. 2005. Bridge evaluation by mean load method per the Canadian Highway Bridge Design Code, *Canadian Journal of Civil Engineering*, Vol. 31, pp. 678-686.

Bakht, B., and L.G. Jaeger. 1990. Bridge Testing – A Surprise Every Time, *Journal of Structural Engineering*, Vol. 116, No. 5, pp. 1370-1383.

Barnes, R.W., J.M. Stallings, and P.W. Porter. 2003. Live-Load Response of Alabama's High-Performance Concrete Bridge, *Transportation Research Record*, No. 1845, pp. 115-124.

Billing, J.R., Dynamic loading and testing of bridges in Ontario. 1984. *Canadian Journal of Civil Engineering*, Vol. 11, pp. 833-843.

Cantieni, R. 1984. Dynamic Load Testing of Highway Bridges, *Transportation Research Record*, Vol. 2, pp. 141-148.

Chajes, M.J., D.R. Mertz, and B. Commander. 1996. Can economical bridge testing reduce posting?, *Better Roads*, Vol. 66, No. 8, pp. 29-32.

Chajes, M.J., D.R. Mertz, and B. Commander. 1997. Experimental Load Rating of a Posted Bridge, *Journal of Bridge Engineering*, Vol. 2, No. 1, pp. 1-10.

Chajes, M.J., H.W. Shenton, III, and D. O'Shea. 2000. Bridge-Condition Assessment and Load Rating Using Nondestructive Evaluation Methods, *Transportation Research Record*, No. 1696, pp. 83-91.

Chan, T.H.T., and C. O'Connor. 1990. Wheel Loads from Highway Bridge Strains: Field Studies, *Journal of Structural Engineering*, Vol. 116, No. 7, pp. 1751-1771.

Cheung, M.S., and W.C. Li. 2002. Reliability assessment in highway bridge design, *Canadian Journal of Civil Engineering*, Vol. 29, pp. 799-805.

CSA. 2000. *Canadian Highway Bridge Design Code: Standard CAN/CSA-S6-00*, Canadian Standards Association, Toronto.

CSA. 2000. *Canadian Highway Bridge Design Code: Standard CAN/CSA-S6-00 Commentary*, Canadian Standards Association, Toronto.

Das, P.C. 1998. Application of reliability analysis in bridge management, *Engineering Structures*, Vol. 20, No. 11, pp. 957-959.

Department of Highways and Transportation (DHT), Government of Saskatchewan. 1956. Design Drawings for the Red Deer River Bridge.

Department of Highways and Transportation (DHT), Government of Saskatchewan. 2007. *E-mail regarding costs for 2006 strengthening*.

Dunker, K.F., and B.G. Rabbat. 1995. Assessing Infrastructure Deficiencies: The Case of Highway Bridges, *Journal of Infrastructure Systems*, Vol. 1, No. 2, pp. 100-119.

Earth Tech (Canada) Inc. 2002. *P.H. 9 Over Red Deer River Bridge Evaluation Bridge File 203-44-28 Phase 1 – Evaluation – Preliminary Design: Design Calculations/Notes*.

Estes, A.C., and D.M. Frangopol (a). 2001. Bridge lifetime system reliability under multiple limit states, *Journal of Bridge Engineering*, Vol. 6, No. 6, pp. 523-528

Estes, A.C., and D.M. Frangopol (b). 2001. Minimum expected cost oriented optimal maintenance planning for deteriorating structures: application to concrete bridge decks. *Reliability Engineering and System Safety*, No. 73, pp. 281-291.

Estes, A.C., and D.M. Frangopol. 1999. Repair Optimization of Highway Bridges Using System Reliability Approach, *Journal of Structural Engineering*, Vol. 125, No. 7, pp. 766-775.

Estes, A.C., and D.M. Frangopol. 2003. Updating bridge reliability based on bridge management systems visual inspection results, *Journal of Bridge Engineering*, Vol. 8, No. 6, pp. 374-382.

Frangopol, D.M., J.S. Kong, and E.S. Gharaibeh. 2001. Reliability-based life-cycle management of highway bridges, *Journal of Computing in Civil Engineering*, Vol. 15, No. 1, pp. 27-34.

Fu, C.C., M. Elhelbawey, M.A. Sahin, and D.R. Schelling. 1996. Lateral Distribution Factor from Bridge Field Testing, *Journal of Structural Engineering*, Vol. 112, No. 9, pp. 1106-1109.

Ghosn, M. 2000. Development of truck weight regulations using bridge reliability model, *Journal of Bridge Engineering*, Vol. 5, No. 4, pp. 293-303.

Ghosn, M., F. Moses, and J. Gobieski. 1986. Evaluation of Steel Bridges Using In-Service Testing, *Transportation Research Record*, No. 1072, pp. 71-78.

GreatWest Kenworth, 5909 6th St. SE, Calgary, AB, T2H 1L8. 2007. *Conversation regarding truck costs*.

Huang, H., H.W. Shenton, and M.J. Chajes. 2004. Load Distribution for a Highly Skewed Bridge: Testing and Analysis, *Journal of Bridge Engineering*, Vol. 9, No. 6, pp. 558-562.

Humar, J.L., and A.M. Kashif. 1993. Dynamic response of bridges under travelling loads, *Canadian Journal of Civil Engineering*, Vol. 20, pp. 287-298.

ISIS Canada. 2001. Reinforcing *Concrete Structures with Fibre Reinforced Polymers*, Intelligent Sensing for Innovative Structures, Winnipeg.

Kim, S., and A.S. Nowak. 1997. Load Distribution and Impact Factors for I-Girder Bridges, *Journal of Bridge Engineering*, Vol. 2, No. 3, pp. 97-104.

Kim, S., A.S. Nowak, and A.F. Sokolik. 1995. Site-Specific Truck Load Study, *Road Transport Technology 4: Proceedings of the Fourth International Symposium on Heavy Vehicle Weights and Dimensions*, pp. 159-163.

Kim, S., A.S. Nowak, and R. Till. 1999. Verification of Site-Specific Live Load on Bridges, *Specialty Conference on Probabilistic Mechanics and Structural Reliability*, pp. 214-217.

Laman, J.A., and A.S. Nowak. 1995. Verification of Truck Loads for Girder Bridges, *Restructuring America and Beyond: Proceedings of Structures Congress XIII*, pp. 907-920.

Lee, E.S.L. 1978. Thesis: Non-Destructive Testing of Concrete Compressive Strength, *University of Saskatchewan*, Saskatoon.

Manac, 15750 128th Ave., Edmonton, AB, T5V 1G1. 2007. *Conversation regarding logging trailer costs*.

Martin, J., M.S.A. Hardy, A.S. Usmani, and M.C. Forde. 1998. Accuracy of NDE in bridge assessment, *Engineering Structures*, Vol. 20, No. 11, pp. 979-984.

MTC. 1979. *Ontario Highway Bridge Design Code*, Ministry of Transportation and Communications, Downsview, Ontario.

MTC. 1983. *Ontario Highway Bridge Design Code*, Ministry of Transportation and Communications, Ontario.

Moses, F., J.P. Lebet, and R. Bez. 1994. Applications of Field Testing to Bridge Evaluation, *Journal of Structural Engineering*, Vol. 120, No. 6, pp. 1745-1762.

Nassif, H.H., and A.S. Nowak (a). 1995. Dynamic Effect of Truck Loads On Girder Bridges, *Road Transport Technology 4: Proceedings of the Fourth International Symposium on Heavy Vehicle Weights and Dimensions*, pp. 383-387.

Nassif, H.H., and A.S. Nowak (b). 1995. Dynamic Load Spectra for Girder Bridges, *Transportation Research Record*, No. 1476, pp. 69-83.

National Instruments Corporation. 2003. *Labview 7 Express User Manual*, National Instruments Corporation, Austin.

Nowak, A.S., Calibration of LRFD Bridge Code, *Journal of Structural Engineering*, Vol. 121, No. 8, pp. 1245-1251.

Nowak, A.S. 1988. Development of Bridge Design Code, *Probabilistic Methods in Civil Engineering: Proceedings of the 5th ASCE Specialty Conference*, pp. 37-40.

Nowak, A.S. 1993. Development of Bridge Load Model for LRFD Code, *Symposium on Structural Engineering in Natural Hazards Mitigation*, pp. 1041-1046, 1993.

Nowak, A.S. 1994. Load and Resistance Factors for Bridge Design Code, *Structures Congress XII: Proceedings of the Papers Presented at the Structures Congress '94*, pp. 538-543.

Nowak, A.S. 1994. Load model for bridge design code, *Canadian Journal of Civil Engineering*, Vol. 21, pp. 36-49.

Nowak, A.S. 1989. Reliability Models for Bridge Structures, *Structural Design, Analysis, and Testing Conference Proceedings*, pp. 786-795.

Nowak, A.S. 1990. System Reliability Models for Bridges, *Structural Safety*, Vol. 7, No. 2, pp. 247-254.

Nowak, A.S., and K.R. Collins. 2000. *Reliability of Structures*, McGraw Hill Companies Inc., Boston.

Nowak, A.S., J. Eom, and A. Sanli. 2000. Control of Live Load on Bridges, *Transportation Research Record*, No. 1696, pp. 136-145.

Nowak, A.S., and H.N. Grouni. 1994. Calibration of the Ontario Highway Bridge Design Code 1991 edition, *Canadian Journal of Civil Engineering*, Vol. 21, pp. 25-35.

Nowak, A.S, and N.C. Lind. 1979. Practical Code Calibration Procedures, *Canadian Journal of Civil Engineering*, Vol. 6, pp. 112-119.

Nowak, A.S., and H. Nassif. 1992. Live Load Models Based on WIM Data, *Probabilistic Mechanics and Structural and Geotechnical Reliability, Proceedings of the Specialty Conference*, pp. 587-590.

Nowak, A.S, A. Sanli, and J. Eom. 1999. Bridge Girder Distribution Factors for Live Load, *Structures Congress Proceedings*, pp. 516-519.

Nowak, A.S., and M.M. Szerszen. 1998. Bridge load and resistance models, *Engineering Structures*, Vol. 20, No. 11, pp. 985-990.

Nowak, A.S., and T. Tharmabala. 1989. Bridge Reliability Evaluation Using Load Tests, *Journal of Structural Engineering*, Vol. 114, No. 10, pp. 2268-2279.

Nowak, A.S., A.S. Yamani, and S.W. Tabsh. 1994. Probabilistic Models for Resistance of Concrete Bridge Girders, *ACI Structural Journal*, Vol. 91, No. 3, pp. 269-276.

Nowak, A.S., and J. Zhou. 1990. System Reliability Models for Bridges, *Structural Safety*, Vol. 7, pp. 247-254.

Paultre, P., J. Proulx, and M. Talbot. 1995. Dynamic Testing Procedures for Highway Bridges Using Traffic Loads, *Journal of Structural Engineering*, Vol. 121, No. 2, pp. 362-376.

Peterson, D. 2001. Heavy Weight Temptations, *Timber Harvesting*, Vol. 49, No. 7, pp. 17.

Reid Crowther and Partners Ltd. 1989. *Design Drawings for Bridge Girder Reinforcing: Bridge over Red Deer River on P.H. No. 9*.

Reid, J.S., M.J. Chajes, D.R. Mertz, and G.H. Reichelt. 1996. Bridge Strength Evaluation Based on Field Tests, *Probabilistic Mechanics and Structural Reliability, Proceedings of the Seventh Specialty Conference*, pp. 294-297.

Ryall, M.J. *2001. Bridge Management,* Butterworth-Heinemann, Oxford.

Schulz, J.L., B. Commander, G.G. Goble, and D.M. Frangopol. 2005. Efficient Field Testing and Load Rating of Short- and Medium-Span Bridges, *Structural Engineering Review*, Vol. 7, No. 3, pp. 181-194.

Sparks, Gordon. 2005. *Conversation regarding Heavy Haul Agreement in Saskatchewan*.

Sparling, Bruce. 2005. *C.E. 816: Structural Dynamics Class Notes*, University of Saskatchewan.

Sparling, Bruce. 2005. *FORTRAN program for strain distribution*.

Stewart, M.G. 2001. Reliability-based assessment of ageing bridges using risk ranking and life cycle cost decision analysis*, Reliability Engineering and System Safety*, No. 74, pp. 263-273.

Stewart, M.G., and D.V. Rosowsky. 1998. Time-dependent reliability of deteriorating reinforced concrete bridge decks*, Structural Safety*, Vol. 20, pp. 91-109.

Tabsh, S.W., and A.S. Nowak. 1991. Reliability of Highway Girder Bridges, *Journal of Structural Engineering*, Vol. 117, No. 8, pp. 2372-2389.

Talbot, R. 1999. Why Install On-Board Scales?, *Timber Harvesting*, Vol. 47, No. 4, pp. 17.

Tokyo Sokki Kenkyujo Company. 2006. Website: www.tokyosokki.co.jp.

Val, D.V., M.G. Stewart, and R.E. Melchers. 1998. Effect of reinforcement corrosion on reliability of highway bridges, *Engineering Structures*, Vol. 20, No. 11, pp. 1010-1019.

APPENDIX A GIRDER SECTION DETAILS

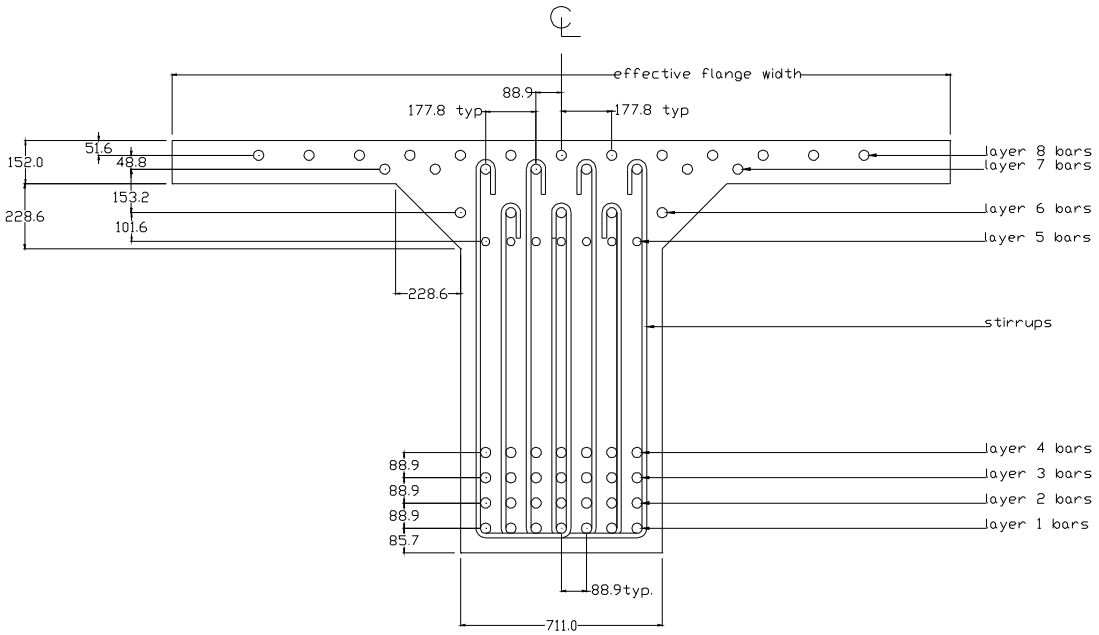

Figure A.1. General girder cross-section, to be used with Table A.1.

Table A.1. Girder cross-section summary (cont'd on next page).

						Number of Reinforcing Bars in Layer			
Girders	**Section**	**SGs**	**Girder Height (mm)**	**Effective flange width (mm)**	**Number of stirrups (#5 bars)**	**1 (#11 bars)**	**2 (#11 bars)**	**3 (#11 bars)**	**4 (#11 bars)**
Interior	End SGs	2-1, 2-5	2472	2743	2	5	0	0	0
	Second SGs	2-2, 2-4	1450	2743	2	7	6	0	0
	Middle SG's	2-3	1204	2743	3	7	7	3	0
	Midspan Center Span	N/A	1194	2743	3	7	7	3	0
	Midspan End Spans	N/A	1194	2743	3	7	7	7	3
	Piers	N/A	2845	2743	4	7	0	0	0
Exterior	End SGs	1-1, 1-5, 3-1, 3-5	2472	2642	2	5	0	0	0
	Second SGs	1-2, 1-4, 3-2, 3-4	1450	2642	2	7	6	0	0
	Middle SG's	1-3, 3-3	1204	2642	3	7	7	3	0
	Midspan Center Span	N/A	1194	2642	3	7	7	3	0
	Midspan End Spans	N/A	1194	2642	3	7	7	7	3
	Piers	N/A	2845	2642	4	7	0	0	0

* Layer 7 bars marked with an asterisk are size #4 bars.

Table A.1. Girder cross-section summary (cont'd).

					Number of Reinforcing Bars in Layer				
Girders	**Section**	**SGs**	**Girder Height (mm)**	**Effective flange width (mm)**	**5 (#9 bars)**	**6 (#11 bars)**	**7 * (#11 bars)**	**8 (#11 bars)**	**ext. (32mm bars)**
Interior	End SGs	2-1, 2-5	2472	2743	6	5	8	13	0
	Second SGs	2-2, 2-4	1450	2743	0	2	2 *	8	4
	Middle SG's	2-3	1204	2743	0	2	0	8	8
	Midspan Center Span	N/A	1194	2743	0	2	0	8	8
	Midspan End Spans	N/A	1194	2743	0	0	0	8	6
	Piers	N/A	2845	2743	7	5	8	13	0
Exterior	End SGs	1-1, 1-5, 3-1, 3-5	2472	2642	6	5	8	10	0
	Second SGs	1-2, 1-4, 3-2, 3-4	1450	2642	0	2	2 *	8	4
	Middle SG's	1-3, 3-3	1204	2642	0	2	0	8	8
	Midspan Center Span	N/A	1194	2642	0	2	0	8	8
	Midspan End Spans	N/A	1194	2642	0	0	0	8	6
	Piers	N/A	2845	2642	7	5	8	10	0

* Layer 7 bars marked with an asterisk are size #4 bars.

APPENDIX B TRUCK DATA

Table B.1. Log trucks recorded at Red Deer River Bridge.

Truck number	Number of axles	Gross Weight	Tare Weight
1	6	60340	18230
2	6	60080	18820
3	6	60880	18240
4	7	69800	20970
5	8	58690	21850
6	8	67830	21080
7	8	72830	21270
8	6	60910	17900
9	7	72930	20800
10	8	71590	21060
11	6	60350	18330
12	8	72150	21000
13	6	60960	17490
14	8	70640	20040
15	7	69030	19650
16	8	68900	21920
17	6	58420	17980
18	8	62440	20220
19	6	60490	18090
20	6	60470	17770
21	8	72310	22260
22	8	68140	20980
23	6	56670	18210
24	8	61430	22250
25	8	72120	21210
26	6	60390	16910
27	6	60310	17040
28	6	60900	17970
	average	64714	19626
	standard deviation	5494	1742

Table B.2. Truck locations which caused maximum bending moments in as-designed analysis.

		62.5 t truck		110 t truck	
Location analysed	**End of bridge**	**lead axle position wrt to N abutment (m)**	**direction of travel**	**lead axle position (m)**	**direction of travel**
piers	N	30.44	NB	35.2	SB
	S	70.08	SB	65.32	NB
midspan exterior span	N	2.38	NB	-2.22	NB
	S	98.14	SB	102.74	SB
midspan interior span	N	63.34	SB	67.93	SB
	S	37.18	NB	32.59	NB
end strain gauges	N	30.44	NB	-1.69	NB
	S	70.08	SB	102.21	SB
second strain gauges	N	55.88	SB	60.49	SB
	S	44.64	NB	40.03	NB
middle strain gauges	one location only	38.62	NB	34	NB

Table B.3. Truck locations which caused maximum shear forces in as-designed analysis.

		62.5 t truck		110 t truck	
Location analysed	**End of bridge**	**lead axle position (m)**	**direction of travel**	**lead axle position (m)**	**direction of travel**
piers	N	46.97	SB	58.98	SB
	S	53.55	NB	41.54	NB
midspan exterior span	N	-0.35	NB	-12.5	NB
	S	100.87	SB	113.02	SB
midspan interior span	N	53.95	SB	57.55	SB
	S	46.57	NB	42.97	NB
end strain gauges	N	49.47	SB	61.61	SB
	S	51.05	NB	38.91	NB
second strain gauges	N	42.81	NB	70.77	SB
	S	57.71	SB	29.75	NB
middle strain gauges	one location only	51.68	SB	79.64	SB

APPENDIX C NON-DESTRUCTIVE EVALUATION RESULTS

Table C.1. Rebound hammers numbers recorded at the Red Deer River Bridge.

Location	Hammer number	Ultimate compressive strength, f'_c
NE corner of deck	47	42.86
	52	48.4
	46	41.76
	47	42.86
	48	43.97
	50	46.19
	49	45.08
	50	46.19
	51	47.3
NW corner of deck	48	43.97
	50	46.19
	48	43.97
	47	42.86
	45	40.65
	48	43.97
	51	47.3
	38	32.89
	48	43.97
SE corner of deck	46	41.76
	40	35.11
	47	42.86
	46	41.76
	46	41.76
	38	32.89
	52	48.4
	42	37.32
	50	46.19
SW corner of deck	38	32.89
	45	40.65
	48	43.97
	36	30.67
	46	41.76
	48	43.97
	45	40.65
	48	43.97
	46	41.76
Midspan of deck	43	38.43
	44	39.54
	38	32.89
	44	39.54
	44	39.54
	42	37.32
	43	38.43
	50	46.19
	42	37.32

Table C.2. Rebound hammer calibration results.

Concrete cylinder	Average hammer number	Ultimate Load (N)	Ultimate compressive strength, f'_c (Mpa)
1	29.33	125500	27.52
2	26.33	107500	23.57
3	27.33	125000	27.41
4	25.00	125000	27.41
5	19.00	65000	14.25
6	21.22	73500	16.12
7	27.11	105000	23.03
8	24.44	97000	21.27
9	33.11	125000	27.41
10	27.11	117000	25.66
11	26.44	120000	26.32
12	25.11	92500	20.29
13	28.67	115000	25.22
14	27.67	137500	30.15
15	28.89	150000	32.89
16	25.67	117500	25.77
17	30.00	120000	26.32
18	27.89	132500	29.06
19	24.33	90000	19.74
20	19.89	90000	19.74
21	22.22	107500	23.57

Table C.3. Rebound hammer results taken from literature (Lee 1978).

Rebound Hammer Number	Lee Mix A f'_c (MPa)	Lee Mix B f'_c (MPa)	Lee Mix C f'_c (MPa)	Rebound Hammer Manufacturer f'_c (MPa)
10	0.15	1.77	4.85	none specified
11	1.34	2.89	5.98	none specified
12	2.53	4.00	7.11	none specified
13	3.72	5.12	8.23	none specified
14	4.91	6.24	9.36	none specified
15	6.09	7.36	10.49	none specified
16	7.28	8.47	11.62	none specified
17	8.47	9.59	12.75	none specified
18	9.66	10.71	13.88	none specified
19	10.85	11.83	15.01	none specified
20	12.03	12.94	16.14	none specified
21	13.22	14.06	17.27	none specified
22	14.41	15.18	18.39	none specified
23	15.60	16.30	19.52	none specified
24	16.79	17.41	20.65	none specified
25	17.97	18.53	21.78	12.41
26	19.16	19.65	22.91	none specified
27	20.35	20.76	24.04	none specified
28	21.54	21.88	25.17	none specified
29	22.73	23.00	26.30	none specified
30	23.92	24.12	27.42	18.96
31	25.10	25.23	28.55	none specified
32	26.29	26.35	29.68	none specified
33	27.48	27.47	30.81	none specified
34	28.67	28.59	31.94	none specified
35	29.86	29.70	33.07	26.89
36	31.04	30.82	34.20	none specified
37	32.23	31.94	35.33	none specified
38	33.42	33.06	36.46	none specified
39	34.61	34.17	37.58	none specified
40	35.80	35.29	38.71	35.51
41	36.98	36.41	39.84	none specified
42	38.17	37.53	40.97	none specified
43	39.36	38.64	42.10	none specified
44	40.55	39.76	43.23	none specified
45	41.74	40.88	44.36	44.13
46	42.93	41.99	45.49	none specified
47	44.11	43.11	46.61	none specified
48	45.30	44.23	47.74	none specified
49	46.49	45.35	48.87	none specified
50	47.68	46.46	50.00	53.43

Table C.3. (cont'd). Rebound hammer results taken from literature (Lee 1978).

Rebound Hammer Number	Lee Mix A f'_c (MPa)	Lee Mix B f'_c (MPa)	Lee Mix C f'_c (MPa)	Rebound Hammer Manufacturer f'_c (MPa)
51	48.87	47.58	51.13	none specified
52	50.05	48.70	52.26	none specified
53	51.24	49.82	53.39	none specified
54	52.43	50.93	54.52	none specified
55	53.62	52.05	55.65	none specified
56	54.81	53.17	56.77	none specified
57	55.99	54.29	57.90	none specified
58	57.18	55.40	59.03	none specified
59	58.37	56.52	60.16	none specified
60	59.56	57.64	61.29	none specified

APPENDIX D AS-DESIGNED RESULTS

Table D.1. Factored bending moments and shear forces.

Girders	Section	SGs	M_f for 62.5 t truck (kNm)	M_f for 110 t truck (kNm)	V_f for 62.5 t truck (kN)	V_f for 110 t truck (kN)
Interior	End SGs	2-1, 2-5	-9875	-11642	1728	2154
	Second SGs	2-2, 2-4	2931	3794	853	1008
	Middle SG's	2-3	5050	6667	459	287
	Midspan Center Span	N/A	5115	6736	360	381
	Midspan End Spans	N/A	5469	6793	803	866
	Piers	N/A	-12979	-15227	2256	2764
Exterior	End SGs	1-1, 1-5, 3-1, 3-5	-9994	-11808	1728	2154
	Second SGs	1-2, 1-4, 3-2, 3-4	3081	3988	853	1008
	Middle SG's	1-3, 3-3	5247	6944	459	287
	Midspan Center Span	N/A	5313	7014	360	381
	Midspan End Spans	N/A	5680	7077	803	866
	Piers	N/A	-13112	-15419	2256	2764

Table D.2. Factored bending moment resistance and shear resistance.

Girders	Section	SGs	M_r (kNm)	V_r for 62.5 t truck (kN)	V_r for 110 t truck (kNm)
Interior	End SGs	2-1, 2-5	15327	2682	2430
	Second SGs	2-2, 2-4	6137	1552	1375
	Middle SGs	2-3	6940	1087	1087
	Midspan Center Span	N/A	6848	1077	1077
	Midspan End Spans	N/A	6756	1115	1133
	Piers	N/A	18759	4807	4893
Exterior	End SGs	1-1, 1-5, 3-1, 3-5	14003	2367	2421
	Second SGs	1-2, 1-4, 3-2, 3-4	6135	1550	1373
	Middle SGs	1-3, 3-3	6925	1110	1110
	Midspan Center Span	N/A	6835	1095	1095
	Midspan End Spans	N/A	7105	1107	1126
	Piers	N/A	17131	4856	4943

Table D.3. Live load capacity factors from load and resistance factor method for bending moment and shear.

			F for Bending Moment		F for Shear	
Girders	**Section**	**SGs**	**62.5 t truck**	**110 t truck**	**62.5 t truck**	**110 t truck**
Interior	End SGs	2-1, 2-5	4.86	3.49	2.03	1.17
	Second SGs	2-2, 2-4	2.32	1.80	2.31	1.51
	Middle SG's	2-3	1.55	1.10	2.57	2.91
	Midspan Center Span	N/A	1.51	1.07	2.98	2.82
	Midspan End Spans	N/A	1.40	1.04	1.53	1.41
	Piers	N/A	5.65	3.90	3.06	2.20
Exterior	End SGs	1-1, 1-5, 3-1, 3-5	4.43	3.18	1.67	1.17
	Second SGs	1-2, 1-4, 3-2, 3-4	2.20	1.72	2.31	1.51
	Middle SG's	1-3, 3-3	1.47	1.05	2.63	2.91
	Midspan Center Span	N/A	1.43	1.02	3.03	2.82
	Midspan End Spans	N/A	1.42	1.05	1.52	1.41
	Piers	N/A	5.17	3.56	3.10	2.20

Table D.4. Unfactored dead load bending moments.

Section	SGs	M_{D1} (kNm)	M_{D2} (kNm)	M_{D3} (kNm)	M_{SD} (kNm)
End SGs	1-1, 1-5, 3-1, 3-5, 2-1, 2-5	-2610	-1826	-374	-4810.4
Second SGs	1-2, 1-4, 2-2, 2-4, 3-2, 3-4	4.68	-73.7	-15.1	-84.2
Middle SG's	1-3, 2-3, 3-3	541	350	71.7	962.9
Midspan Center Span	N/A	561	366	75	1001.8
Midspan End Spans	N/A	735	598	123	1455
Piers	N/A	-3997	-2619	-537	-7152.5

Table D.5. Unfactored dead load shear forces.

Section	SGs	V_{D1} (kN)	V_{D2} (kN)	V_{D3} (kN)	V_{SD} (kN)
End SGs	1-1, 1-5, 3-1, 3-5, 2-1, 2-5	443.1	264.5	54.2	761.8
Second SGs	1-2, 1-4, 2-2, 2-4, 3-2, 3-4	154.3	118.5	24.3	297
Middle SG's	1-3, 2-3, 3-3	27.8	22.6	4.63	55
Midspan Center Span	N/A	0.196	0.16	0.033	0.389
Midspan End Spans	N/A	118.6	84.7	17.4	220.6
Piers	N/A	560.8	308.7	63.2	932.7

Table D.6. Unfactored live load bending moments and shear forces.

Girders	Section	SGs	M_u for 62.5 t truck (kNm)	M_u for 110 t truck (kNm)	V_u for 62.5 t truck (kN)	V_u for 110 t truck (kN)
Interior	End SGs	2-1, 2-5	-3088	-4302	570.9	850.9
	Second SGs	2-2, 2-4	2079	2672	338.7	440.7
	Middle SG's	2-3	2728	3838	260.8	230.2
	Midspan Center Span	N/A	2742	3855	237.3	251.1
	Midspan End Spans	N/A	2633	3542	363.4	404.9
	Piers	N/A	-3430	-4974	792	1126.3
Exterior	End SGs	1-1, 1-5, 3-1, 3-5	-3172	-4418	570.9	850.9
	Second SGs	1-2, 1-4, 3-2, 3-4	2187	2810	338.7	440.7
	Middle SG's	1-3, 3-3	2869	4036	260.8	230.2
	Midspan Center Span	N/A	2884	4054	237.3	251.1
	Midspan End Spans	N/A	2781	3742	363.4	404.9
	Piers	N/A	-3523	-5109	792	1126.3

Table D.7. Unfactored bending moment resistance and shear resistance.

Girders	Section	SGs	M_{ru} (kNm)	V_{ru} for 62.5 t truck (kN)	V_{ru} for 110 t truck (kNm)
Interior	End SGs	2-1, 2-5	17457	3287	3250
	Second SGs	2-2, 2-4	6821	2050	2050
	Middle SG's	2-3	7779	1556	1556
	Midspan Center Span	N/A	7676	1542	1542
	Midspan End Spans	N/A	7970	1551	1551
	Piers	N/A	21250	6292	5431
Exterior	End SGs	1-1, 1-5, 3-1, 3-5	15897	3280	3278
	Second SGs	1-2, 1-4, 3-2, 3-4	6818	2048	2048
	Middle SG's	1-3, 3-3	7765	1549	1549
	Midspan Center Span	N/A	7664	1535	1535
	Midspan End Spans	N/A	7954	1543	1543
	Piers	N/A	19357	6341	5473

Table D.8. Live load capacity factors from the mean load method for bending moment and shear.

			F for Bending Moments		F for Shear	
Girders	**Section**	**SGs**	**62.5 t truck**	**110 t truck**	**62.5 t truck**	**110 t truck**
Interior	End SGs	2-1, 2-5	3.34	2.37	2.10	1.35
	Second SGs	2-2, 2-4	1.95	1.49	2.65	2.01
	Middle SG's	2-3	1.48	1.04	3.02	3.44
	Midspan Center Span	N/A	1.45	1.01	3.33	3.15
	Midspan End Spans	N/A	1.59	1.16	1.84	1.64
	Piers	N/A	3.72	2.53	3.52	1.99
Exterior	End SGs	1-1, 1-5, 3-1, 3-5	2.93	2.08	2.10	1.37
	Second SGs	1-2, 1-4, 3-2, 3-4	1.84	1.41	2.65	2.00
	Middle SG's	1-3, 3-3	1.40	0.98	3.00	3.42
	Midspan Center Span	N/A	1.37	0.96	3.32	3.14
	Midspan End Spans	N/A	1.49	1.09	1.83	1.63
	Piers	N/A	3.27	2.22	3.55	2.01

Table D.9. Reliability indices for bending moment and shear.

			β for Bending Moment		β for Shear	
Girders	**Section**	**SGs**	**62.5 t truck**	**110 t truck**	**62.5 t truck**	**110 t truck**
Interior	End SGs	2-1, 2-5	9.71	7.80	5.77	4.32
	Second SGs	2-2, 2-4	5.71	4.42	7.21	6.13
	Middle SG's	2-3	5.00	3.18	8.64	9.28
	Midspan Center Span	N/A	4.88	3.07	9.32	9.03
	Midspan End Spans	N/A	5.35	3.77	5.80	5.33
	Piers	N/A	10.40	8.22	8.19	5.94
Exterior	End SGs	1-1, 1-5, 3-1, 3-5	8.93	7.04	5.76	4.38
	Second SGs	1-2, 1-4, 3-2, 3-4	5.45	4.16	7.20	6.12
	Middle SG's	1-3, 3-3	4.72	2.90	8.62	9.26
	Midspan Center Span	N/A	4.61	2.79	9.29	9.01
	Midspan End Spans	N/A	5.05	3.47	5.76	5.29
	Piers	N/A	9.63	7.47	8.24	5.99

APPENDIX E IN-SITU RESULTS

Table E.1. Measured curvatures.

Girder	SG Location	Mean Curvature ($x10^{-6}$/m)	Standard Deviation of Curvature (x10-6/m)	Coefficient of Variation
1	1-1	-14.29	8.77	0.614
	1-2	17.82	9.43	0.529
	1-3	N/A	N/A	N/A
	1-4	24.55	12.16	0.495
	1-5	-16.72	10.19	0.609
2	2-1	-18.26	8.8	0.482
	2-2	12.51	7.89	0.631
	2-3	48.25	23.44	0.486
	2-4	16.45	10.67	0.649
	2-5	-10.88	5.03	0.462
3	3-1	-15.25	8.24	0.540
	3-2	13.91	5.59	0.402
	3-3	3.6	3.22	0.894
	3-4	8.03	3.38	0.421
	3-5	-11.23	4.15	0.370

Table E.2. Measured neutral axis locations.

Girder	SG Location	Mean NA (m)	Standard Deviation of NA (m)	Coefficient of Variation
1	1-1	1.24	0.22	0.177
	1-2	1.69	0.07	0.041
	1-3	N/A	N/A	N/A
	1-4	1.77	0.08	0.045
	1-5	1.16	0.16	0.138
2	2-1	1.19	0.13	0.109
	2-2	1.88	0.11	0.059
	2-3	2.11	0.03	0.014
	2-4	1.8	0.07	0.039
	2-5	1.28	0.13	0.102
3	3-1	0.91	0.41	0.451
	3-2	1.9	0.11	0.058
	3-3	1.74	0.37	0.213
	3-4	1.84	0.15	0.082
	3-5	1.26	0.13	0.103

Table E.3. Measured strains in lower strain gauges.

Girder	SG Location	Mean Strain ($x10^{-6}$)	Standard Deviation of Strain ($x10^{-6}$)	Coefficient of Variation
1	1-1	-13.86	9.44	0.681
	1-2	4.06	1.71	0.421
	1-3	N/A	N/A	N/A
	1-4	13	6.7	0.515
	1-5	-14.73	9.93	0.674
2	2-1	-17.1	7.96	0.465
	2-2	14.59	6.92	0.474
	2-3	28.58	13.9	0.486
	2-4	N/A	N/A	N/A
	2-5	-9.46	4.59	0.485
3	3-1	-6.22	3.81	0.613
	3-2	10.45	5.37	0.514
	3-3	0.85	1.03	1.212
	3-4	5.43	2.71	0.499
	3-5	-9.97	4.2	0.421

Table E.4. Distribution factors for bending moments determined using measured curvatures.

Girder	SG Location	Mean DF	Standard Deviation of DF	Coefficient of Variation	Mean 2DF
1	1-1	0.294	0.159	0.541	0.588
	1-2	0.34	0.037	0.109	0.68
	1-3	0.485	0.139	0.287	0.97
	1-4	0.492	0.054	0.110	0.984
	1-5	0.404	0.212	0.525	0.808
2	2-1	0.396	0.127	0.321	0.792
	2-2	0.392	0.042	0.107	0.784
	2-3	0.474	0.062	0.131	0.948
	2-4	0.338	0.053	0.157	0.676
	2-5	0.308	0.095	0.308	0.616
3	3-1	0.31	0.137	0.442	0.62
	3-2	0.268	0.02	0.075	0.536
	3-3	0.041	0.009	0.220	0.082
	3-4	0.17	0.014	0.082	0.34
	3-5	0.288	0.076	0.264	0.576

Table E.5. Distribution factors for bending moments determined using measured neutral axis locations and strains.

Girder	SG Location	Mean DF	Standard Deviation of DF	Coefficient of Variation	Mean 2DF
1	1-1	0.296	0.143	0.483	0.592
	1-2	0.171	0.048	0.281	0.342
	1-3	0.512	0.191	0.373	1.024
	1-4	0.511	0.179	0.350	1.022
	1-5	0.391	0.164	0.419	0.782
2	2-1	0.41	0.108	0.263	0.82
	2-2	0.429	0.136	0.317	0.858
	2-3	0.442	0.128	0.290	0.884
	2-4	0.227	0.061	0.269	0.454
	2-5	0.261	0.072	0.276	0.522
3	3-1	0.294	0.201	0.684	0.588
	3-2	0.401	0.14	0.349	0.802
	3-3	0.046	0.162	3.522	0.092
	3-4	0.262	0.1	0.382	0.524
	3-5	0.348	0.076	0.218	0.696

Table E.6. Distribution factors for shear determined using measured curvatures.

Girder	SG Location	Mean DF	Standard Deviation of DF	Coefficient of Variation	Mean 2DF
1	1-1	0.218	0.121	0.555	0.436
	1-2	0.44	0.053	0.120	0.88
	1-3	0.251	0.067	0.267	0.502
	1-4	0.482	0.058	0.120	0.964
	1-5	0.366	0.191	0.522	0.732
2	2-1	0.3	0.1	0.333	0.6
	2-2	0.51	0.061	0.120	1.02
	2-3	0.733	0.083	0.113	1.466
	2-4	0.471	0.079	0.168	0.942
	2-5	0.155	0.047	0.303	0.31
3	3-1	0.482	0.22	0.456	0.964
	3-2	0.05	0.004	0.080	0.1
	3-3	0.016	0.003	0.188	0.032
	3-4	0.047	0.004	0.085	0.094
	3-5	0.48	0.126	0.263	0.96

Table E.7. Distribution factors for shear determined using measured neutral axis locations and strains.

Girder	SG Location	Mean DF	Standard Deviation of DF	Coefficient of Variation	Mean 2DF
1	1-1	0.188	0.097	0.516	0.376
	1-2	0.465	0.128	0.275	0.93
	1-3	0.057	0.026	0.456	0.114
	1-4	0.429	0.147	0.343	0.858
	1-5	0.404	0.171	0.423	0.808
2	2-1	0.381	0.113	0.297	0.762
	2-2	0.434	0.136	0.313	0.868
	2-3	0.796	0.29	0.364	1.592
	2-4	0.446	0.117	0.262	0.892
	2-5	0.154	0.043	0.279	0.308
3	3-1	0.43	0.309	0.719	0.86
	3-2	0.1	0.035	0.350	0.2
	3-3	0.147	0.528	3.592	0.294
	3-4	0.126	0.047	0.373	0.252
	3-5	0.442	0.099	0.224	0.884

Table E.8. Estimated bending moment resistance determined using site-specific parameters.

Girders	Section	SGs	Mean M_r (kNm)	Standard Deviaton of M_r (kNm)	Coefficient of Variation
Interior	End SGs	2-1, 2-5	20736	2244	0.108
	Second SGs	2-2, 2-4	9356	1152	0.123
	Middle SG's	2-3	9436	1083	0.115
Exterior	End SGs	1-1, 1-5, 3-1, 3-5	18771	2047	0.109
	Second SGs	1-2, 1-4, 3-2, 3-4	9258	1142	0.123
	Middle SG's	1-3, 3-3	9333	1090	0.117

Table E.9. Estimated shear resistance using site-specific parameters for 62.5 t trucks.

Girder	SG Location	Mean V_r for 62.5 t truck (kN)	Standard Deviation of V_r for 62.5 t truck (kN)	Coefficient of Variation
1	1-1	4489.9	323.4	0.072
	1-2	2850	262.2	0.092
	1-3	1984.7	221.2	0.111
	1-4	2585.2	301.2	0.117
	1-5	4339.8	338.6	0.078
2	2-1	4489.9	324.6	0.072
	2-2	2623.9	289	0.110
	2-3	2145.3	199.4	0.093
	2-4	2811.3	259.2	0.092
	2-5	4691.6	346.4	0.074
3	3-1	4691.6	348.1	0.074
	3-2	2811.3	272.8	0.097
	3-3	2209.5	218.1	0.099
	3-4	2850	288.5	0.101
	3-5	4741.6	347.2	0.073

Table E.10. Estimated shear resistance determined using site-specific parameters for 110 t trucks.

Girder	SG Location	Mean V_r for 110 t truck (kN)	Standard Deviation of V_r for 110 t truck (kN)	Coefficient of Variation
1	1-1	4489.9	324.9	0.072
	1-2	2850	263.1	0.092
	1-3	1958.5	220.1	0.112
	1-4	2662.6	290.9	0.109
	1-5	4346.7	319.6	0.074
2	2-1	4346.7	314	0.072
	2-2	2662.6	273.9	0.103
	2-3	2209.5	245.5	0.111
	2-4	2662.6	264.1	0.099
	2-5	4608.1	335.1	0.073
3	3-1	4608.1	334.9	0.073
	3-2	2262.6	294.4	0.130
	3-3	2209.5	205.6	0.093
	3-4	2850	273.4	0.096
	3-5	4489.9	323	0.072

Table E.11. Bias ratios relating to bending moments determined using measured curvatures.

		Bias Ratio			
Girder	SG Location	Bending Moment	Bending Moment Resistance	Distribution Factor	Dynamic Load Allowance
1	1-1	0.212	1.181	0.817	0.800
	1-2	0.093	1.358	0.953	0.800
	1-3	0.167	1.202	1.36	0.800
	1-4	0.125	1.358	1.38	0.800
	1-5	0.242	1.182	1.124	0.800
2	2-1	0.294	1.188	1.131	0.800
	2-2	0.113	1.372	1.157	0.800
	2-3	0.172	1.213	1.397	0.800
	2-4	0.091	1.372	0.998	0.800
	2-5	0.190	1.188	0.88	0.800
3	3-1	0.224	1.181	0.863	0.800
	3-2	0.073	1.358	0.752	0.800
	3-3	0.014	1.202	0.116	0.800
	3-4	0.043	1.358	0.476	0.800
	3-5	0.173	1.181	0.801	0.800

Table E.12. Bias ratios relating to bending moments determined using measured neutral axis locations and strains.

Girder	SG Location	Bending Moment	Bending Moment Resistance	Distribution Factor	Dynamic Load Allowance
1	1-1	0.215	1.181	0.824	0.800
	1-2	0.045	1.358	0.479	0.800
	1-3	0.145	1.202	1.435	0.800
	1-4	0.117	1.358	1.434	0.800
	1-5	0.243	1.182	1.088	0.800
2	2-1	0.301	1.188	1.171	0.800
	2-2	0.116	1.372	1.264	0.800
	2-3	0.132	1.213	1.305	0.800
	2-4	0.041	1.372	0.669	0.800
	2-5	0.170	1.188	0.746	0.800
3	3-1	0.157	1.181	0.818	0.800
	3-2	0.078	1.358	1.124	0.800
	3-3	0.013	1.202	0.129	0.800
	3-4	0.046	1.358	0.735	0.800
	3-5	0.160	1.181	0.967	0.800

Table E.13. Bias ratios relating to shear determined using measured curvatures.

Girder	SG Location	Shear	Shear Resistance 62.5 t	Shear Resistance 110 t	Distribution Factor	Dynamic Load Allowance
1	1-1	0.215	1.369	1.370	0.570	0.800
	1-2	0.194	1.392	1.392	1.152	0.800
	1-3	0.023	1.281	1.265	0.657	0.800
	1-4	0.189	1.262	1.300	1.262	0.800
	1-5	0.293	1.323	1.326	0.957	0.800
2	2-1	0.296	1.366	1.338	0.785	0.800
	2-2	0.225	1.280	1.299	1.335	0.800
	2-3	0.067	1.379	1.420	1.919	0.800
	2-4	0.185	1.371	1.299	1.233	0.800
	2-5	0.124	1.427	1.418	0.405	0.800
3	3-1	0.476	1.430	1.406	1.263	0.800
	3-2	0.022	1.373	1.105	0.131	0.800
	3-3	0.001	1.427	1.427	0.041	0.800
	3-4	0.018	1.392	1.392	0.123	0.800
	3-5	0.384	1.446	1.370	1.255	0.800

Table E.14. Bias ratios relating to shear determined using measured neutral axis locations and strains.

Girder	SG Location	Shear	Shear Resistance 62.5 t	Shear Resistance 110 t	Distribution Factor	Dynamic Load Allowance
1	1-1	0.175	1.369	1.370	0.493	0.800
	1-2	0.193	1.392	1.392	1.218	0.800
	1-3	0.007	1.281	1.265	0.150	0.800
	1-4	0.169	1.262	1.300	1.123	0.800
	1-5	0.303	1.323	1.326	1.056	0.800
2	2-1	0.355	1.366	1.338	0.998	0.800
	2-2	0.180	1.280	1.299	1.137	0.800
	2-3	0.104	1.379	1.420	2.082	0.800
	2-4	0.176	1.371	1.299	1.166	0.800
	2-5	0.116	1.427	1.418	0.404	0.800
3	3-1	0.401	1.430	1.406	1.127	0.800
	3-2	0.042	1.373	1.105	0.263	0.800
	3-3	0.019	1.427	1.427	0.385	0.800
	3-4	0.049	1.392	1.392	0.329	0.800
	3-5	0.332	1.446	1.370	1.157	0.800

Table E.15. Live load capacity factors and reliability indices for bending moments determined using measured curvatures.

		62.5 t trucks		110 t trucks	
Girder	SG Location	Live Load Capacity Factor, F	Reliability Index, β	Live Load Capacity Factor, F	Reliability Index, β
1	1-1	11.29	7.78	6.49	6.17
	1-2	25.82	14.18	19.85	13.55
	1-3	4.56	6.29	2.7	4.91
	1-4	12.75	12.26	9.65	11.22
	1-5	5.43	5.78	3.04	4.6
2	2-1	7.16	7.64	4.43	6.17
	2-2	18.35	13.40	14	12.54
	2-3	7.22	10.47	4.84	8.73
	2-4	46.47	13.90	20.2	13.13
	2-5	19.04	12.03	12.13	9.82
3	3-1	10.97	8.26	6.52	6.59
	3-2	42.46	15.16	32.99	14.89
	3-3	1124	16.56	799.1	16.55
	3-4	113.9	15.66	88.7	15.58
	3-5	22.12	13.70	14.48	11.4

Table E.16. Live load capacity factors and reliability indices for bending moments determined using measured neutral axis locations and strains.

		62.5 t trucks		110 t trucks	
Girder	SG Location	Live Load Capacity Factor, F	Reliability Index, β	Live Load Capacity Factor, F	Reliability Index, β
1	1-1	12.24	8.55	7.27	6.82
	1-2	107.6	15.49	83.54	15.31
	1-3	5.38	6.65	3.17	5.20
	1-4	10.77	9.15	7.64	7.88
	1-5	7.15	7.04	4.24	5.63
2	2-1	7.89	8.89	5.06	7.24
	2-2	14.27	10.54	10.44	9.26
	2-3	8.78	9.12	5.53	7.36
	2-4	90.00	15.45	69.75	15.22
	2-5	28.17	14.82	18.48	12.38
3	3-1	15.60	8.25	8.79	6.49
	3-2	24.04	12.25	17.81	11.09
	3-3	1084	16.40	767.10	16.25
	3-4	67.53	14.83	51.90	14.35
	3-5	20.11	13.86	13.28	11.59

Table E.17. Live load capacity factors and reliability indices for shear determined using measured curvatures.

		62.5 t trucks		110 t trucks	
Girder	SG Location	Live Load Capacity Factor, F	Reliability Index, β	Live Load Capacity Factor, F	Reliability Index, β
1	1-1	45.04	13.61	28.98	12.42
	1-2	16.51	11.51	11.96	10.29
	1-3	4167	22.82	4658.00	22.75
	1-4	17.02	10.29	12.99	9.63
	1-5	9.03	8.44	5.07	6.59
2	2-1	9.76	10.11	5.60	7.99
	2-2	16.44	10.59	12.38	9.87
	2-3	12.99	9.57	15.25	9.89
	2-4	19.33	12.27	13.12	10.69
	2-5	88.39	14.32	58.12	14.14
3	3-1	4.21	5.32	1.68	3.81
	3-2	383.9	14.97	215.80	12.60
	3-3	582.8	18.48	682.10	19.44
	3-4	259.8	14.30	205.30	14.96
	3-5	9.69	10.33	5.58	8.35

Table E.18. Live load capacity factors and reliability indices for shear determined using measured neutral axis locations and strains.

		62.5 t trucks		110 t trucks	
Girder	SG Location	Live Load Capacity Factor, F	Reliability Index, β	Live Load Capacity Factor, F	Reliability Index, β
1	1-1	30.33	12.40	18.76	10.66
	1-2	19	13.30	14.29	12.47
	1-3	287.2	22.08	321.80	22.14
	1-4	13.97	11.20	11.74	11.09
	1-5	10.09	8.36	5.55	6.49
2	2-1	15.58	11.37	9.36	9.66
	2-2	11.95	11.10	9.30	10.66
	2-3	35.31	18.74	38.47	17.14
	2-4	17.90	12.71	12.31	11.20
	2-5	82.40	14.28	54.11	14.05
3	3-1	3.74	5.65	1.75	4.08
	3-2	1471	15.02	827.10	12.68
	3-3	87720	24.84	139130.00	24.85
	3-4	1792	14.41	1418.00	15.12
	3-5	7.06	8.80	3.86	6.72

Table E.19. Bias ratios for bending moments determined using measured curvatures for different bearing restraint cases.

Bearing Restraint	Girder	SG Location	Bias Ratio of M	Bias Ratio of DF
Fixed	1	1-1	0.493	0.851
		1-2	0.000	0.000
		1-3	0.110	1.281
		1-4	0.000	0.000
		1-5	0.563	1.160
	2	2-1	0.614	1.059
		2-2	0.000	0.000
		2-3	0.127	1.488
		2-4	0.000	0.000
		2-5	0.397	0.816
	3	3-1	0.521	0.899
		3-2	0.000	0.000
		3-3	0.009	0.109
		3-4	0.000	0.000
		3-5	0.402	0.827
Free	1	1-1	0.151	0.821
		1-2	0.124	0.918
		1-3	0.199	1.388
		1-4	0.168	1.337
		1-5	0.173	1.128
	2	2-1	0.207	1.240
		2-2	0.165	1.221
		2-3	0.196	1.366
		2-4	0.133	1.059
		2-5	0.134	0.873
	3	3-1	0.160	0.867
		3-2	0.098	0.725
		3-3	0.017	0.119
		3-4	0.058	0.461
		3-5	0.123	0.804

Table E.20. Bias ratios for bending moments determined using measured neutral axis locations and strains for different bearing restraint cases.

Bearing Restraint	Girder	SG Location	Bias Ratio of M	Bias Ratio of DF
Fixed	1	1-1	0.367	0.938
		1-2	0.000	0.000
		1-3	0.071	1.168
		1-4	0.000	0.000
		1-5	0.418	1.239
	2	2-1	0.469	1.201
		2-2	0.000	0.000
		2-3	0.098	1.608
		2-4	0.000	0.000
		2-5	0.258	0.765
	3	3-1	0.264	0.675
		3-2	0.000	0.000
		3-3	0.007	0.109
		3-4	0.000	0.000
		3-5	0.269	0.798
Free	1	1-1	0.113	0.901
		1-2	0.045	0.508
		1-3	0.129	1.276
		1-4	0.119	1.144
		1-5	0.128	1.207
	2	2-1	0.158	1.267
		2-2	0.129	1.470
		2-3	0.150	1.483
		2-4	0.134	1.284
		2-5	0.087	0.819
	3	3-1	0.081	0.648
		3-2	0.079	0.900
		3-3	0.012	0.119
		3-4	0.046	0.440
		3-5	0.083	0.778

Table E.21. Bias ratios for shear determined using measured curvatures for different bearing restraint cases.

Bearing Restraint	Girder	SG Location	Bias Ratio of V	Bias Ratio of DF
Fixed	1	1-1	0.483	0.712
		1-2	0.265	1.004
		1-3	0.047	0.845
		1-4	0.271	1.273
		1-5	0.552	1.027
	2	2-1	0.556	0.819
		2-2	0.329	1.248
		2-3	0.083	1.492
		2-4	0.257	1.206
		2-5	0.298	0.555
	3	3-1	0.738	1.087
		3-2	0.096	0.366
		3-3	0.016	0.281
		3-4	0.029	0.138
		3-5	0.557	1.036
Free	1	1-1	0.146	0.456
		1-2	0.197	1.172
		1-3	0.024	0.585
		1-4	0.195	1.198
		1-5	0.240	0.850
	2	2-1	0.253	0.794
		2-2	0.190	1.130
		2-3	0.082	1.963
		2-4	0.194	1.193
		2-5	0.143	0.505
	3	3-1	0.437	1.368
		3-2	0.053	0.315
		3-3	0.003	0.070
		3-4	0.037	0.227
		3-5	0.356	1.263

Table E.22. Bias ratios for shear determined using measured neutral axis locations and strains for different bearing restraint cases.

Bearing Restraint	Girder	SG Location	Bias Ratio of V	Bias Ratio of DF
Fixed	1	1-1	0.386	0.853
		1-2	0.176	0.974
		1-3	0.030	0.744
		1-4	0.185	1.102
		1-5	0.441	1.124
	2	2-1	0.416	0.920
		2-2	0.252	1.399
		2-3	0.071	1.730
		2-4	0.192	1.143
		2-5	0.171	0.436
	3	3-1	0.382	0.845
		3-2	0.044	0.245
		3-3	0.006	0.144
		3-4	0.063	0.373
		3-5	0.414	1.057
Free	1	1-1	0.060	0.271
		1-2	0.148	1.178
		1-3	0.008	0.518
		1-4	0.136	1.335
		1-5	0.193	0.830
	2	2-1	0.228	1.033
		2-2	0.127	1.008
		2-3	0.028	1.896
		2-4	0.103	1.011
		2-5	0.148	0.636
	3	3-1	0.290	1.314
		3-2	0.054	0.433
		3-3	0.003	0.204
		3-4	0.028	0.272
		3-5	0.267	1.152

Table E.23. Live load capacity factors and reliability indices for bending moments determined using measured curvatures for different bearing restraint cases.

			62.5 t Trucks		110 t Trucks	
Bearing Restraint	**Girder**	**SG Location**	**Live Load Capacity Factor, F**	**Reliability Index, β**	**Live Load Capacity Factor, F**	**Reliability Index, β**
Fixed	1	1-1	2.43	4.20	1.33	3.35
		1-2	infinite	15.88	infinite	15.88
		1-3	10.18	9.43	6.41	7.65
		1-4	infinite	15.88	infinite	15.88
		1-5	1.14	3.16	0.63	2.50
	2	2-1	2.71	4.94	1.69	3.96
		2-2	infinite	15.96	infinite	15.96
		2-3	9.51	11.69	6.43	9.99
		2-4	infinite	15.96	infinite	15.96
		2-5	7.59	7.94	4.72	6.42
	3	3-1	2.63	4.52	1.53	3.61
		3-2	infinite	15.88	infinite	15.88
		3-3	1781	16.57	1323	16.56
		3-4	infinite	15.88	infinite	15.88
		3-5	6.96	8.15	4.41	6.60
Free	1	1-1	19.08	9.80	11.35	7.80
		1-2	19.85	13.55	15.18	12.74
		1-3	3.97	6.09	2.38	4.74
		1-4	9.48	11.15	7.13	10.01
		1-5	9.50	7.30	5.44	5.79
	2	2-1	11.89	9.59	7.42	7.77
		2-2	11.47	11.83	8.63	10.72
		2-3	6.34	9.91	4.25	8.17
		2-4	16.42	12.44	12.35	11.37
		2-5	30.22	14.68	19.70	12.21
	3	3-1	18.00	10.30	10.97	8.26
		3-2	32.74	14.88	25.39	14.51
		3-3	902.30	16.55	642	16.54
		3-4	87.24	15.58	67.90	15.47
		3-5	33.35	16.10	22.29	13.74

Table E.24. Live load capacity factors and reliability indices for bending moments determined using measured neutral axis locations and strains for different bearing restraint cases.

			62.5 t Trucks		110 t Trucks	
Bearing Restraint	**Girder**	**SG Location**	**Live Load Capacity Factor, F**	**Reliability Index, β**	**Live Load Capacity Factor, F**	**Reliability Index, β**
Fixed	1	1-1	4.01	5.25	2.28	4.19
		1-2	infinite	15.88	infinite	15.88
		1-3	18.68	11.22	11.99	9.36
		1-4	infinite	15.98	infinite	15.88
		1-5	2.27	4.26	1.33	3.40
	2	2-1	4.03	6.37	2.58	5.14
		2-2	infinite	15.96	infinite	15.96
		2-3	9.88	9.62	6.27	7.83
		2-4	infinite	15.96	infinite	15.96
		2-5	15.59	11.22	9.91	9.15
	3	3-1	8.16	6.14	4.29	4.83
		3-2	infinite	15.98	infinite	15.88
		3-3	2389	16.54	1697	16.50
		3-4	infinite	15.88	infinite	15.88
		3-5	12.92	11.10	8.34	9.09
Free	1	1-1	26.92	11.98	16.71	9.68
		1-2	101.40	15.45	78.68	15.25
		1-3	7.37	7.53	4.39	5.94
		1-4	14.12	10.21	10.17	8.92
		1-5	15.48	9.67	9.38	7.74
	2	2-1	12.43	8.75	10.46	9.90
		2-2	10.20	9.16	7.26	7.89
		2-3	6.23	7.79	3.85	6.18
		2-4	12.09	10.25	8.78	8.98
		2-5	55.30	18.62	37.44	16.25
	3	3-1	56.98	14.23	35.93	11.62
		3-2	30.46	13.02	22.82	12.00
		3-3	1274.00	16.45	902.80	16.33
		3-4	114.30	15.41	88.52	15.18
		3-5	54.73	19.07	37.70	17.11

Table E.25. Live load capacity factors and reliability indices for shear determined using measured curvatures for different bearing restraint cases.

			62.5 t Trucks		110 t Trucks	
Bearing Restraint	**Girder**	**SG Location**	**Live Load Capacity Factor, F**	**Reliability Index, β**	**Live Load Capacity Factor, F**	**Reliability Index, β**
Fixed	1	1-1	7.80	7.46	3.97	5.55
		1-2	15.76	12.79	11.80	11.84
		1-3	103.80	19.57	117.40	20.01
		1-4	9.90	10.33	7.78	9.84
		1-5	3.19	5.09	1.41	3.69
	2	2-1	6.64	8.16	3.55	6.09
		2-2	8.45	10.08	6.50	9.42
		2-3	36.80	18.99	40.11	17.32
		2-4	12.64	11.51	8.58	9.90
		2-5	23.96	12.62	15.02	11.26
	3	3-1	2.24	4.53	0.960	3.20
		3-2	121.00	14.85	68.04	12.44
		3-3	1121.00	24.75	1270.00	24.77
		3-4	1047.00	14.40	828.10	15.11
		3-5	5.56	7.92	2.97	5.89
Free	1	1-1	58.92	13.96	38.28	12.99
		1-2	18.00	13.22	13.80	12.37
		1-3	309.50	22.17	346.70	22.21
		1-4	15.09	11.37	12.02	11.16
		1-5	51.24	13.36	9.15	8.12
	2	2-1	18.41	11.93	11.01	10.07
		2-2	17.15	11.99	13.50	11.84
		2-3	27.34	17.32	30.01	16.11
		2-4	17.62	12.67	12.12	11.16
		2-5	57.06	14.04	37.24	13.60
	3	3-1	3.75	5.66	1.75	4.08
		3-2	254.30	14.95	143.00	12.58
		3-3	23978.00	24.84	27165.00	24.84
		3-4	499.00	14.38	394.80	15.08
		3-5	7.75	9.18	4.29	7.11

Table E.26. Live load capacity factors and reliability indices for shear determined using measured neutral axis locations and strains for different bearing restraint cases.

			62.5 t Trucks		110 t Trucks	
Bearing Restraint	**Girder**	**SG Location**	**Live Load Capacity Factor, F**	**Reliability Index, β**	**Live Load Capacity Factor, F**	**Reliability Index, β**
Fixed	1	1-1	8.54	7.88	4.68	6.14
		1-2	23.79	12.74	17.54	11.71
		1-3	189.10	20.82	213.60	21.19
		1-4	178.00	14.23	11.85	9.32
		1-5	4.68	6.31	2.37	4.68
	2	2-1	8.93	9.84	5.10	7.71
		2-2	8.23	8.31	5.92	7.33
		2-3	30.19	13.98	34.34	13.82
		2-4	17.73	11.85	11.95	10.23
		2-5	55.27	14.03	36.10	13.59
	3	3-1	7.43	6.58	3.35	4.80
		3-2	15.61	10.04	221.10	12.60
		3-3	5672.00	23.54	6590.00	24.73
		3-4	393.40	14.97	140.60	14.83
		3-5	8.12	9.48	4.55	7.42
Free	1	1-1	246.80	14.89	164.80	14.70
		1-2	23.39	12.73	17.26	11.69
		1-3	1052.00	22.58	1180.00	22.66
		1-4	17.82	10.40	13.63	9.76
		1-5	21.63	11.52	13.60	10.11
	2	2-1	15.63	11.67	9.32	9.77
		2-2	28.10	12.06	21.82	11.79
		2-3	84.79	19.94	92.89	18.24
		2-4	40.44	14.21	28.31	12.99
		2-5	43.57	13.80	28.28	13.17
	3	3-1	5.24	5.63	2.11	4.05
		3-2	181.10	14.85	101.70	12.44
		3-3	8018.00	23.61	9312.00	24.78
		3-4	550.10	14.37	435.10	15.07
		3-5	12.46	11.12	7.30	9.28